Technical Paper 3701

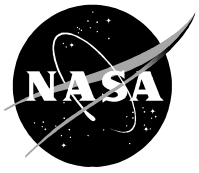

Measurement of Momentum Transfer Coefficients for H_2, N_2, CO, and CO_2 Incident Upon Spacecraft Surfaces

Steven R. Cook and Mark A. Hoffbauer

November 1997

The NASA STI Program Office . . . in Profile

Since its founding, NASA has been dedicated to the advancement of aeronautics and space science. The NASA Scientific and Technical Information (STI) Program Office plays a key part in helping NASA maintain this important role.

The NASA STI Program Office is operated by Langley Research Center, the lead center for NASA's scientific and technical information. The NASA STI Program Office provides access to the NASA STI Database, the largest collection of aeronautical and space science STI in the world. The Program Office is also NASA's institutional mechanism for disseminating the results of its research and development activities. These results are published by NASA in the NASA STI Report Series, which includes the following report types:

- TECHNICAL PUBLICATION. Reports of completed research or a major significant phase of research that present the results of NASA programs and include extensive data or theoretical analysis. Includes compilations of significant scientific and technical data and information deemed to be of continuing reference value. NASA's counterpart of peer-reviewed formal professional papers but has less stringent limitations on manuscript length and extent of graphic presentations.

- TECHNICAL MEMORANDUM. Scientific and technical findings that are preliminary or of specialized interest, e.g., quick release reports, working papers, and bibliographies that contain minimal annotation. Does not contain extensive analysis.

- CONTRACTOR REPORT. Scientific and technical findings by NASA-sponsored contractors and grantees.

- CONFERENCE PUBLICATION. Collected papers from scientific and technical conferences, symposia, seminars, or other meetings sponsored or cosponsored by NASA.
- SPECIAL PUBLICATION. Scientific, technical, or historical information from NASA programs, projects, and mission, often concerned with subjects having substantial public interest.

- TECHNICAL TRANSLATION. English-language translations of foreign scientific and technical material pertinent to NASA's mission.

Specialized services that complement the STI Program Office's diverse offerings include creating custom thesauri, building customized databases, organizing and publishing research results . . . even providing videos.

For more information about the NASA STI Program Office, see the following:

- Access the NASA STI Program Home Page at ***http://www.sti.nasa.gov***

- E-mail your question via the Internet to help@sti.nasa.gov

- Fax your question to the NASA Access Help Desk at (301) 621-0134

- Telephone the NASA Access Help Desk at (301) 621-0390

- Write to:
  NASA Access Help Desk
  NASA Center for AeroSpace Information
  800 Elkridge Landing Road
  Linthicum Heights, MD 21090-2934

Technical Paper 3701

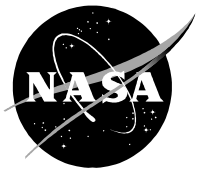

Measurement of Momentum Transfer Coefficients for H_2, N_2, CO, and CO_2 Incident Upon Spacecraft Surfaces

Steven R. Cook and Mark A. Hoffbauer
Los Alamos National Laboratory

National Aeronautics
and Space Administration

Lyndon B Johnson Space Center
Houston, Texas 77058-4406

November 1997

Available from:

NASA Center for AeroSpace Information
800 Elkridge Landing Road
Linthicum Heights, MD 21090-2934
Price Code: A17

National Technical Information Service
5285 Port Royal Road
Springfield, VA 22161
Price Code: A10

Contents

List of Figures

List of Tables

Abstract

Measurements of momentum transfer coefficients were made for gas-surface interactions between the Space Shuttle reaction control jet plume gases and the solar panel array materials to be used on the International Space Station. Actual conditions were simulated using a supersonic nozzle source to produce beams of the gases with approximately the same average velocities as the gases have in the Shuttle plumes. Samples of the actual solar panel materials were mounted on a torsion balance that was used to measure the force exerted on the surfaces by the molecular beams. Measurements were made with H_2, N_2, CO, and CO_2 incident upon the solar array material, Kapton, SiO_2-coated Kapton, and Z-93-coated Al. The measurements showed that molecules scatter from the surfaces more specularly as the angle of incidence increases and that the scattering behavior has a strong dependence upon both the incident gas and velocity. These results show that for some technical surfaces the simple assumption of diffuse scattering with complete thermal accommodation is entirely inadequate. It is clear that additional measurements are required to produce models that more accurately describe the gas-surface interactions encountered in rarefied flow regimes.

1 Background

This project was motivated by the need to accurately model the forces exerted on the large solar panel arrays to be used on the International Space Station by gases emitted from the reaction control jets on the Space Shuttle. This effort has been one of the largest ever undertaken to measure and characterize momentum transferred to surfaces by incident gases. The experimental effort has resulted in the most comprehensive and accurate measurements ever made in this field. Using this data it is now possible to construct a limited number of accurate empirical models of forces exerted on spacecraft surfaces by incident gases in rarefied flow regimes. The high accuracy of these measurements also makes it possible to obtain an understanding of fundamental microscopic gas-surface interaction properties. The results of these experiments show that, even from technical surfaces, molecules scatter more specularly as the angle of incidence increases, and that the scattering has a strong dependence upon both the incident gas and velocity.

Theoretical advances were made in addition to the experimental contributions. Traditionally, the momentum accommodation coefficients have been used to analyze the momentum transferred to surfaces by incident gases in rarefied flow regimes. However, the momentum accommodation coefficients contain singularities that render them unusable for a large number of gas-surface interactions, including those that are of specific interest to NASA under investigation at LANL. Therefore, a new formalism was developed based upon two momentum transfer parameters called the reduced force coefficients. We have shown that the macroscopic average momentum transferred to a surface by incident molecules in rarefied flow regimes can be completely characterized using the reduced force coefficients. These coefficients can also be used to determined the magnitude and direction of the flux-weighted average velocity of the scattered molecules.

In the past, a knowledge of the energy accommodation coefficient was required to determine the flux-weighted average translational energy of the scattered molecules. Accurate measurements of energy accommodation coefficients are difficult, however, and would introduce an additional source of uncertainty. A formula was derived using the reduced force coefficients that accurately

approximates the flux-weighted average translational energy of the scattered molecules, thereby eliminating the need to measure energy accommodation coefficients. This breakthrough makes it possible to uniquely determine the adjustable parameters in the Nocilla gas-surface interaction model solely from measurements of the momentum transferred to surfaces by incident gases.

This project to date has resulted in one Ph.D. dissertation and six refereed publications [1, 2, 3, 4, 5, 6, 7]. Four additional manuscripts are near completion and will be submitted to Physical Review E. The apparatus has been extensively improved and is now fully operational. In addition, many new and exciting results have been recently obtained and will be published in future articles.

Recently, a differentially pumped time-of-flight system was added to the apparatus that will allow accurate measurements of the velocity distribution functions of molecules scattered from surfaces. This system was designed so that during time-of-flight measurements, the torsion balance can be used to simultaneously measure the momentum transferred to the surface by the incident gas. This experimental capability will make it possible to compare approximate velocity distribution functions of the scattered molecules constructed from the macroscopic average transfer of momentum and energy to the surfaces by the incident gases, such as the Nocilla model, with the actual measured velocity distribution functions of the scattered molecules.

In addition, an improved torsion balance has been fabricated that can be used to measure both the momentum transfer coefficients and the absolute flux densities of the molecular beams. This new torsion balance will simplify the experimental procedures, reduce the time taken to complete a set of measurements, and increase the accuracy of the results. Accuracy is increased mainly due to eliminating the use of mass spectrometers to measure the percentage of each gas species in the molecular beams.

2 The Momentum Accommodation Coefficients

The tangential σ and normal σ' momentum accommodation coefficients can be expressed as [8]

$$\sigma = \frac{\overline{v}_i \sin\theta_i - \overline{v}_s \sin\theta_s}{\overline{v}_i \sin\theta_i}, \tag{1}$$

$$\sigma' = \frac{\overline{v}_i \cos\theta_i - \overline{v}_s \cos\theta_s}{\overline{v}_i \cos\theta_i - \sqrt{\pi kT/2m}}, \tag{2}$$

where $\overline{v}$ is the magnitude of the flux-weighted average (hereafter referred to as average) velocity, θ is the angle between the average velocity and the surface normal, the subscripts i and s represent the incident and scattered molecules respectively, k is Boltzmann's constant, T is the temperature of the scattering surface, and m is the mass of the individual gas molecules. The quantity $\sqrt{\pi kT/2m}$ is the average velocity of the scattered molecules assuming diffuse scattering from the surface with complete thermal accommodation [8].

For many applications the tangential momentum accommodation coefficient has a removable singularity at an angle of incidence θ_i normal to the surface and is well behaved. However, for applications where θ_s is not equal to zero at normal angles of incidence, the tangential coefficient would diverge. Problems with the singularity in the normal momentum accommodation coefficient result in divergent behavior for essentially every application involving a directed gas

flow. In addition, the angle of incidence at which the singularity occurs is a function of the average velocity of the incident molecules and the temperature of the scattering surface. For the gas-surface interactions considered in this report, the angle of incidence at which the singularity occurred ranged from 55° to 85°. The divergent behavior caused by this singularity made it nearly impossible to use the normal coefficient.

To overcome this singularity problem, Knuth [9] defined a normal momentum transfer coefficient that eliminates the functional dependence of the singularity upon the average velocity of the incident molecules and the surface temperature. However, the coefficient diverges at large angles of incidence for all non specular scattering processes. Therefore, a new formalism was developed that completely eliminated the problems caused by singularities.

3 The Reduced Force Coefficients

The definitions of the reduced force coefficients were arrived at by considering the force exerted on a surface by an incident molecular beam. The singularity problems were eliminated by defining the coefficients with denominators that are independent of the incident flow direction. The tangential f_t and normal f_n reduced force coefficients are defined as

$$f_t = \frac{\overline{p}_{it} - \overline{p}_{st}}{\overline{p}_i}, \tag{3}$$

$$f_n = \frac{\overline{p}_{in} + \overline{p}_{sn}}{\overline{p}_i}, \tag{4}$$

where $\overline{p}$ is the magnitude of the average momentum, and the subscripts t and n are the tangential and normal components, respectively. The reduced force coefficients can also be written as

$$f_t = F_t / N_i m \overline{v}_i, \tag{5}$$

$$f_n = F_n / N_i m \overline{v}_i, \tag{6}$$

where F is the magnitude of the force exerted on the surface by the incident gas, and N_i is the total incident flux. Thus, the coefficients can be determined from measurements of F_t, F_n, N_i, and $\overline{v}_i$. Equations (3) and (4) can be used to express the magnitude and direction of the average velocity of the scattered molecules as

$$\overline{v}_s = \overline{v}_i \sqrt{(f_t - \sin\theta_i)^2 + (f_n - \cos\theta_i)^2}, \tag{7}$$

$$\theta_s = \tan^{-1}\left(\frac{\sin\theta_i - f_t}{f_n - \cos\theta_i}\right). \tag{8}$$

Spherical polar coordinates are used to define the directions of the average velocities of the incident and scattered molecules. The polar angle is measured from the surface normal, the azimuthal angle is 180° for the average velocity of the incident molecules and is assumed to be 0° for the average velocity of the scattered molecules, and the scattering surface is in the plane defined by the polar angle of 90°.

A new parameter μ, called the scalar momentum accommodation coefficient is introduced and defined as

$$\mu = \frac{\overline{p}_i - \overline{p}_s}{\overline{p}_i - \overline{p}_d}. \tag{9}$$

The quantity $\overline{p}_d$ is the magnitude of the average momentum of the scattered molecules assuming diffuse scattering and is given by $\sqrt{\pi kTm/2}$. The scalar momentum accommodation coefficient ranges between zero for specular scattering and one for diffuse scattering with complete thermal accommodation and is well defined for all angles of incidence.

For applications where differences between the average energies associated with the internal-state distribution functions of the incident and scattered molecules can be neglected, the energy accommodation coefficient ϵ can be written as [8, 10]

$$\epsilon = \frac{\overline{v_i^2} - \overline{v_s^2}}{\overline{v_i^2} - 4kT/m}, \tag{10}$$

where $\overline{v^2}$ is the average of the velocity squared, and $4kT/m$ is the average of the velocity squared of the scattered molecules assuming diffuse scattering. A knowledge of the reduced force coefficients is not sufficient to determine the energy accommodation coefficient using Eq. (10). Additional information is required to determine $\overline{v_s^2}$. The simple assumption of equating $\overline{v}_s^2$ with $\overline{v_s^2}$ can result in errors as large as 60%. A more accurate approximation for $\overline{v_s^2}$ can be made with an energy accommodation coefficient ϵ' based on the average velocities of the incident and scattered molecules. The coefficient is defined as

$$\epsilon' = \frac{\overline{v}_i^2 - \overline{v}_s^2}{\overline{v}_i^2 - \pi kT/2m}. \tag{11}$$

From a knowledge of the reduced force coefficients and the velocity distribution function of the molecular beam, the coefficient ϵ' can be calculated. The uncertainty associated with the approximation of equating ϵ' with ϵ has been shown to be less than $\pm 1\%$ for gas-surface interactions where the average energy of the incident molecules is large compared to kT [1]. With this approximation, $\overline{v_s^2}$ can be written as

$$\overline{v_s^2} = \overline{v_i^2} - \epsilon' \left(\overline{v_i^2} - 4kT/m \right). \tag{12}$$

The quantity $\overline{v_i^2}$ can be determined from a knowledge of the velocity distribution function of the incident molecules. The average translational energy of the scattered molecules can be obtained using Eq. (12).

4 The Nocilla Gas-Surface Interaction Model

The Nocilla gas-surface interaction model assumes that the velocity distribution function of the scattered molecules can be approximated using a drifting Maxwellian distribution function with most probable velocity $\mathbf{U}$ defined as [11]

$$N(\mathbf{v}) = n \left(\frac{m}{2\pi kT_s} \right)^{3/2} \exp\left(-\frac{m(\mathbf{v} - \mathbf{U})^{\mathbf{2}}}{2kT_s} \right), \tag{13}$$

where n and T_s are the number density and temperature of the scattered molecules, respectively. The adjustable parameters in the Nocilla model are n, T_s, and $\mathbf{U}$. The most probable velocity of the scattered molecules is assumed to lie in the plane formed by the surface normal and the

average velocity of the incident molecules. Equations (14)–(17), obtained by integrating Eq. (13), can be used to determine the four Nocilla model parameters:

$$\Phi_s = \frac{nU}{2\pi S}\left(e^{-\Lambda^2} + \sqrt{\pi}\Lambda\Sigma\right), \tag{14}$$

$$\overline{v}_s \sin\theta_s = U \sin\theta_u, \tag{15}$$

$$\overline{v}_s \cos\theta_s = \frac{U}{S}\frac{\Lambda e^{-\Lambda^2} + \sqrt{\pi}\left(\frac{1}{2} + \Lambda^2\right)\Sigma}{e^{-\Lambda^2} + \sqrt{\pi}\Lambda\Sigma}, \tag{16}$$

$$\overline{v_s^2} = \frac{U^2}{S^2}\frac{\left(2 + S^2\right)e^{-\Lambda^2} + \sqrt{\pi}\left(\frac{5}{2} + S^2\right)\Lambda\Sigma}{e^{-\Lambda^2} + \sqrt{\pi}\Lambda\Sigma}, \tag{17}$$

where

$$S = \frac{U}{\sqrt{2kT_s/m}}, \tag{18}$$

$$\Lambda = S\cos\theta_u, \tag{19}$$

$$\Sigma = 1 + \mathrm{erf}\Lambda, \tag{20}$$

Φ_s is the flux density of the scattered molecules, and θ_u is the angle between the surface normal and the most probable velocity $\mathbf{U}$. Using Eqs. (15), (16) and (17) it can be shown that

$$\tan\theta_s = \frac{S\sin\theta_u\left(e^{-\Lambda^2} + \sqrt{\pi}\Lambda\Sigma\right)}{\Lambda e^{-\Lambda^2} + \sqrt{\pi}\left(\frac{1}{2} + \Lambda^2\right)\Sigma}, \tag{21}$$

$$\frac{\left(\overline{v}_s \sin\theta_s\right)^2}{\overline{v_s^2}} = \frac{\left(S\sin\theta_u\right)^2\left(e^{-\Lambda^2} + \sqrt{\pi}\Lambda\Sigma\right)}{\left(2 + S^2\right)e^{-\Lambda^2} + \sqrt{\pi}\left(\frac{5}{2} + S^2\right)\Lambda\Sigma}. \tag{22}$$

To determine S and θ_u, Eqs. (21) and (22) can be evaluated iteratively. Then Eq. (15) is used to determine U, and Eq. (18) is used to obtain T_s.

When the scattering angle θ_s is equal to zero, Eq. (15) implies θ_u must equal zero or 180°. For this special case, S can be determined from an equation obtained by combining Eqs. (21) and (22), given by

$$\frac{\overline{v_s^2}}{\overline{v}_s^2} = \frac{\Delta\left(e^{-S^2} \pm \sqrt{\pi}S\Sigma'\right)}{\left(\sqrt{\pi}\left(\frac{1}{2} + S^2\right)\Sigma' \pm Se^{-S^2}\right)^2}, \tag{23}$$

where

$$\Sigma' = 1 \pm \mathrm{erf}S, \tag{24}$$

$$\Delta = \left(2 + S^2\right)e^{-S^2} \pm \sqrt{\pi}\left(\frac{5}{2} + S^2\right)S\Sigma'. \tag{25}$$

The plus sign is used if θ_u equals zero while the minus sign is used if θ_u equals 180°. Once S is known, U can be evaluated iteratively using Eq. (16). For all cases, after θ_u, U, and S have been determined, n can be obtained from Eq. (14) by equating the incident and exit flux-densities.

The angular distribution function I is defined by letting $I\left(\theta,\phi\right)d\Omega$ represent the fraction of Φ_s that scatters into the differential solid angle $d\Omega$ about the direction defined by θ and ϕ, where ϕ is

the spherical coordinate azimuthal angle. Using the Nocilla model to approximate the angular distribution function of the scattered molecules gives

$$I(\theta,\phi) = \frac{\Theta}{\pi}\cos\theta\frac{e^{-S^2}}{e^{-\Lambda^2}+\sqrt{\pi}\Lambda\Sigma}, \tag{26}$$

where

$$\Theta = 1+\rho^2+\sqrt{\pi}\rho\left(\frac{3}{2}+\rho^2\right)(1+\mathrm{erf}\rho)\,e^{\rho^2}, \tag{27}$$

and

$$\rho = S\left(\sin\theta\cos\phi\sin\theta_u+\cos\theta\cos\theta_u\right). \tag{28}$$

The angular distribution function can also be thought of as representing the probability that a molecule with incident velocity $\mathbf{v}_i$ scatters into the solid angle $d\Omega$ about the direction defined by θ and ϕ. Once the Nocilla model parameters have been determined, Eq. (26) can be used to approximate the angular distribution function of the scattered molecules.

5 Experimental Results

The experimental results were obtained from measurements of the forces exerted on surfaces by molecular beams of the gases using a torsion balance. The torsion balance apparatus used to measure the forces, along with the techniques used to measure the flux-densities and velocity distribution functions of the molecular beams are described elsewhere[1, 2]. The average velocities of the molecular beams ranged from 1670 m/s for CO_2 to 4620 m/s for H_2. The total uncertainty in the reduced force coefficient measurements is estimated to be less than $\pm 10\%$.

Measurements of the reduced force coefficients for N_2, CO, and CO_2 incident upon the solar panel, SiO_2-coated Kapton, and Kapton showed that these gas-surface interactions have many similarities. Scanning electron microscope measurements revealed that the solar panel, SiO_2-coated Kapton, and Kapton had similar surface roughness and were smooth on a scale of less than 1 μm, while the Z-93-coated aluminum surface was rough on a 100 μm scale. This contrast in surface roughness could account for the significant differences between the way the four gases scattered from Z-93-coated aluminum and the other three surfaces.

Figures 1–32 are plots of the reduced force coefficients, $\overline{v}_s/\overline{v}_i$, θ_s, and μ as a function of the angle of incidence θ_i for the various gas-surface interactions, while Tables 1–32 contain all actual experimental data. The gases N_2, CO, and CO_2 can be seen to scatter from Z-93-coated aluminum diffusely with almost complete thermal accommodation by noting that θ_s is close to zero and μ is close to one at all angles of incidence. H_2 can be seen to scatter from Z-93-coated aluminum diffusely by noting that θ_s is close to zero for all angles of incidence. However, μ varies widely over the range of angles of incidence.

For the gases incident upon the solar panel, SiO_2-coated Kapton, and Kapton $\overline{v}_s$ and θ_s increase as the angle of incidence increases, consistent with the scattering becoming more specular. For large angles of incidence, the scattering angles for CO_2 are larger than for N_2 and CO, and the scattering angles for N_2 and CO are larger than for H_2. This effect can be explained by noting that the mass of H_2 is significantly smaller than the mass of N_2 and CO, and the masses of N_2 and CO are smaller than the mass of CO_2 and that a given force perpendicular to the direction of motion would deflect H_2 more than N_2 and CO, and would deflect N_2 and CO more than CO_2.

Thus, for large angles of incidence where the scattering becomes more specular, it is reasonable to assume that the large repulsive force exerted on the molecules by the surface will deflect H_2 more than N_2 and CO, and will deflect N_2 and CO more than CO_2.

In Figs. 33–64, polar plots of the angular distribution functions of the scattered molecules are shown for the various gas-surface interactions. The Nocilla model parameters are shown in Tables 33–64 and were obtained for the gas-surface interactions using the previously outlined procedure. Negative values for θ_u imply that ϕ_u is 180°. Equation (26) was then used to calculate the angular distribution functions. In these figures, the origin can be thought of as the impingement point of the molecular beam, the vertical axis is perpendicular to the scattering surface, and the horizontal axis is defined by the projection of **U** onto the plane of the scattering surface. Figures 33–64 show the intersection of the plane formed by the average velocity of the incident molecules and the surface normal with the three-dimensional angular distribution functions. The distance from the origin to a point on a lobe times $d\Omega$ represents the probability that a molecule with the indicated average velocity scatters from the surface into a differential solid angle $d\Omega$ about the direction defined by θ and ϕ. These distances are defined by the tick marks on the horizontal and vertical axis. The portion of the horizontal axis to the right of the vertical axis corresponds to $\phi = 0$, and the portion to the left of the vertical axis corresponds to $\phi = 180°$. The polar angle is given along the circular axis of the graphs.

The general trend that the scattering becomes more specular with increasing angles of incidence for gases scattering from the solar panel, SiO_2-coated Kapton, and Kapton can be inferred from Figs. 33–64. As the angle of incidence increases, the lobes become much larger because of the way in which the angular distribution function is normalized according to the equation

$$\int I\,(\theta, \phi)\; d\Omega = 1. \tag{29}$$

This behavior has fundamental physical significance. As the angle of incidence increases, the size of the lobes also increases, meaning fewer particles scatter out of the plane formed by the average velocity of the incident molecules and the surface normal. This effect is more pronounced for N_2, CO, and CO_2 than for H_2 and for the larger incident velocities.

The figures show that scattering from Z-93-coated aluminum is nearly diffuse for all angles of incidence. This result was observed for all gases incident upon Z-93-coated aluminum and at all incident velocities. Nearly diffuse scattering is most likely due to the extremely rough surface morphology of Z-93-coated aluminum.

Tables 65–67 compare measurements of the reduced force coefficients for N_2, CO, and CO_2 made with the carrier gases H_2 and He. The data agree to within the uncertainty of the measurements for all angles of incidence except 85°. At this angle of incidence alignment of the sample with the molecular beam is extremely critical. A minor misalignment could result in a fraction of the beam missing the sample. The large discrepancy at the angle of incidence of 85° could be due to this effect.

6 Conclusions

A new formalism has been used to analyze the average momentum transferred to surfaces by incident gases. This new formalism eliminates the singularity problems associated with the

momentum accommodation coefficients and can be used to uniquely determine the Nocilla gas-surface interaction model parameters. The formalism eliminates the need to measure energy accommodation coefficients, thereby reducing the number of experimentally determined parameters required to obtain the Nocilla model parameters.

The results discussed in this report show that molecules scatter from technical surfaces more specularly as the angle of incidence increases, and that the scattering has a strong dependence upon both the incident gas and velocity. These results show that for some technical surfaces the simple assumption of diffuse scattering with complete thermal accommodation is entirely inadequate.

References

[1] S. R. Cook, Ph.D. thesis, The University of Texas at Austin, 1995.

[2] S. R. Cook, M. A. Hoffbauer, J. B. Cross, H. Wellenstein, and M. Fink, Rev. Sci. Instrum. **67**, 1781 (1996).

[3] S. R. Cook and M. A. Hoffbauer, Phys. Rev. E **55**, R3828 (1997).

[4] S. R. Cook, J. B. Cross, and M. A. Hoffbauer, in *Rarefied Gas Dynamics 19*, edited by J. Harvey and G. Lord (Oxford University Press, Oxford, 1995), Vol. 2, pp. 967–973.

[5] S. R. Cook and M. A. Hoffbauer, in *Rarefied Gas Dynamics 20*, edited by C. Shen (Peking University Press, Beijing, 1997), pp. 467–472.

[6] S. R. Cook and M. A. Hoffbauer, J. of Spacecraft and Rockets **34**, 379 (1997).

[7] S. R. Cook and M. A. Hoffbauer, J. of Vac. Sci. and Tech. A **15**, 1 (1997).

[8] S. A. Schaaf, in *Encyclopedia of Physics*, edited by S. Flügge and C. Truesdell (Springer-Verlag, Berlin, 1963), No. 2, pp. 591–624.

[9] E. L. Knuth, AIAA Journal **18**, 602 (1980).

[10] *Dynamics of Gas-Surface Interactions*, edited by C. T. Rettner and M. N. R. Ashfold (The Royal Society of Chemistry, Cambridge, 1991).

[11] S. Nocilla, in *Rarefied Gas Dynamics*, edited by J. A. Laurmann (Academic Press, New York, 1963), Vol. 1, pp. 327–346.

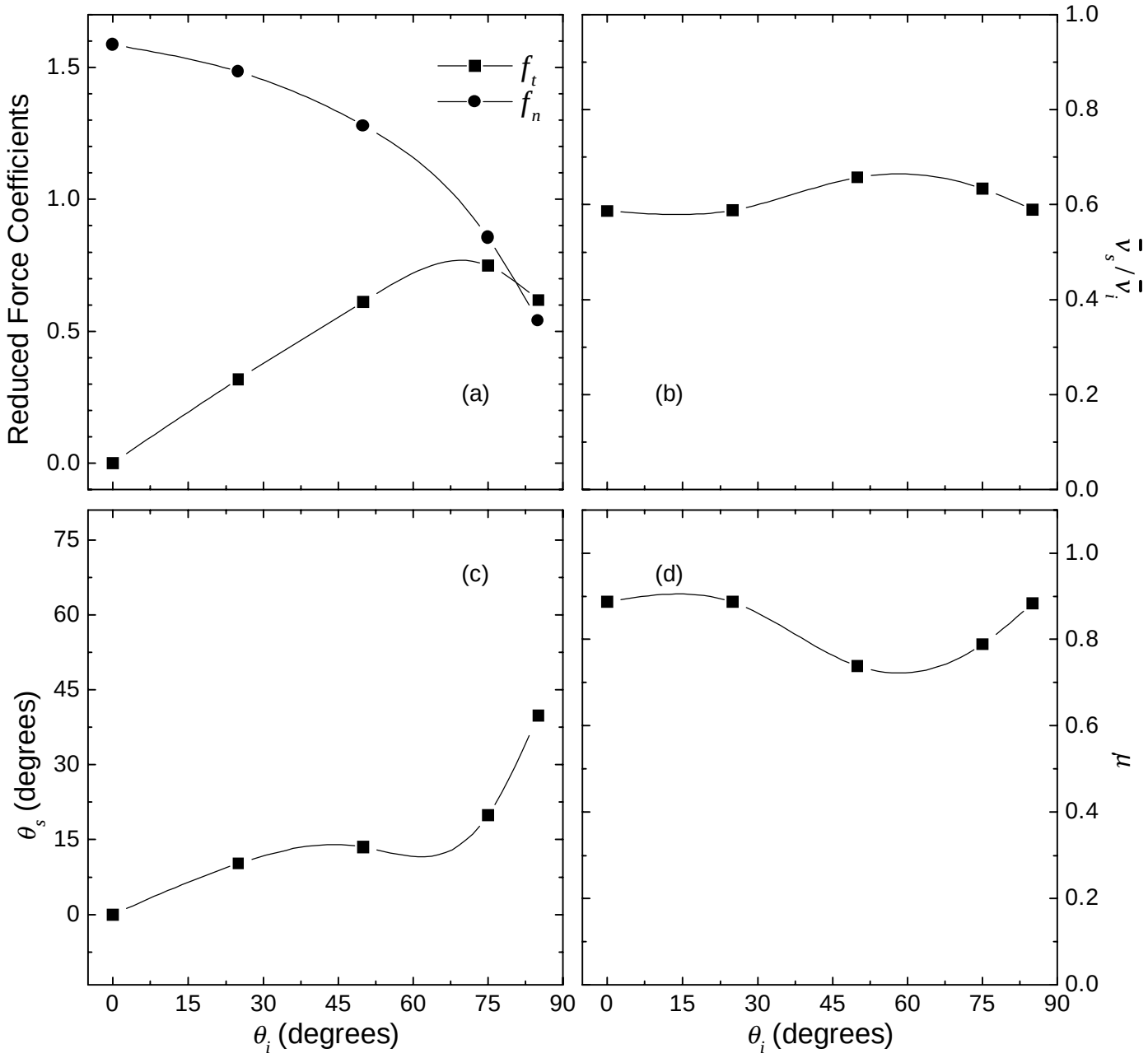

Figure 1: The data for 2590 m/s H_2 incident upon the solar panel.

Table 1: 2590 m/s H_2 incident upon the solar panel

θ_i (degrees)	f_t	f_n	$\overline{v}_s/\overline{v}_i$	$\overline{v}_s$ (m/s)	θ_s (degrees)	μ	ϵ'	$\overline{v_s^2}$ $(\mathrm{m/s})^2$
0	0	1.59	0.586	1520	0	0.888	0.918	5.02×10^6
25	0.317	1.48	0.587	1520	10.3	0.886	0.916	5.02×10^6
50	0.612	1.28	0.656	1700	13.6	0.738	0.796	5.25×10^6
75	0.750	0.854	0.633	1640	19.9	0.788	0.839	5.17×10^6
85	0.619	0.539	0.588	1520	39.8	0.883	0.915	5.03×10^6

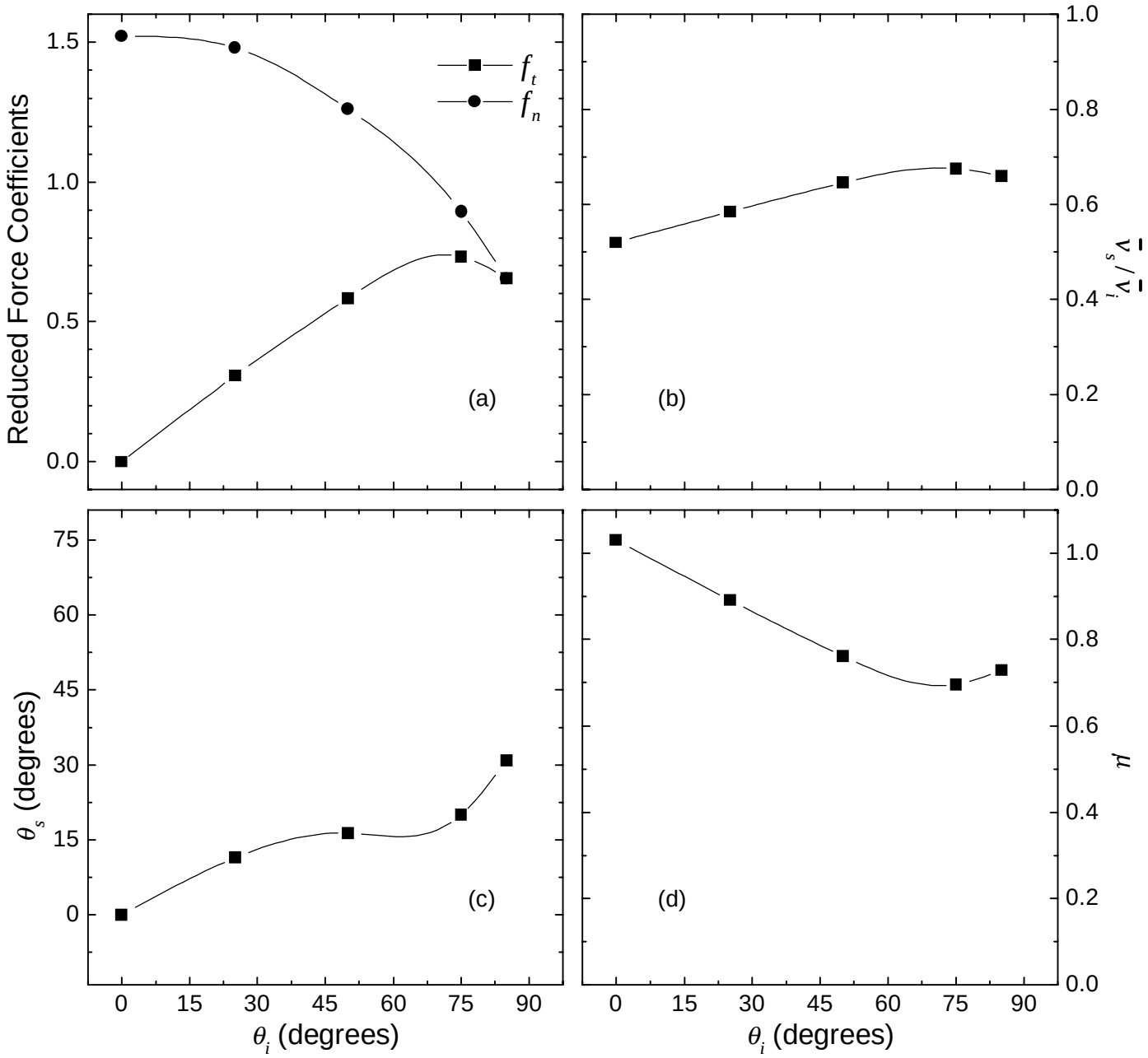

Figure 2: The data for 2590 m/s H_2 incident upon SiO_2-coated Kapton.

Table 2: 2590 m/s H_2 incident upon SiO_2-coated Kapton

θ_i (degrees)	f_t	f_n	$\overline{v}_s/\overline{v}_i$	$\overline{v}_s$ (m/s)	θ_s (degrees)	μ	ϵ'	$\overline{v_s^2}$ $(\mathrm{m/s})^2$
0	0	1.52	0.520	1350	0	1.03	1.02	4.82×10^6
25	0.307	1.48	0.585	1510	11.4	0.891	0.920	5.02×10^6
50	0.584	1.26	0.645	1670	16.4	0.761	0.816	5.22×10^6
75	0.733	0.893	0.676	1750	20.1	0.696	0.760	5.32×10^6
85	0.656	0.653	0.660	1710	31.0	0.729	0.789	5.27×10^6

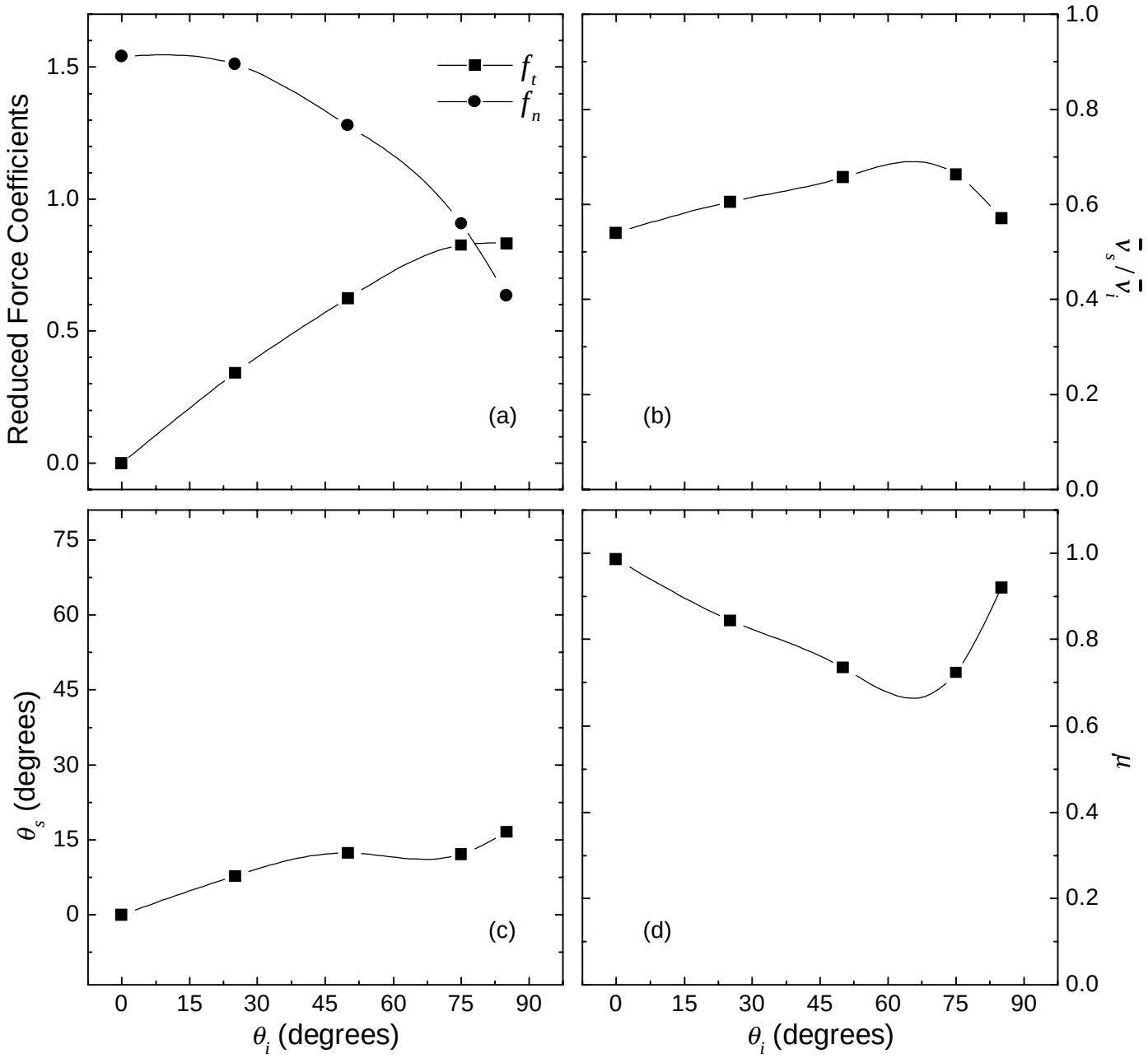

Figure 3: The data for 2590 m/s H_2 incident upon Kapton.

Table 3: 2590 m/s H_2 incident upon Kapton

θ_i (degrees)	f_t	f_n	$\overline{v}_s/\overline{v}_i$	$\overline{v}_s$ (m/s)	θ_s (degrees)	μ	ϵ'	$\overline{v_s^2}$ (m/s)^2
0	0	1.54	0.540	1400	0	0.986	0.990	4.88×10^6
25	0.340	1.51	0.606	1570	7.80	0.845	0.885	5.08×10^6
50	0.625	1.28	0.657	1700	12.4	0.735	0.794	5.26×10^6
75	0.826	0.907	0.663	1720	12.2	0.724	0.784	5.28×10^6
85	0.833	0.635	0.571	1480	16.6	0.920	0.942	4.97×10^6

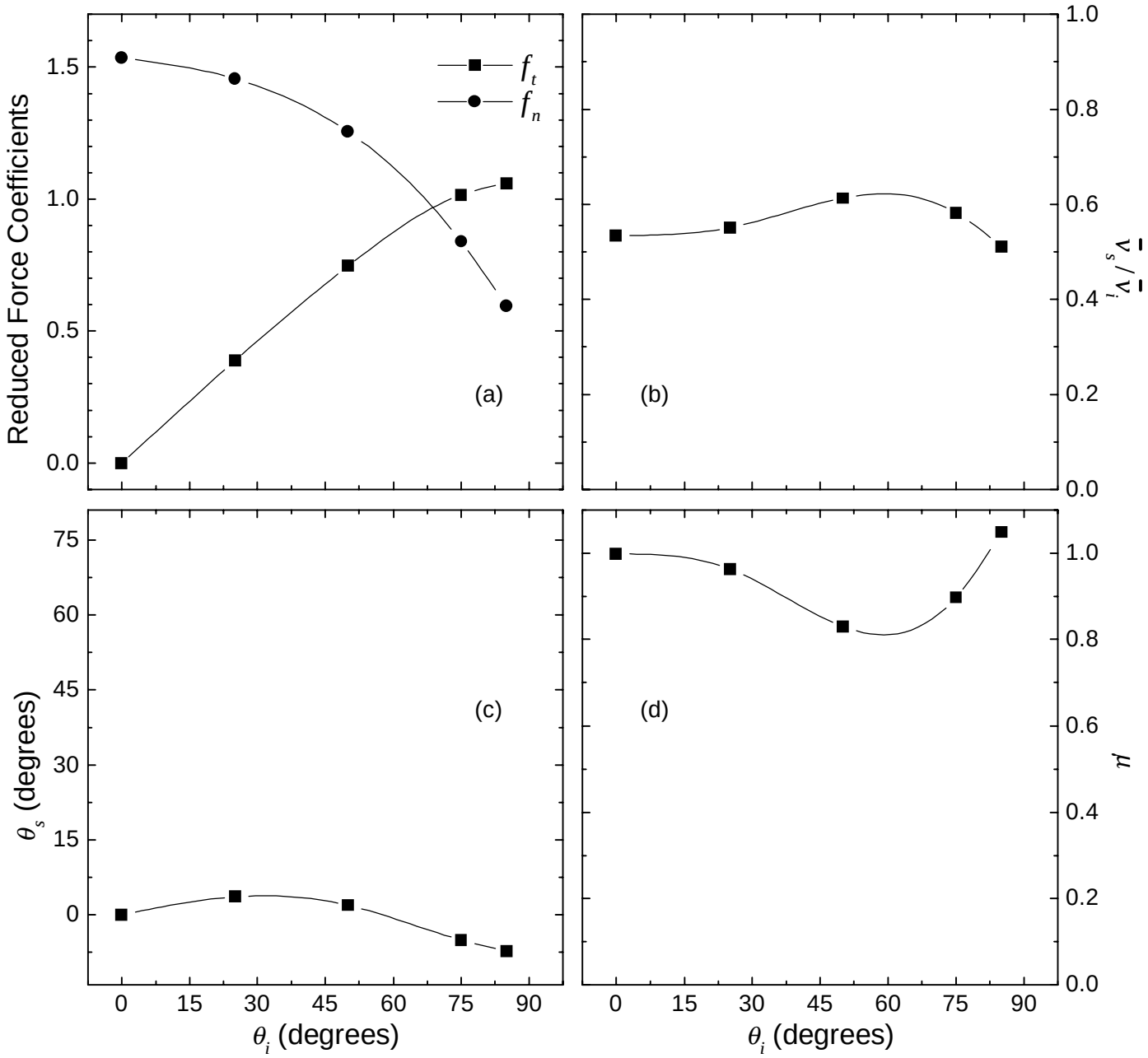

Figure 4: The data for 2590 m/s H_2 incident upon Z-93-coated aluminum.

Table 4: 2590 m/s H_2 incident upon Z-93-coated aluminum

θ_i (degrees)	f_t	f_n	$\overline{v}_s/\overline{v}_i$	$\overline{v}_s$ (m/s)	θ_s (degrees)	μ	ϵ'	$\overline{v_s^2}$ (m/s)^2
0	0	1.53	0.535	1380	0	0.998	0.999	4.87×10^6
25	0.388	1.46	0.551	1430	3.59	0.963	0.973	4.91×10^6
50	0.745	1.26	0.613	1590	1.96	0.830	0.873	5.11×10^6
75	1.02	0.839	0.582	1510	-5.02	0.897	0.925	5.01×10^6
85	1.06	0.594	0.511	1320	-7.25	1.05	1.03	4.80×10^6

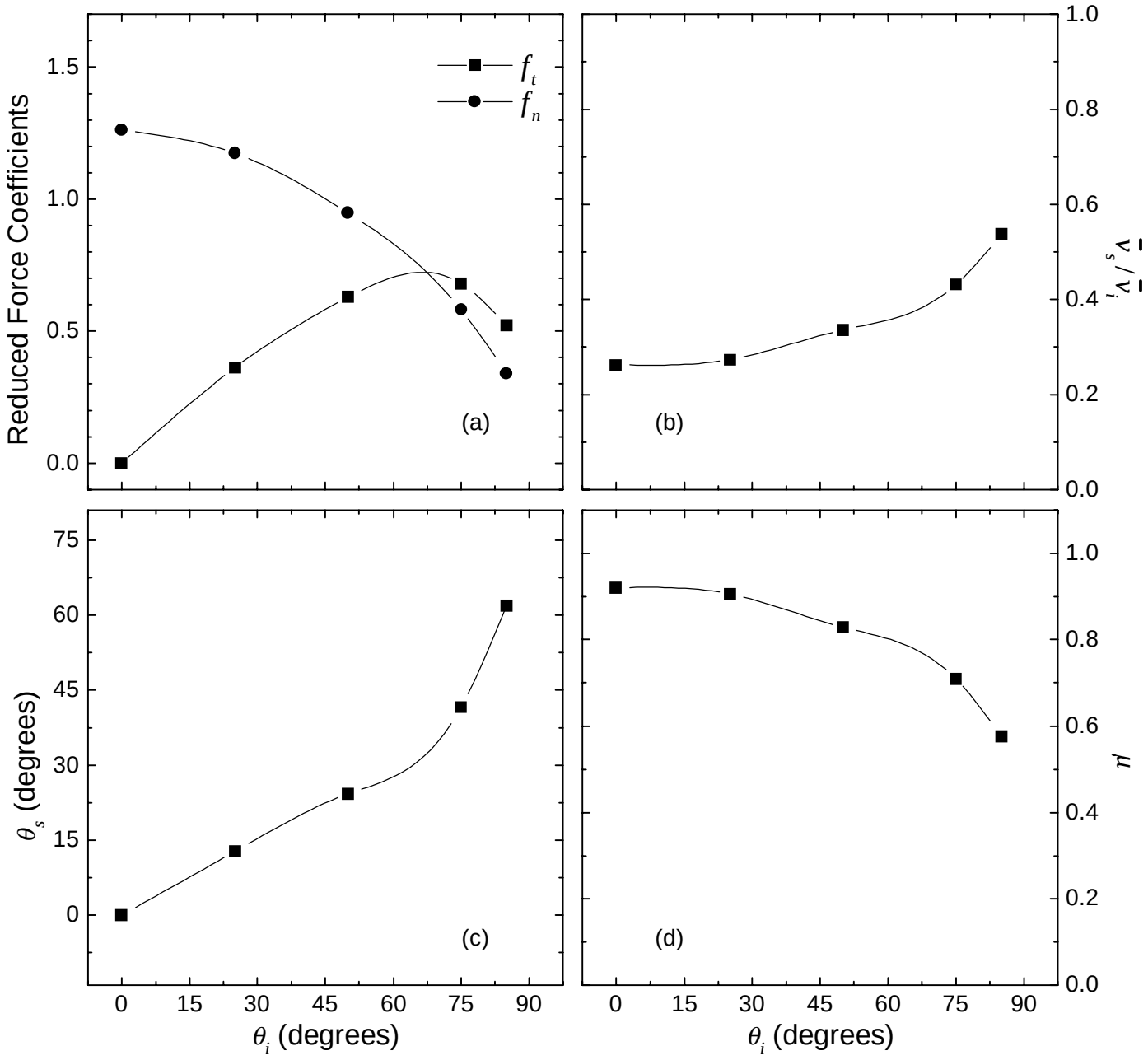

Figure 5: The data for 1870 m/s N_2 incident upon the solar panel.

Table 5: 1870 m/s N_2 incident upon the solar panel

θ_i (degrees)	f_t	f_n	$\overline{v}_s/\overline{v}_i$	$\overline{v}_s$ (m/s)	θ_s (degrees)	μ	ϵ'	$\overline{v_s^2}$ (m/s)^2
0	0	1.26	0.262	491	0	0.920	0.969	4.48×10^5
25	0.362	1.17	0.274	513	12.8	0.905	0.963	4.69×10^5
50	0.628	0.949	0.335	629	24.3	0.828	0.924	5.94×10^5
75	0.679	0.581	0.431	808	41.7	0.709	0.847	8.37×10^5
85	0.522	0.340	0.537	1010	61.9	0.577	0.740	1.18×10^6

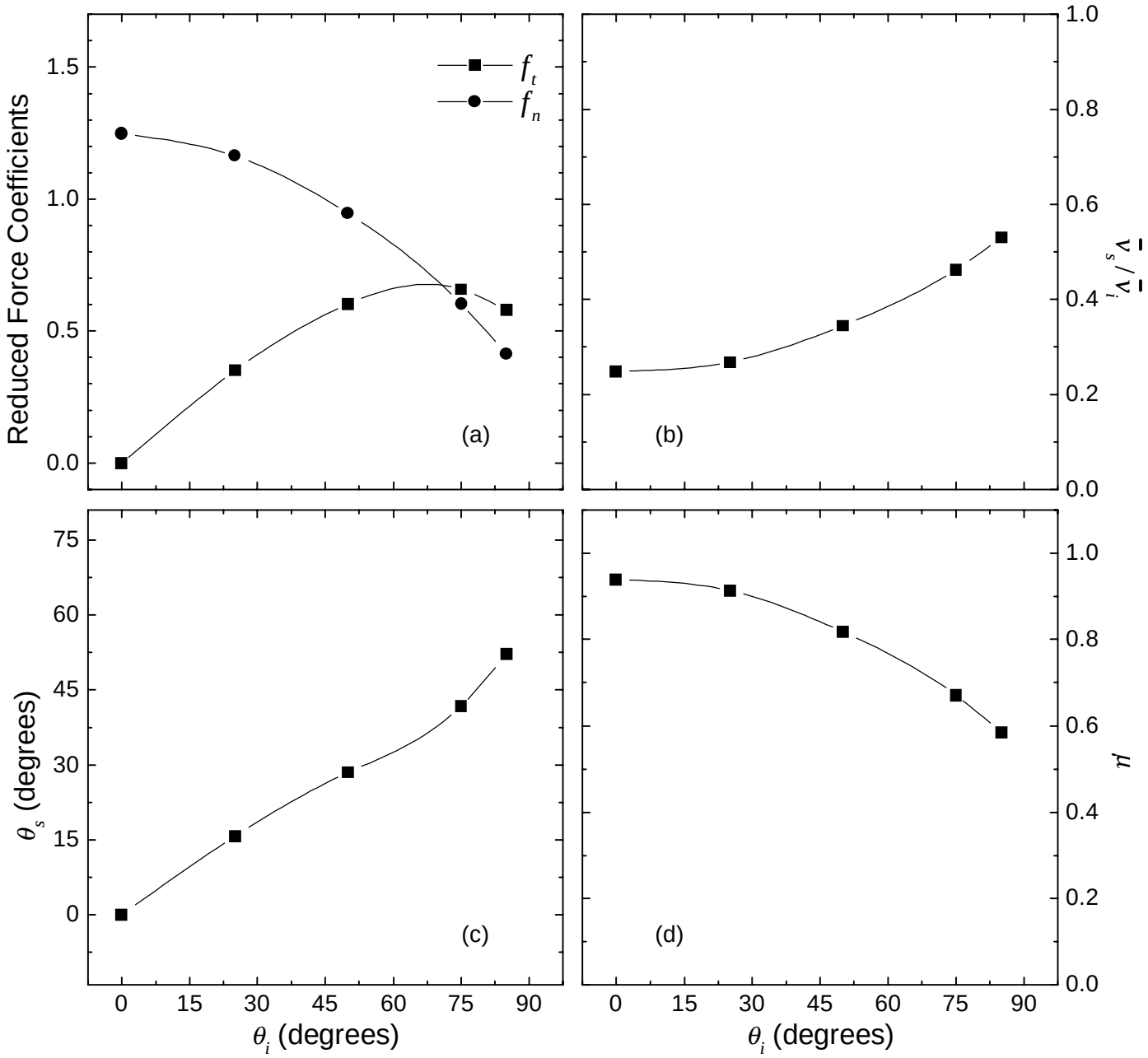

Figure 6: The data for 1870 m/s N_2 incident upon SiO_2-coated Kapton.

Table 6: 1870 m/s N_2 incident upon SiO_2-coated Kapton

θ_i (degrees)	f_t	f_n	$\overline{v}_s/\overline{v}_i$	$\overline{v}_s$ (m/s)	θ_s (degrees)	μ	ϵ'	$\overline{v_s^2}$ $(\mathrm{m/s})^2$
0	0	1.25	0.247	464	0	0.938	0.977	4.23×10^5
25	0.350	1.16	0.267	501	15.8	0.913	0.966	4.57×10^5
50	0.602	0.945	0.344	645	28.5	0.818	0.918	6.13×10^5
75	0.658	0.603	0.462	865	41.9	0.671	0.819	9.29×10^5
85	0.578	0.412	0.530	993	52.1	0.586	0.748	1.15×10^6

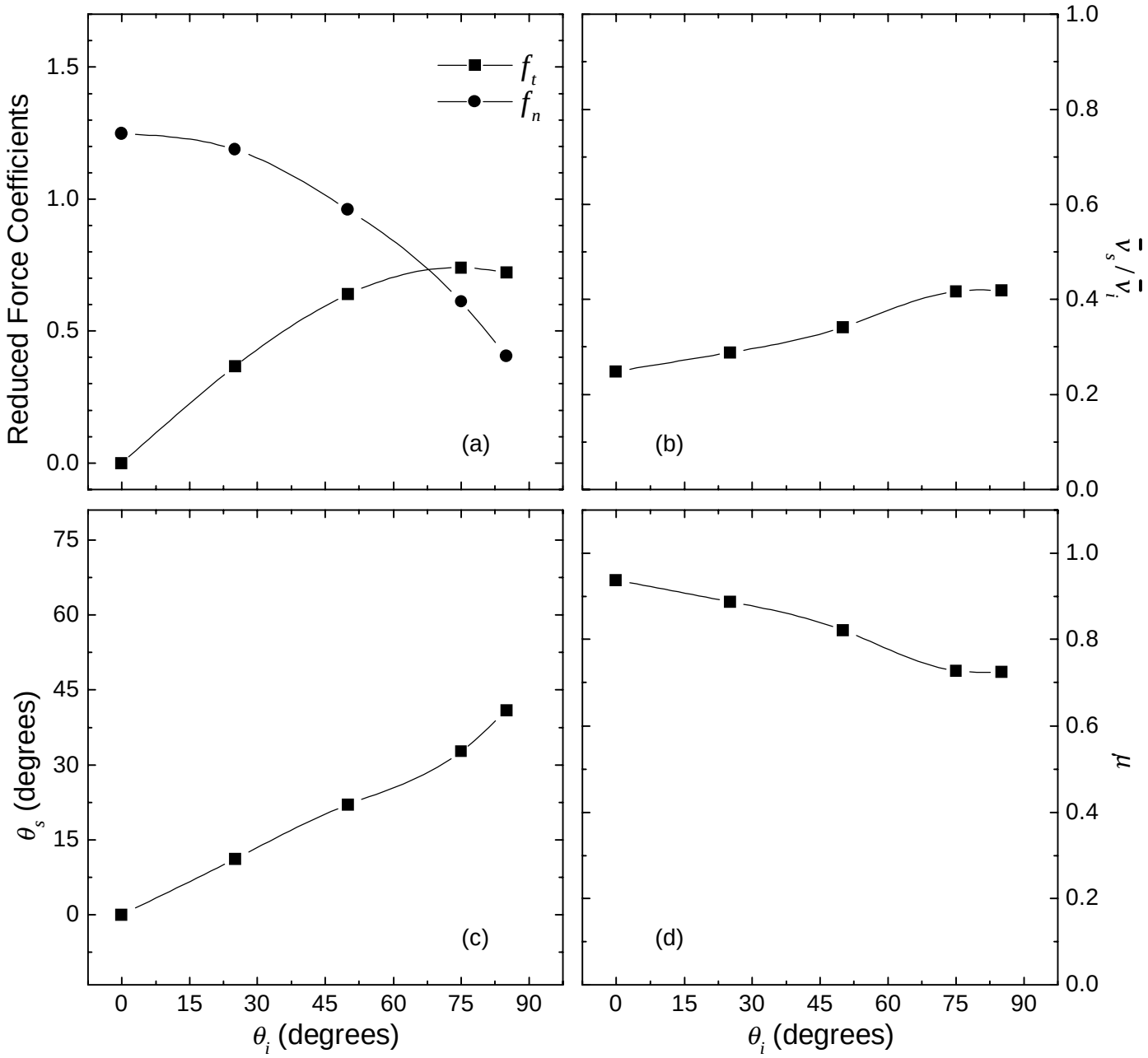

Figure 7: The data for 1870 m/s N_2 incident upon Kapton.

Table 7: 1870 m/s N_2 incident upon Kapton

θ_i (degrees)	f_t	f_n	$\overline{v}_s/\overline{v}_i$	$\overline{v}_s$ (m/s)	θ_s (degrees)	μ	ϵ'	$\overline{v_s^2}$ $(\mathrm{m/s})^2$
0	0	1.25	0.248	465	0	0.937	0.977	4.25×10^5
25	0.366	1.19	0.288	540	11.3	0.888	0.954	4.96×10^5
50	0.638	0.959	0.341	639	22.1	0.821	0.920	6.07×10^5
75	0.740	0.609	0.417	781	32.8	0.727	0.860	7.98×10^5
85	0.722	0.403	0.418	784	40.9	0.725	0.858	8.02×10^5

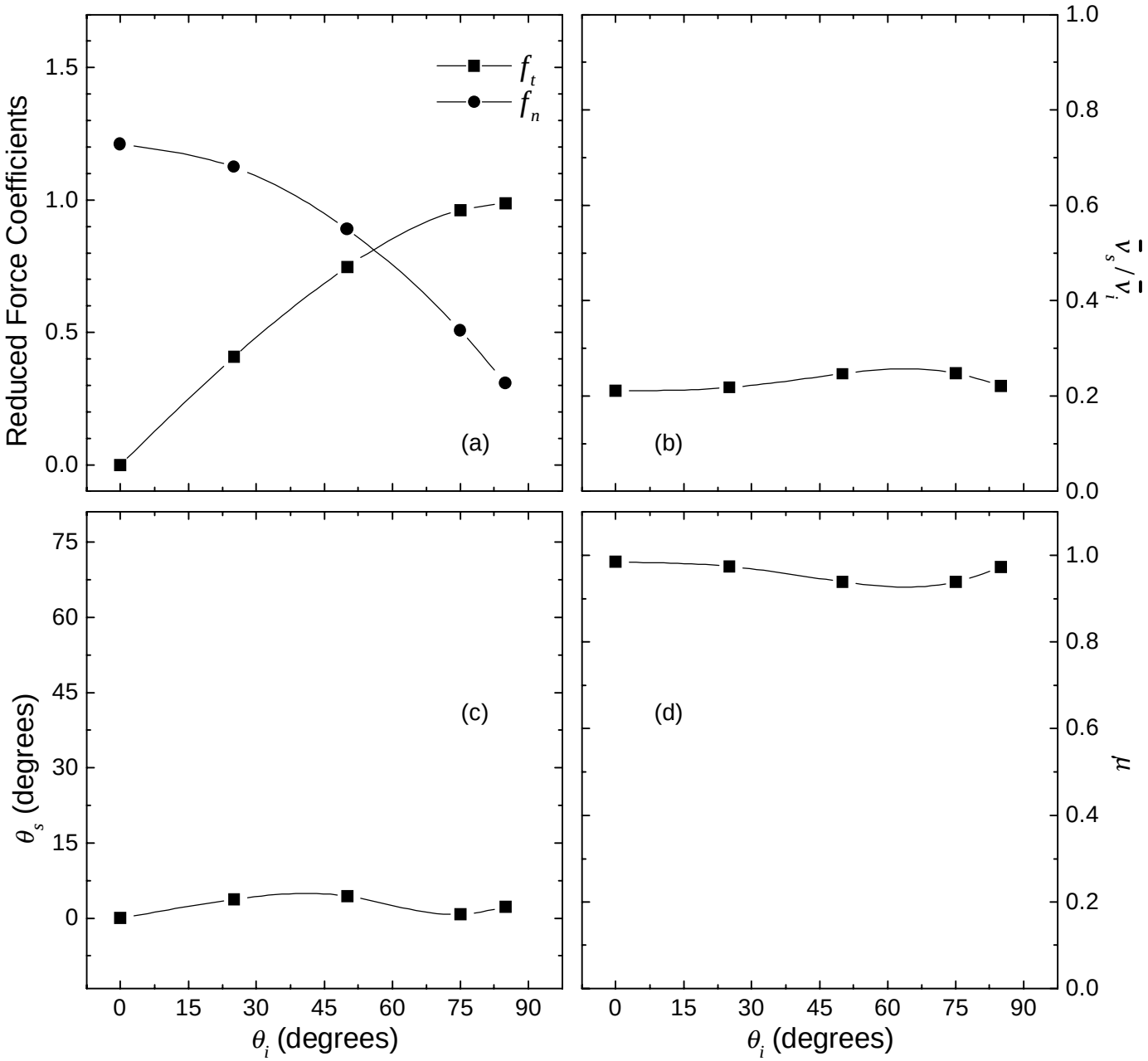

Figure 8: The data for 1870 m/s N_2 incident upon Z-93-coated aluminum.

Table 8: 1870 m/s N_2 incident upon Z-93-coated aluminum

θ_i (degrees)	f_t	f_n	$\overline{v}_s/\overline{v}_i$	$\overline{v}_s$ (m/s)	θ_s (degrees)	μ	ϵ'	$\overline{v_s^2}$ $(\mathrm{m/s})^2$
0	0	1.21	0.211	395	0	0.984	0.994	3.68×10^5
25	0.408	1.12	0.218	409	3.82	0.975	0.991	3.78×10^5
50	0.747	0.889	0.247	463	4.45	0.939	0.977	4.23×10^5
75	0.962	0.506	0.247	464	0.857	0.938	0.977	4.23×10^5
85	0.987	0.308	0.221	414	2.34	0.971	0.990	3.82×10^5

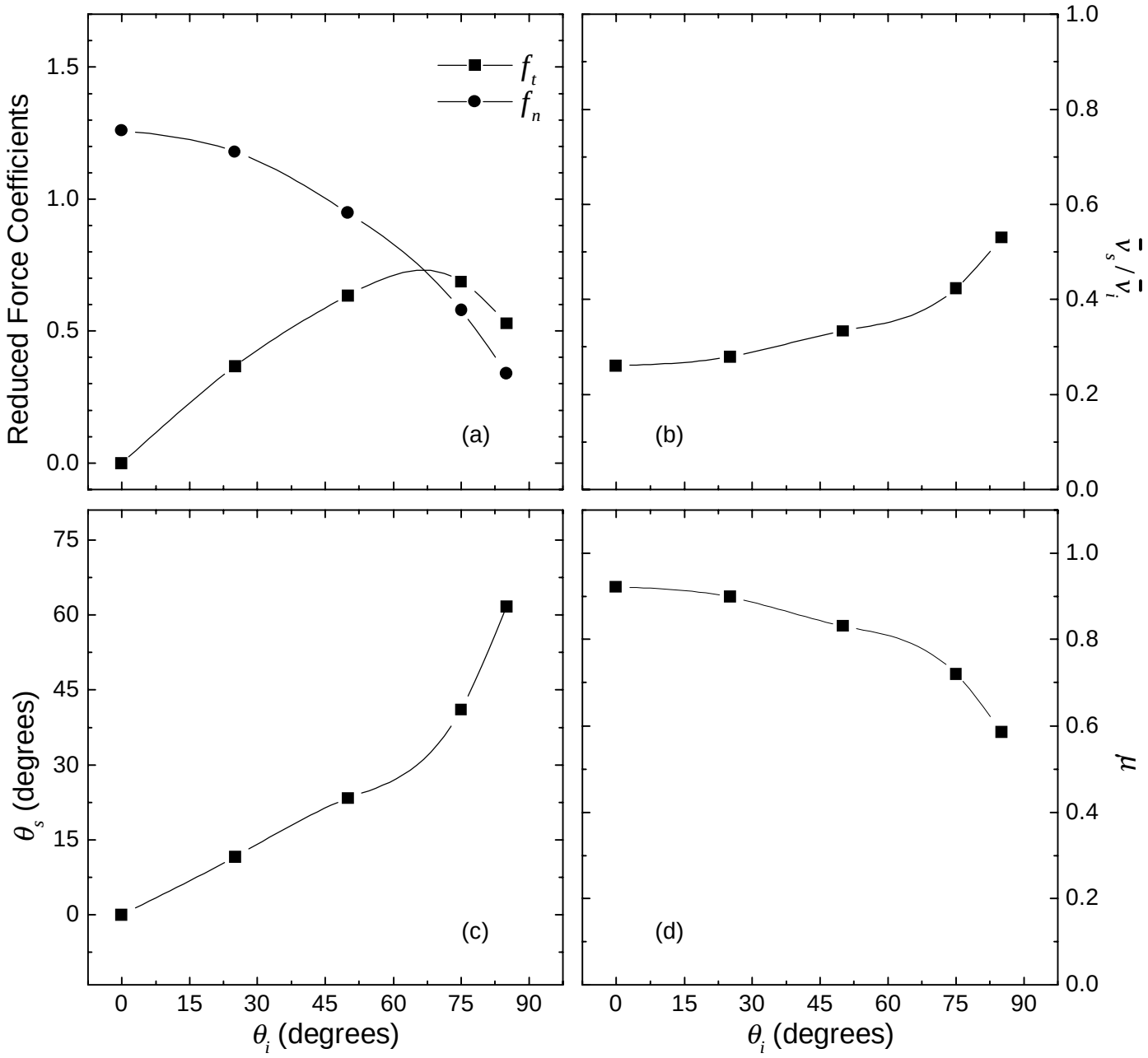

Figure 9: The data for 1870 m/s CO incident upon the solar panel.

Table 9: 1870 m/s CO incident upon the solar panel

θ_i (degrees)	f_t	f_n	$\overline{v}_s/\overline{v}_i$	$\overline{v}_s$ (m/s)	θ_s (degrees)	μ	ϵ'	$\overline{v_s^2}$ (m/s)^2
0	0	1.26	0.260	488	0	0.922	0.970	4.46×10^5
25	0.366	1.18	0.279	524	11.7	0.898	0.959	4.80×10^5
50	0.634	0.948	0.333	624	23.4	0.832	0.925	5.89×10^5
75	0.688	0.577	0.423	793	41.2	0.719	0.855	8.15×10^5
85	0.530	0.338	0.530	993	61.7	0.586	0.749	1.15×10^6

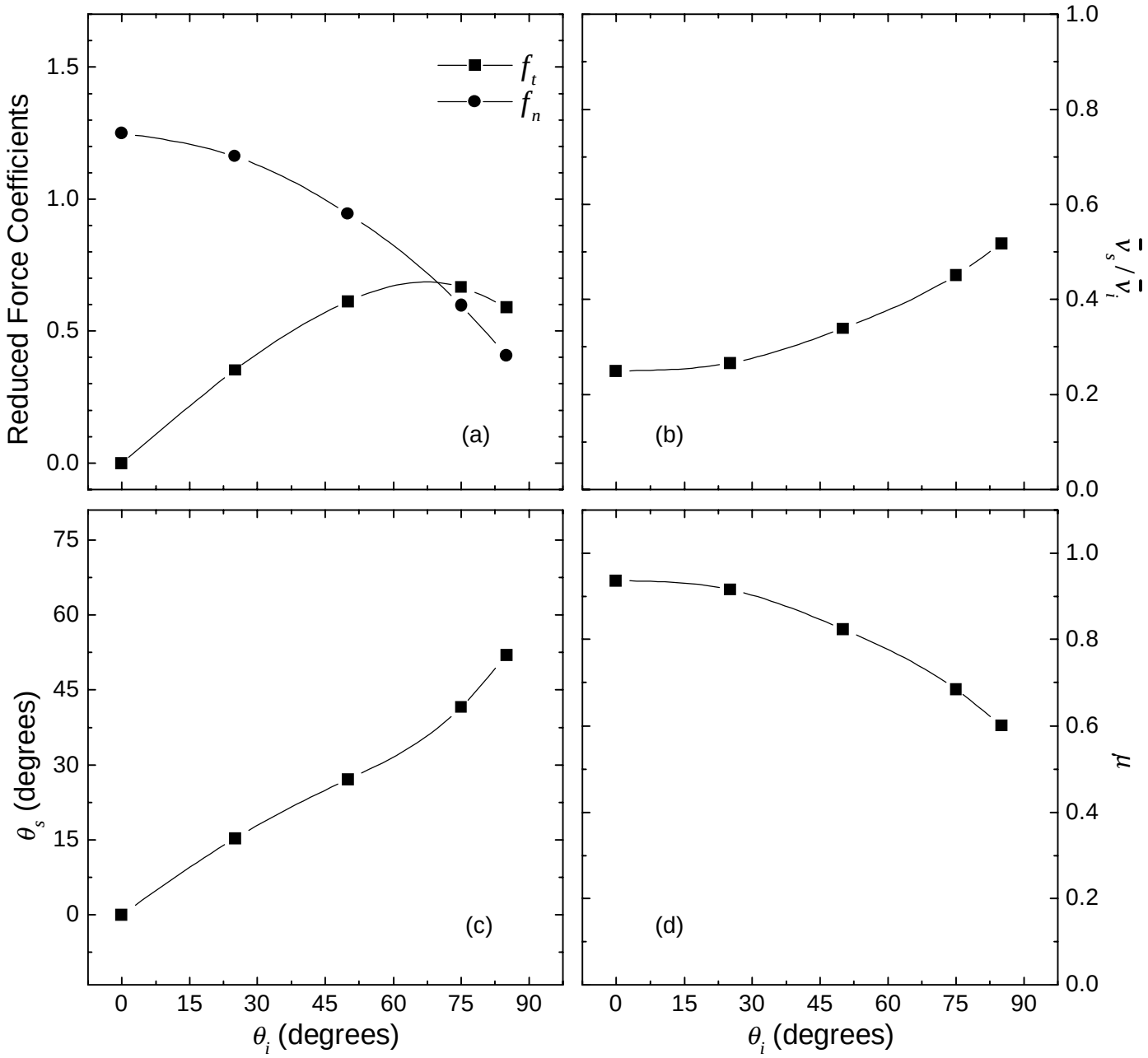

Figure 10: The data for 1870 m/s CO incident upon SiO_2-coated Kapton.

Table 10: 1870 m/s CO incident upon SiO_2-coated Kapton

θ_i (degrees)	f_t	f_n	$\overline{v}_s/\overline{v}_i$	$\overline{v}_s$ (m/s)	θ_s (degrees)	μ	ϵ'	$\overline{v_s^2}$ $(\mathrm{m/s})^2$
0	0	1.25	0.249	467	0	0.936	0.976	4.26×10^5
25	0.352	1.16	0.265	497	15.4	0.916	0.968	4.54×10^5
50	0.611	0.944	0.339	635	27.2	0.824	0.921	6.02×10^5
75	0.666	0.596	0.451	845	41.7	0.685	0.829	8.96×10^5
85	0.589	0.406	0.517	970	51.9	0.602	0.762	1.11×10^6

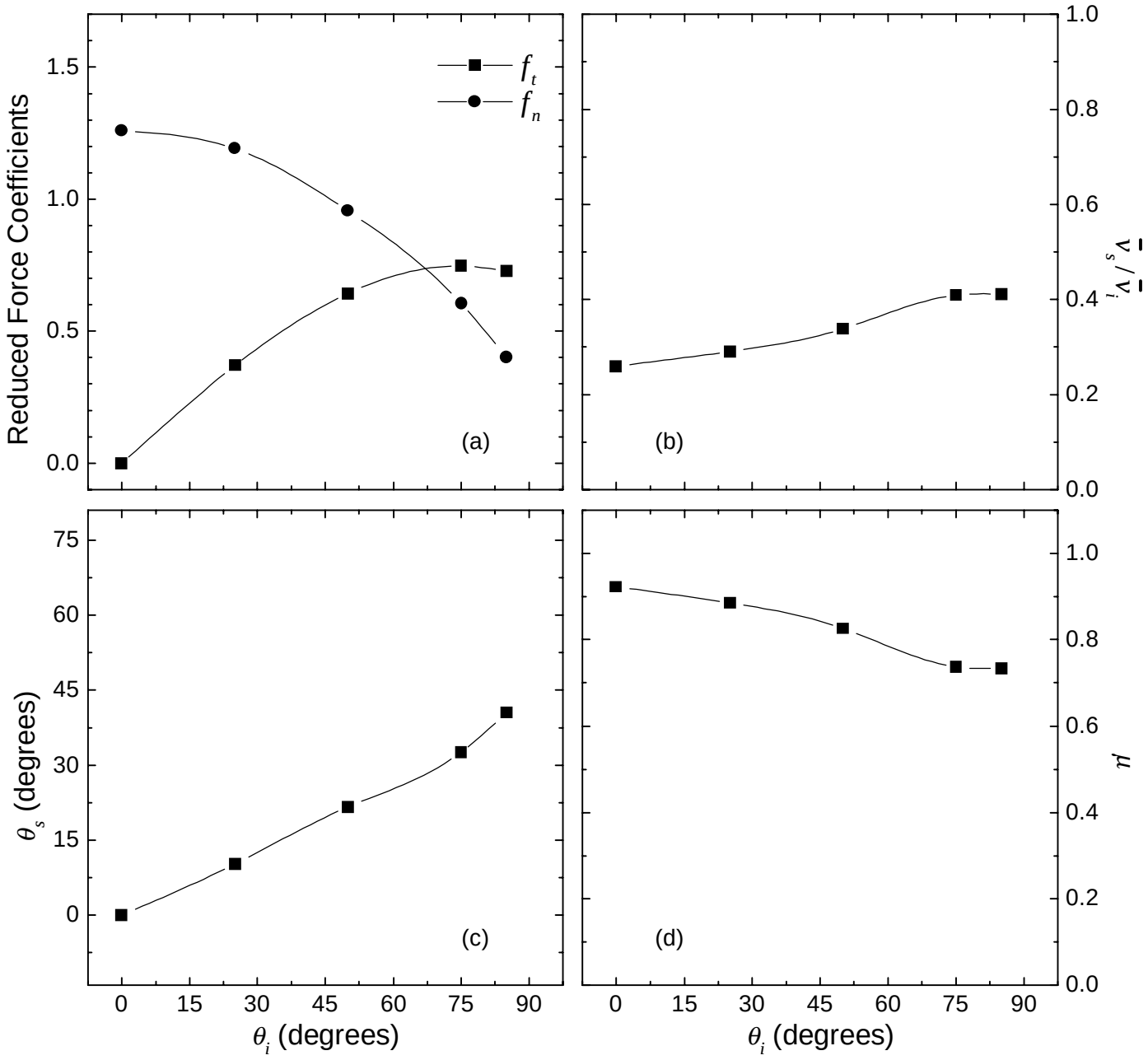

Figure 11: The data for 1870 m/s CO incident upon Kapton.

Table 11: 1870 m/s CO incident upon Kapton

θ_i (degrees)	f_t	f_n	$\overline{v}_s/\overline{v}_i$	$\overline{v}_s$ (m/s)	θ_s (degrees)	μ	ϵ'	$\overline{v_s^2}$ (m/s)^2
0	0	1.26	0.259	486	0	0.923	0.971	4.44×10^5
25	0.371	1.19	0.290	544	10.3	0.885	0.953	5.00×10^5
50	0.641	0.956	0.337	633	21.7	0.826	0.922	5.99×10^5
75	0.745	0.603	0.409	766	32.6	0.737	0.867	7.76×10^5
85	0.728	0.400	0.412	772	40.6	0.733	0.864	7.84×10^5

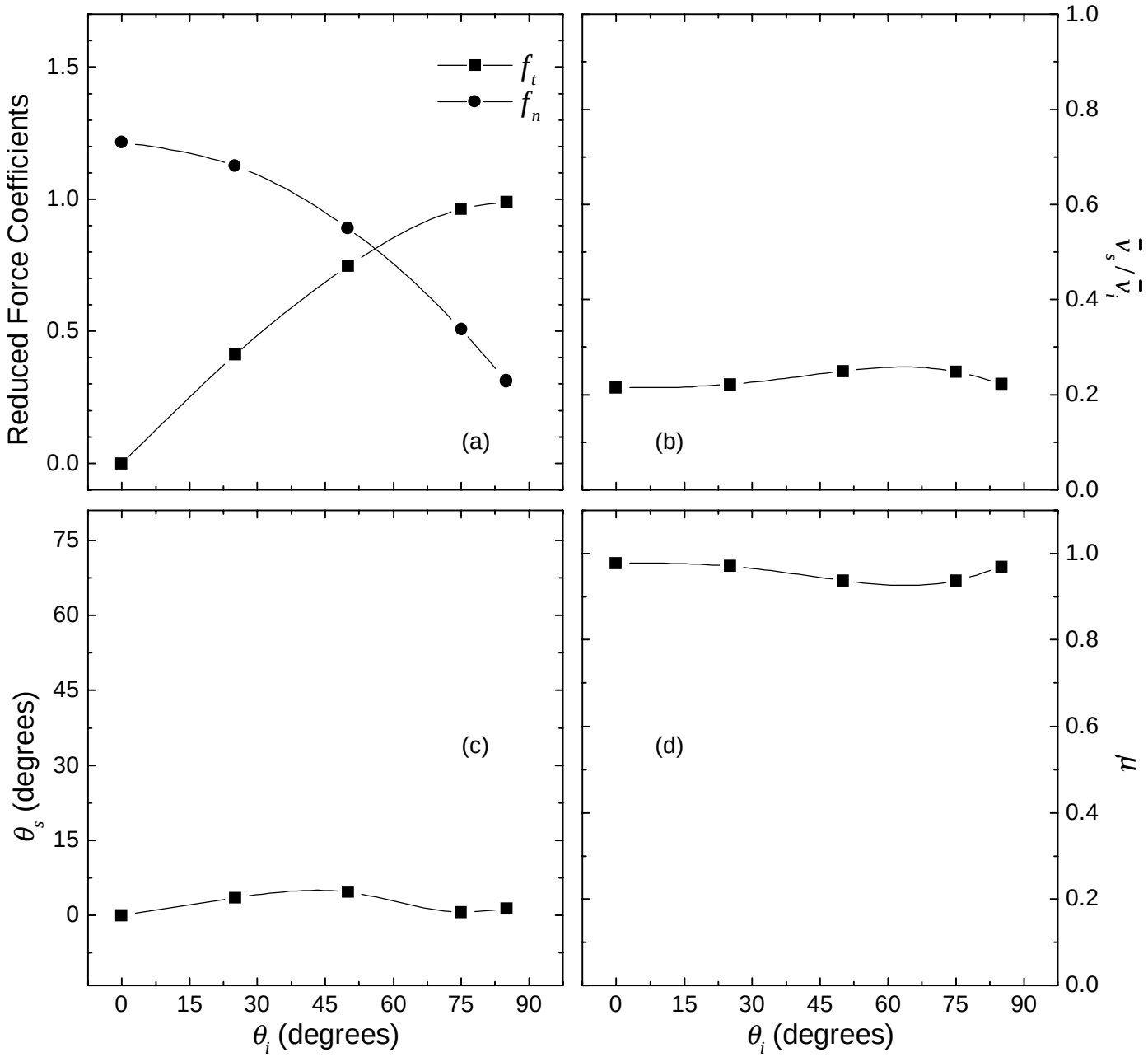

Figure 12: The data for 1870 m/s CO incident upon Z-93-coated aluminum.

Table 12: 1870 m/s CO incident upon Z-93-coated aluminum

θ_i (degrees)	f_t	f_n	$\overline{v}_s/\overline{v}_i$	$\overline{v}_s$ (m/s)	θ_s (degrees)	μ	ϵ'	$\overline{v_s^2}$ (m/s)^2
0	0	1.22	0.215	404	0	0.978	0.992	3.74×10^5
25	0.409	1.13	0.221	414	3.52	0.971	0.990	3.83×10^5
50	0.746	0.890	0.248	466	4.65	0.937	0.976	4.25×10^5
75	0.963	0.507	0.248	465	0.687	0.938	0.977	4.24×10^5
85	0.991	0.309	0.222	416	1.45	0.970	0.989	3.84×10^5

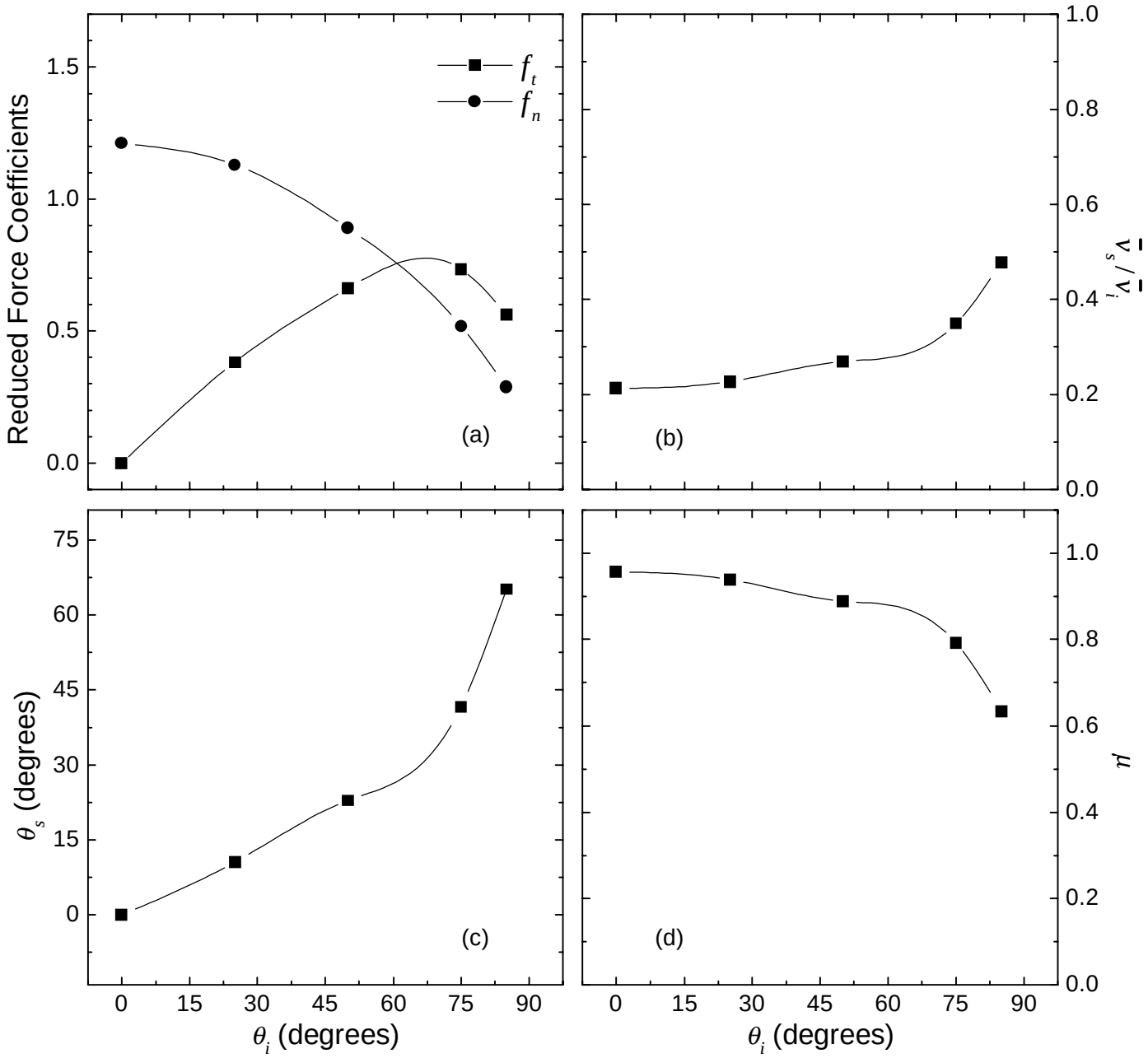

Figure 13: The data for 1670 m/s CO_2 incident upon the solar panel.

Table 13: 1670 m/s CO_2 incident upon the solar panel

θ_i (degrees)	f_t	f_n	$\overline{v}_s/\overline{v}_i$	$\overline{v}_s$ (m/s)	θ_s (degrees)	μ	ϵ'	$\overline{v_s^2}$ $(\mathrm{m/s})^2$
0	0	1.21	0.213	355	0	0.957	0.986	2.60×10^5
25	0.381	1.13	0.227	379	10.5	0.939	0.979	2.77×10^5
50	0.661	0.891	0.269	449	22.9	0.888	0.958	3.33×10^5
75	0.734	0.519	0.348	582	41.7	0.792	0.907	4.64×10^5
85	0.562	0.288	0.478	799	65.2	0.634	0.796	7.52×10^5

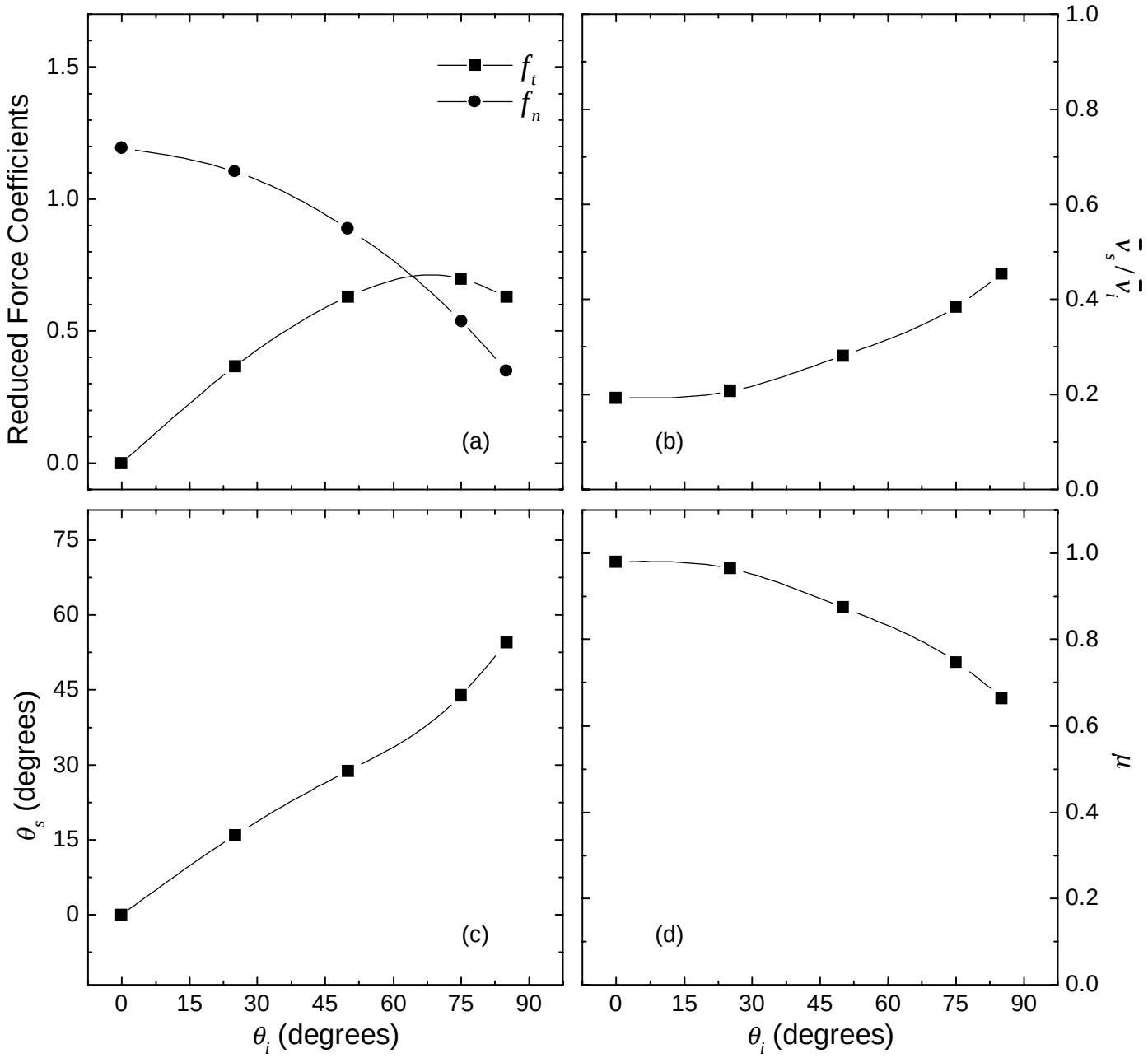

Figure 14: The data for 1670 m/s CO_2 incident upon SiO_2-coated Kapton.

Table 14: 1670 m/s CO_2 incident upon SiO_2-coated Kapton

θ_i (degrees)	f_t	f_n	$\overline{v}_s/\overline{v}_i$	$\overline{v}_s$ (m/s)	θ_s (degrees)	μ	ϵ'	$\overline{v_s^2}$ $(\mathrm{m/s})^2$
0	0	1.19	0.194	324	0	0.980	0.994	2.39×10^5
25	0.366	1.10	0.206	344	16.0	0.965	0.988	2.53×10^5
50	0.630	0.889	0.281	469	28.9	0.874	0.951	3.50×10^5
75	0.699	0.536	0.385	642	44.0	0.748	0.880	5.35×10^5
85	0.627	0.350	0.453	757	54.5	0.664	0.820	6.89×10^5

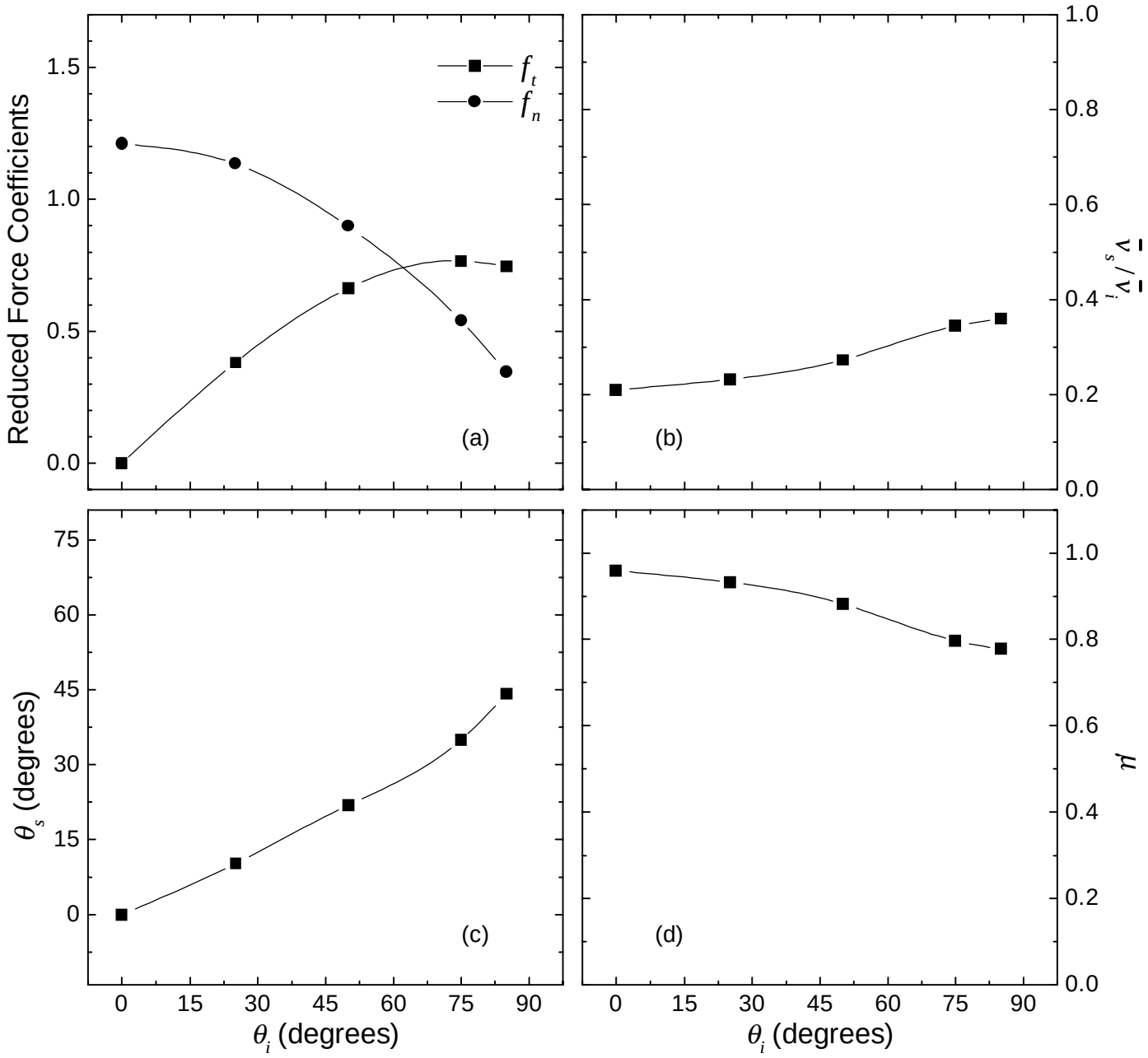

Figure 15: The data for 1670 m/s CO_2 incident upon Kapton.

Table 15: 1670 m/s CO_2 incident upon Kapton

θ_i (degrees)	f_t	f_n	$\overline{v}_s/\overline{v}_i$	$\overline{v}_s$ (m/s)	θ_s (degrees)	μ	ϵ'	$\overline{v_s^2}$ $(\mathrm{m/s})^2$
0	0	1.21	0.210	351	0	0.960	0.987	2.57×10^5
25	0.381	1.13	0.232	388	10.3	0.933	0.977	2.83×10^5
50	0.664	0.897	0.274	457	21.9	0.883	0.955	3.39×10^5
75	0.769	0.541	0.344	574	35.0	0.797	0.910	4.56×10^5
85	0.745	0.345	0.360	601	44.2	0.778	0.899	4.86×10^5

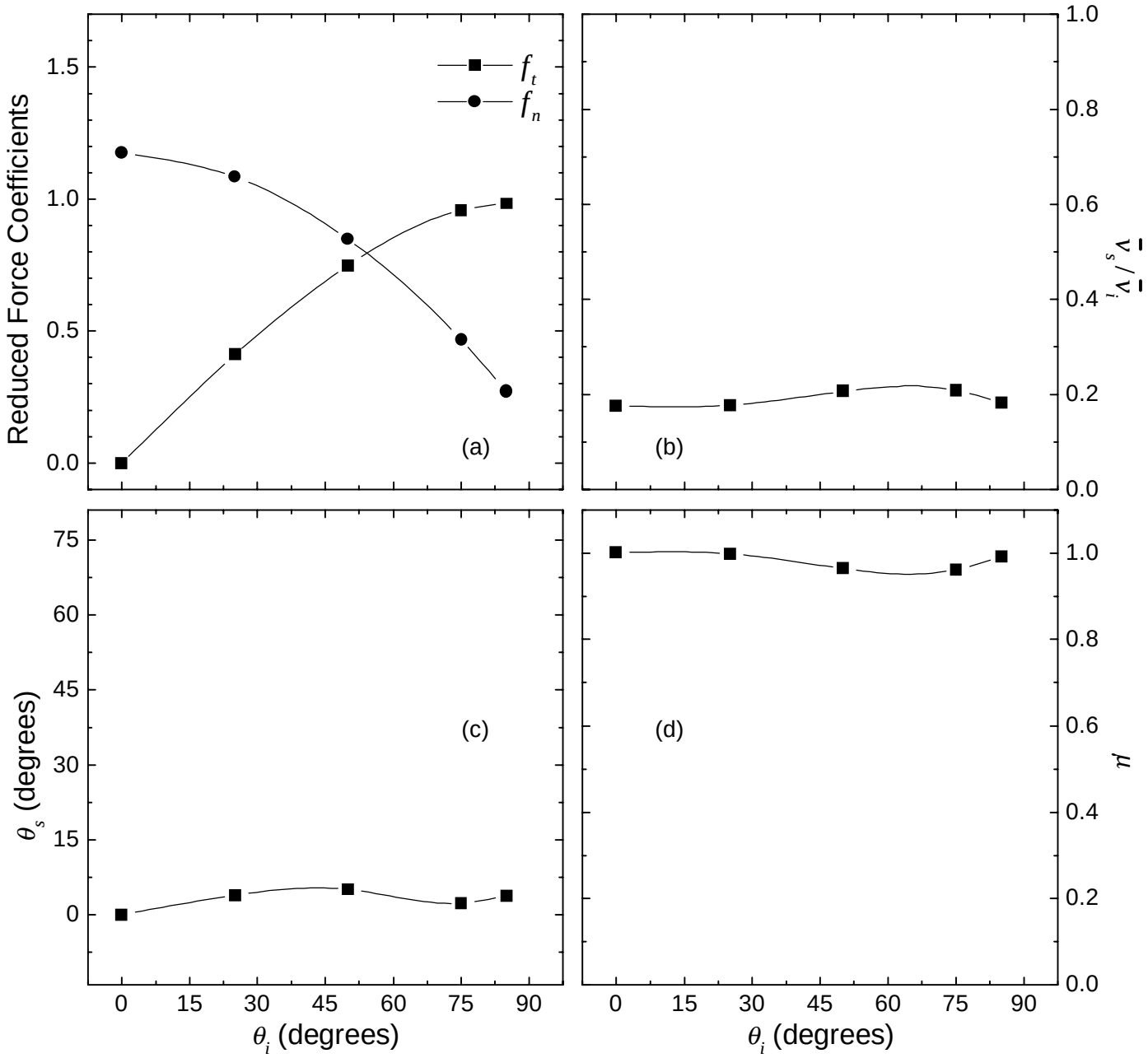

Figure 16: The data for 1670 m/s CO_2 incident upon Z-93-coated aluminum.

Table 16: 1670 m/s CO_2 incident upon Z-93-coated aluminum

θ_i (degrees)	f_t	f_n	$\overline{v}_s/\overline{v}_i$	$\overline{v}_s$ (m/s)	θ_s (degrees)	μ	ϵ'	$\overline{v_s^2}$ (m/s)^2
0	0	1.18	0.177	295	0	1.00	1.00	2.22×10^5
25	0.410	1.08	0.178	297	3.93	0.999	1.00	2.23×10^5
50	0.748	0.848	0.206	345	5.07	0.964	0.988	2.53×10^5
75	0.957	0.467	0.208	348	2.34	0.962	0.988	2.55×10^5
85	0.984	0.270	0.184	307	3.85	0.992	0.998	2.29×10^5

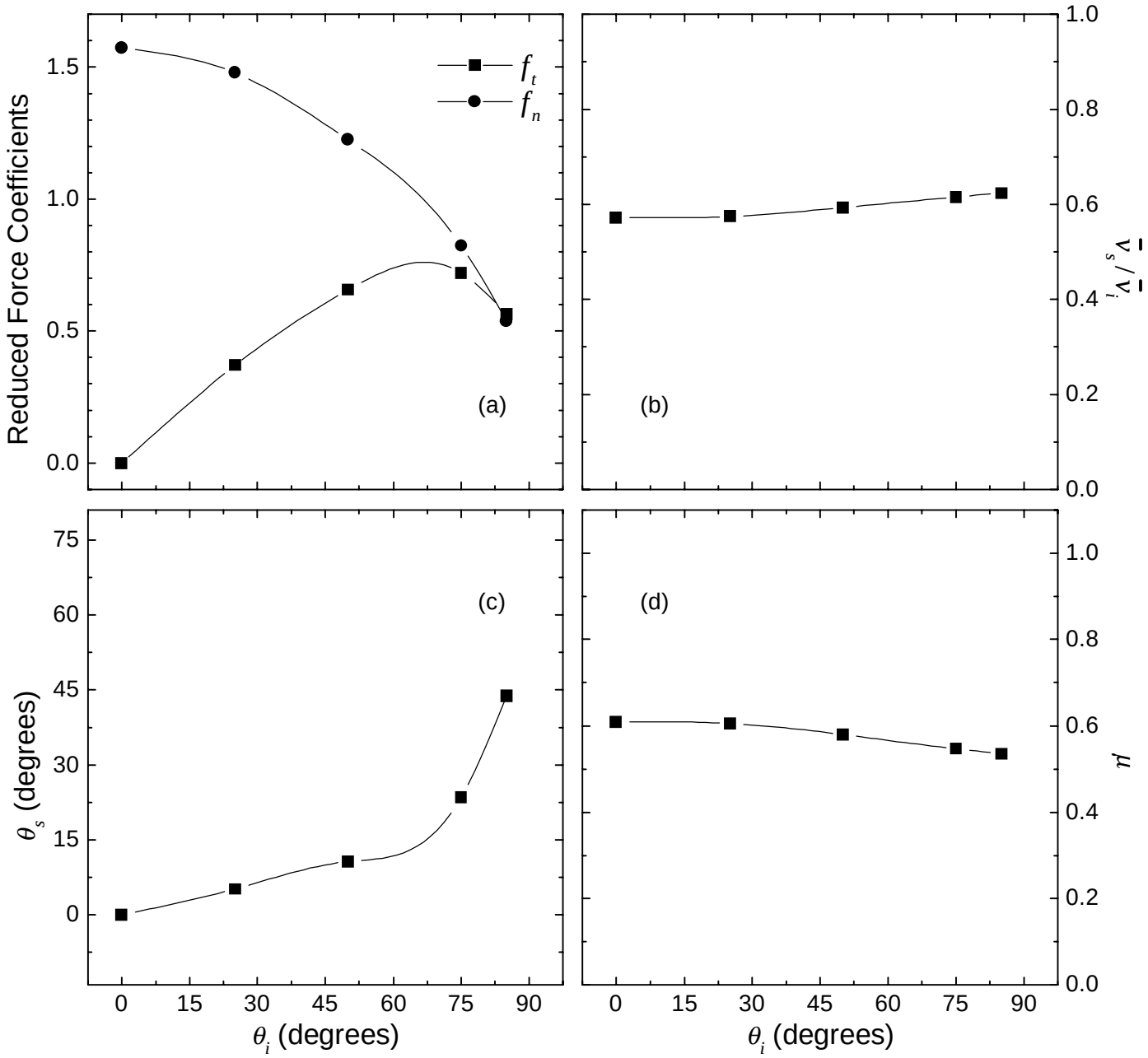

Figure 17: The data for 4620 m/s H_2 incident upon the solar panel.

Table 17: 4620 m/s H_2 incident upon the solar panel

θ_i (degrees)	f_t	f_n	$\overline{v}_s/\overline{v}_i$	$\overline{v}_s$ (m/s)	θ_s (degrees)	μ	ϵ'	$\overline{v_s^2}$ $(\mathrm{m/s})^2$
0	0	1.57	0.572	2650	0	0.610	0.738	9.32×10^6
25	0.370	1.48	0.575	2660	5.25	0.607	0.735	9.36×10^6
50	0.656	1.23	0.593	2740	10.7	0.580	0.712	9.77×10^6
75	0.720	0.823	0.616	2850	23.5	0.548	0.682	1.03×10^7
85	0.564	0.538	0.624	2800	43.8	0.536	0.670	1.05×10^7

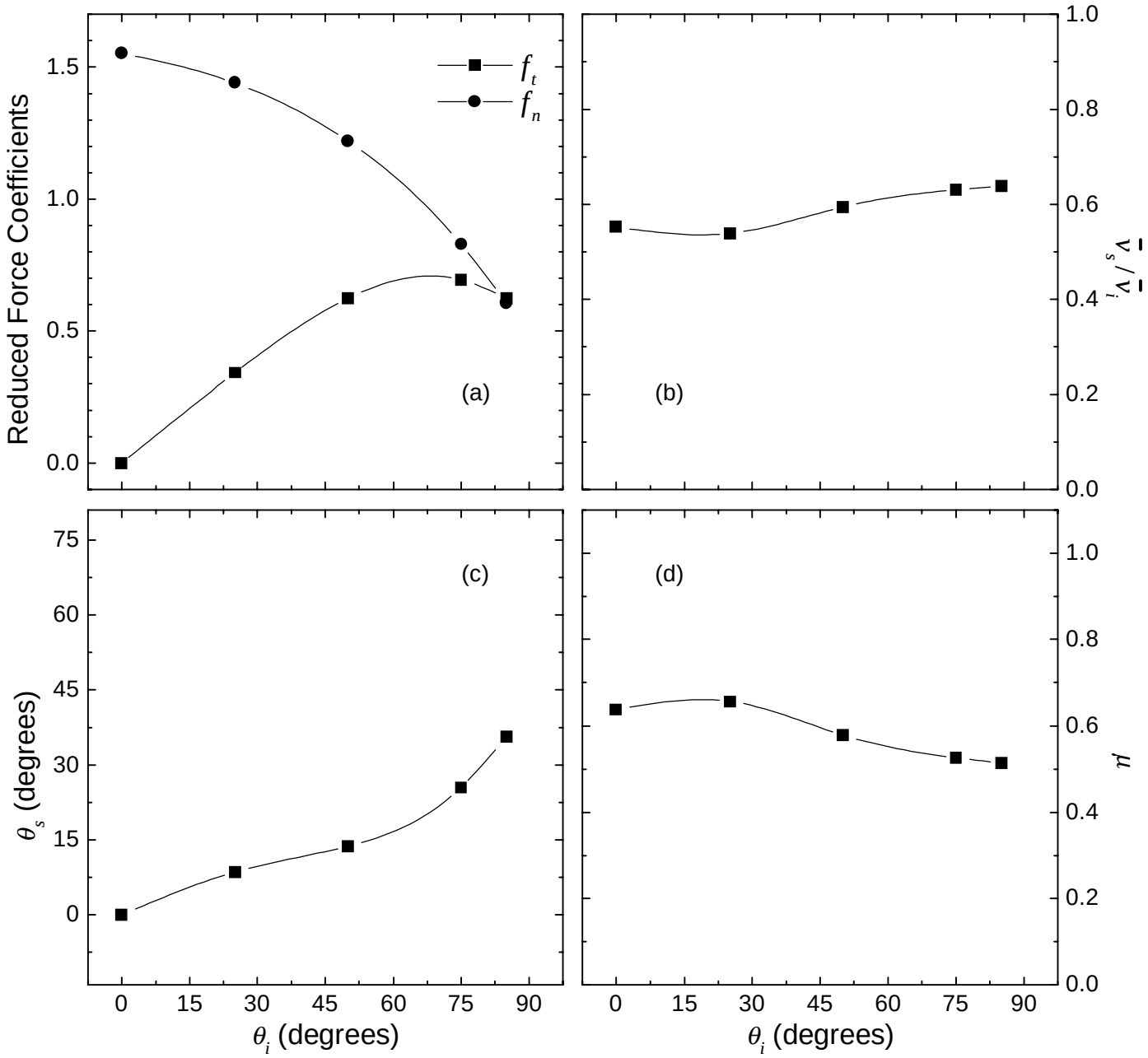

Figure 18: The data for 4620 m/s H_2 incident upon SiO_2-coated Kapton.

Table 18: 4620 m/s H_2 incident upon SiO_2-coated Kapton

θ_i (degrees)	f_t	f_n	$\overline{v}_s/\overline{v}_i$	$\overline{v}_s$ (m/s)	θ_s (degrees)	μ	ϵ'	$\overline{v_s^2}$ $(\mathrm{m/s})^2$
0	0	1.55	0.552	2550	0	0.638	0.763	8.90×10^6
25	0.343	1.44	0.539	2490	8.54	0.658	0.779	8.62×10^6
50	0.624	1.22	0.594	2750	13.8	0.579	0.711	9.79×10^6
75	0.693	0.828	0.631	2920	25.6	0.526	0.661	1.06×10^7
85	0.624	0.606	0.639	2950	35.7	0.515	0.650	1.08×10^7

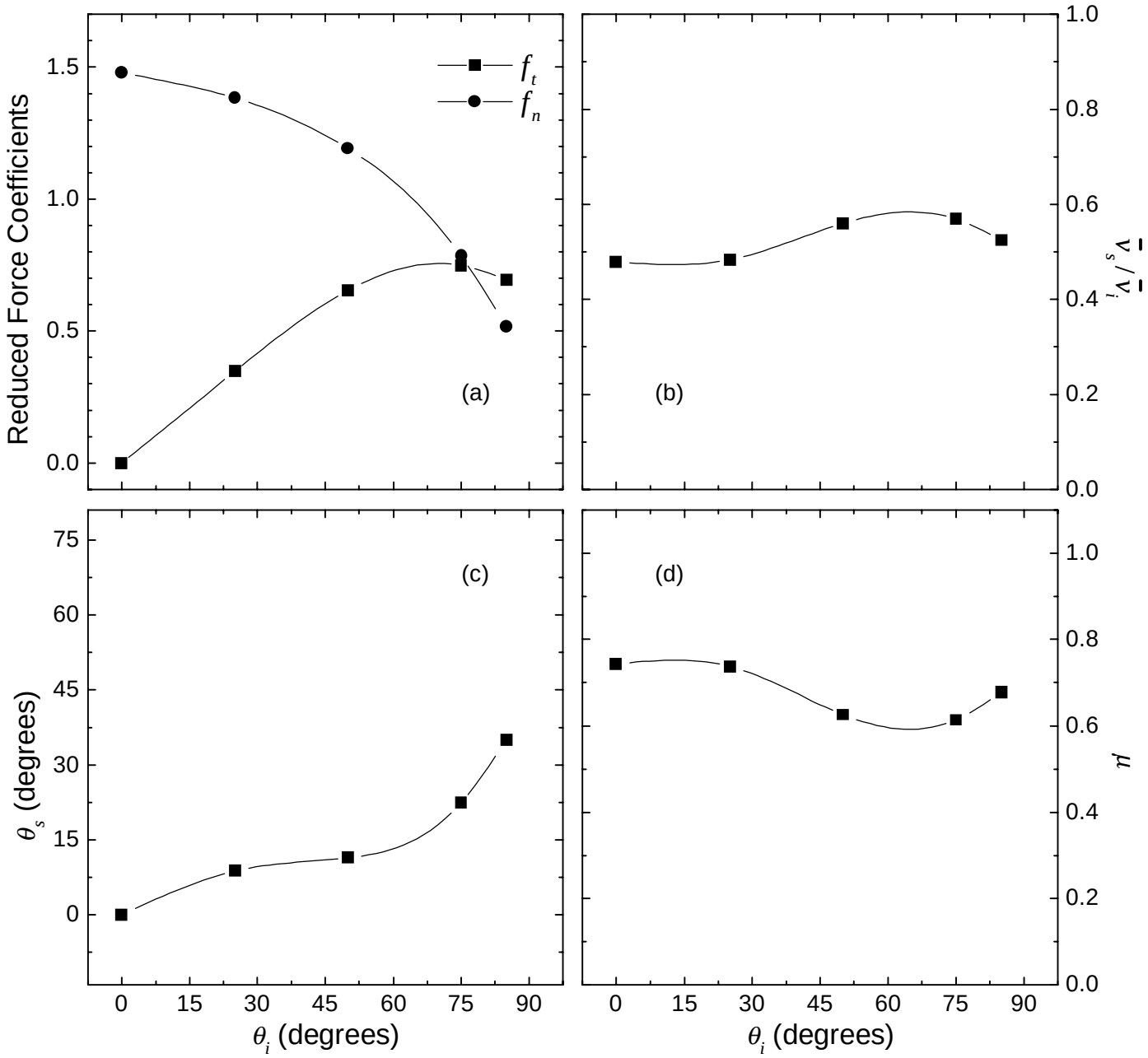

Figure 19: The data for 4620 m/s H_2 incident upon Kapton.

Table 19: 4620 m/s H_2 incident upon Kapton

θ_i (degrees)	f_t	f_n	$\overline{v}_s/\overline{v}_i$	$\overline{v}_s$ (m/s)	θ_s (degrees)	μ	ϵ'	$\overline{v_s^2}$ $(\mathrm{m/s})^2$
0	0	1.48	0.479	2210	0	0.743	0.846	7.48×10^6
25	0.349	1.38	0.484	2240	8.81	0.737	0.841	7.56×10^6
50	0.655	1.19	0.561	2590	11.4	0.627	0.753	9.06×10^6
75	0.748	0.784	0.569	2630	22.5	0.615	0.743	9.24×10^6
85	0.694	0.517	0.525	2430	35.1	0.678	0.796	8.34×10^6

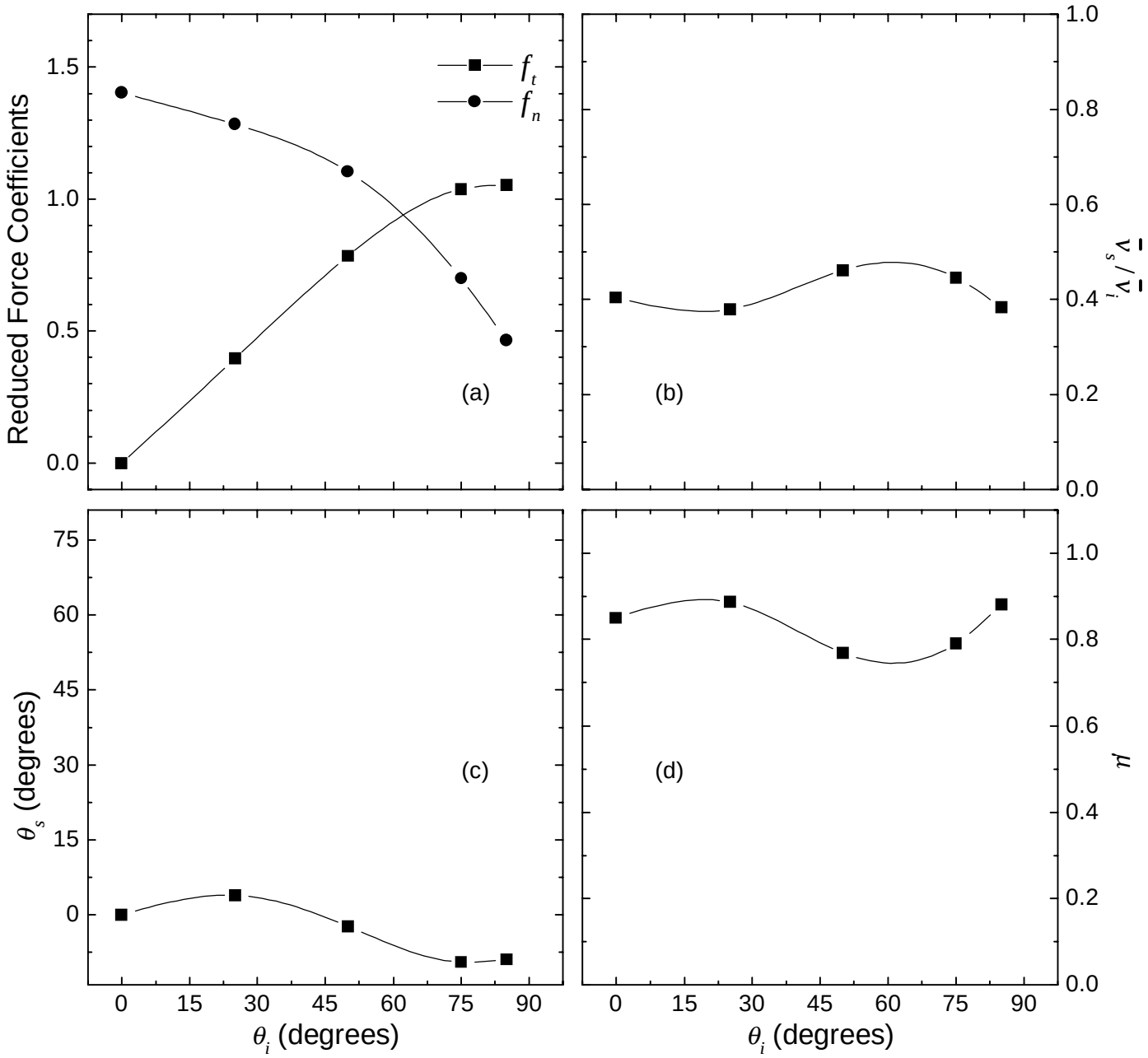

Figure 20: The data for 4620 m/s H_2 incident upon Z-93-coated aluminum.

Table 20: 4620 m/s H_2 incident upon Z-93-coated aluminum

θ_i (degrees)	f_t	f_n	$\overline{v}_s/\overline{v}_i$	$\overline{v}_s$ (m/s)	θ_s (degrees)	μ	ϵ'	$\overline{v_s^2}$ $(\mathrm{m/s})^2$
0	0	1.40	0.404	1870	0	0.851	0.919	6.24×10^6
25	0.396	1.28	0.379	1750	3.99	0.886	0.940	5.88×10^6
50	0.785	1.10	0.461	2130	-2.31	0.769	0.865	7.17×10^6
75	1.04	0.698	0.445	2060	-9.41	0.791	0.880	6.90×10^6
85	1.05	0.465	0.382	1770	-8.85	0.882	0.938	5.92×10^6

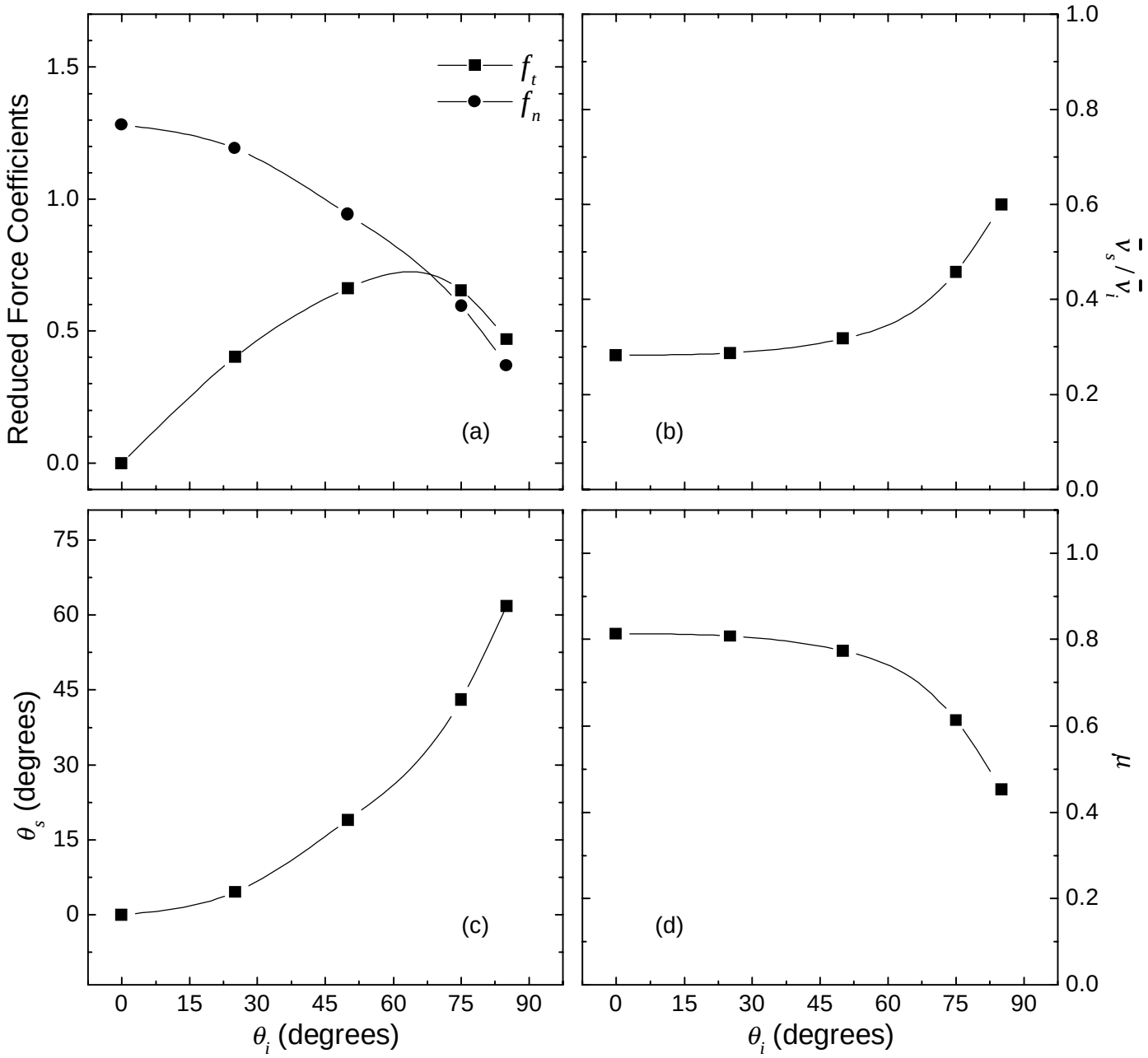

Figure 21: The data for 3180 m/s N_2 incident upon the solar panel.

Table 21: 3180 m/s N_2 incident upon the solar panel

θ_i (degrees)	f_t	f_n	$\overline{v}_s/\overline{v}_i$	$\overline{v}_s$ (m/s)	θ_s (degrees)	μ	ϵ'	$\overline{v_s^2}$ (m/s)^2
0	0	1.28	0.282	896	0	0.813	0.933	1.02×10^6
25	0.400	1.19	0.287	912	4.60	0.807	0.930	1.05×10^6
50	0.662	0.942	0.317	1010	19.1	0.773	0.912	1.24×10^6
75	0.653	0.593	0.458	1460	43.1	0.614	0.801	2.35×10^6
85	0.468	0.371	0.600	1910	61.8	0.453	0.649	3.88×10^6

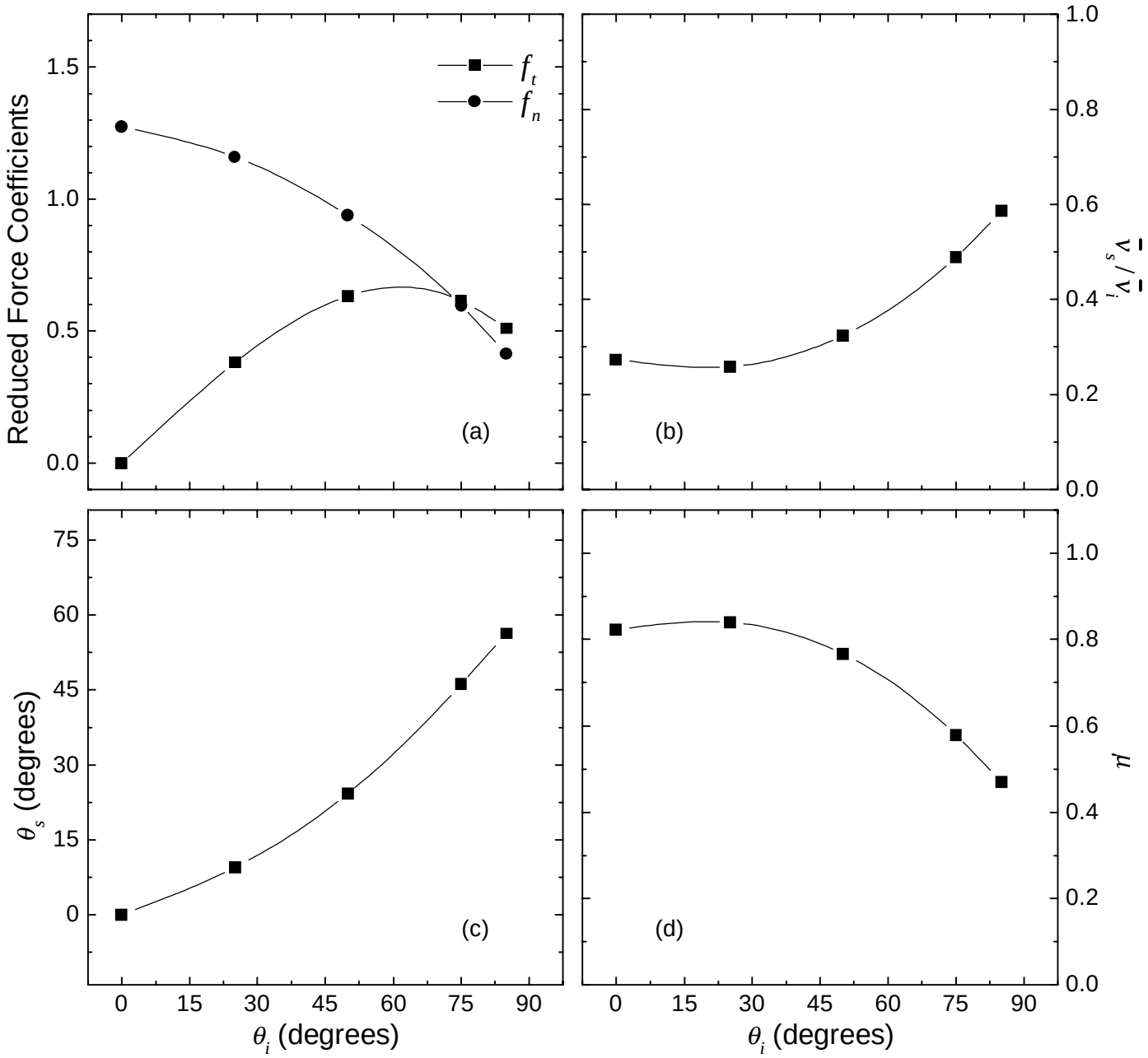

Figure 22: The data for 3180 m/s N_2 incident upon SiO_2-coated Kapton.

Table 22: 3180 m/s N_2 incident upon SiO_2-coated Kapton

θ_i (degrees)	f_t	f_n	$\overline{v}_s/\overline{v}_i$	$\overline{v}_s$ (m/s)	θ_s (degrees)	μ	ϵ'	$\overline{v_s^2}$ (m/s)^2
0	0	1.27	0.273	869	0	0.823	0.938	9.72×10^5
25	0.380	1.16	0.258	820	9.52	0.840	0.946	8.89×10^5
50	0.633	0.937	0.323	1028	24.3	0.766	0.908	1.28×10^6
75	0.613	0.597	0.488	1554	46.2	0.579	0.772	2.65×10^6
85	0.509	0.412	0.585	1862	56.2	0.469	0.666	3.71×10^6

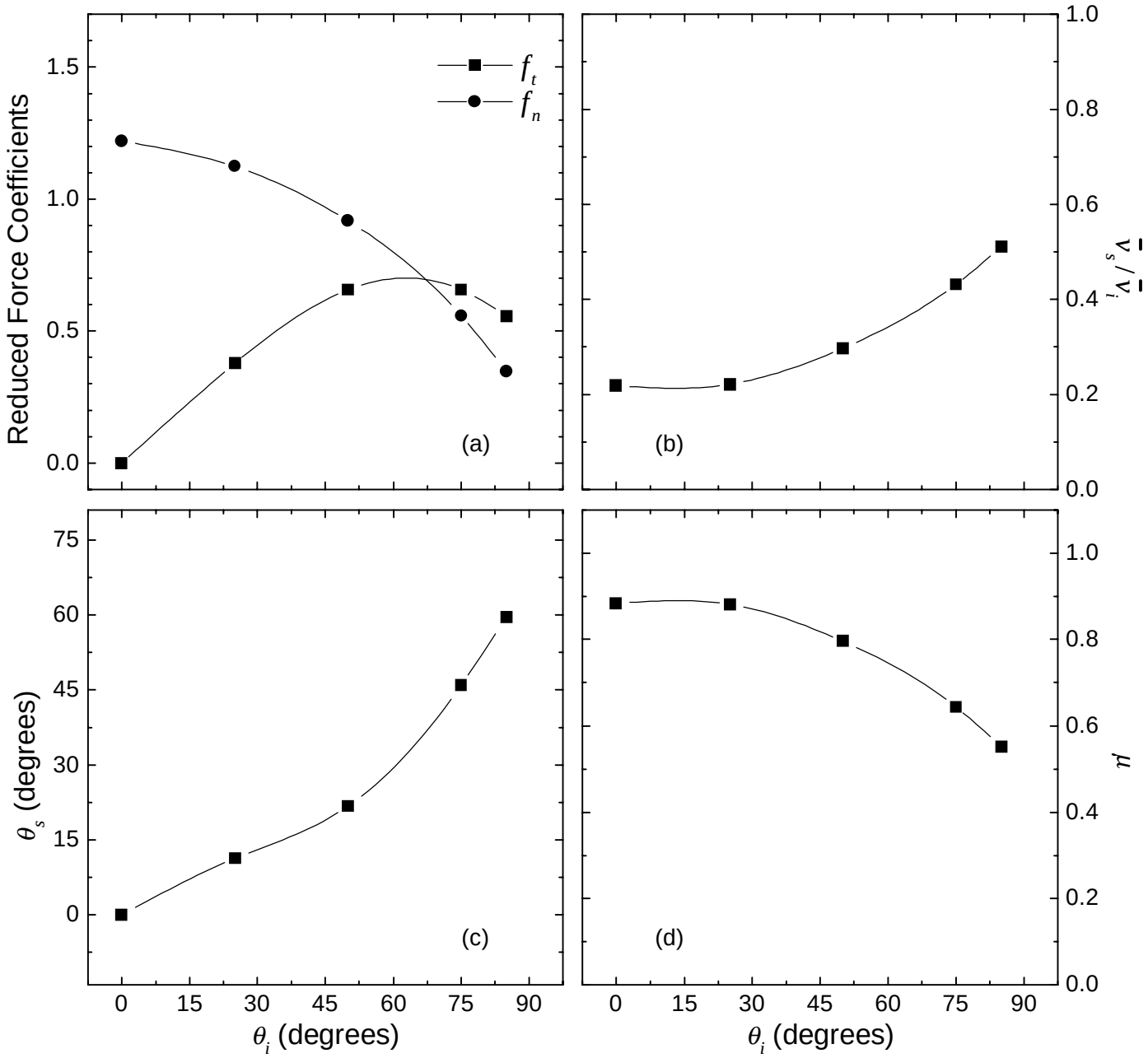

Figure 23: The data for 3180 m/s N_2 incident upon Kapton.

Table 23: 3180 m/s N_2 incident upon Kapton

θ_i (degrees)	f_t	f_n	$\overline{v}_s/\overline{v}_i$	$\overline{v}_s$ (m/s)	θ_s (degrees)	μ	ϵ'	$\overline{v_s^2}$ $(\mathrm{m/s})^2$
0	0	1.22	0.219	698	0	0.884	0.965	7.02×10^5
25	0.379	1.12	0.221	704	11.4	0.881	0.964	7.11×10^5
50	0.656	0.918	0.297	943	21.8	0.796	0.925	1.11×10^6
75	0.656	0.559	0.431	1370	45.9	0.644	0.825	2.11×10^6
85	0.555	0.347	0.512	1630	59.5	0.553	0.748	2.88×10^6

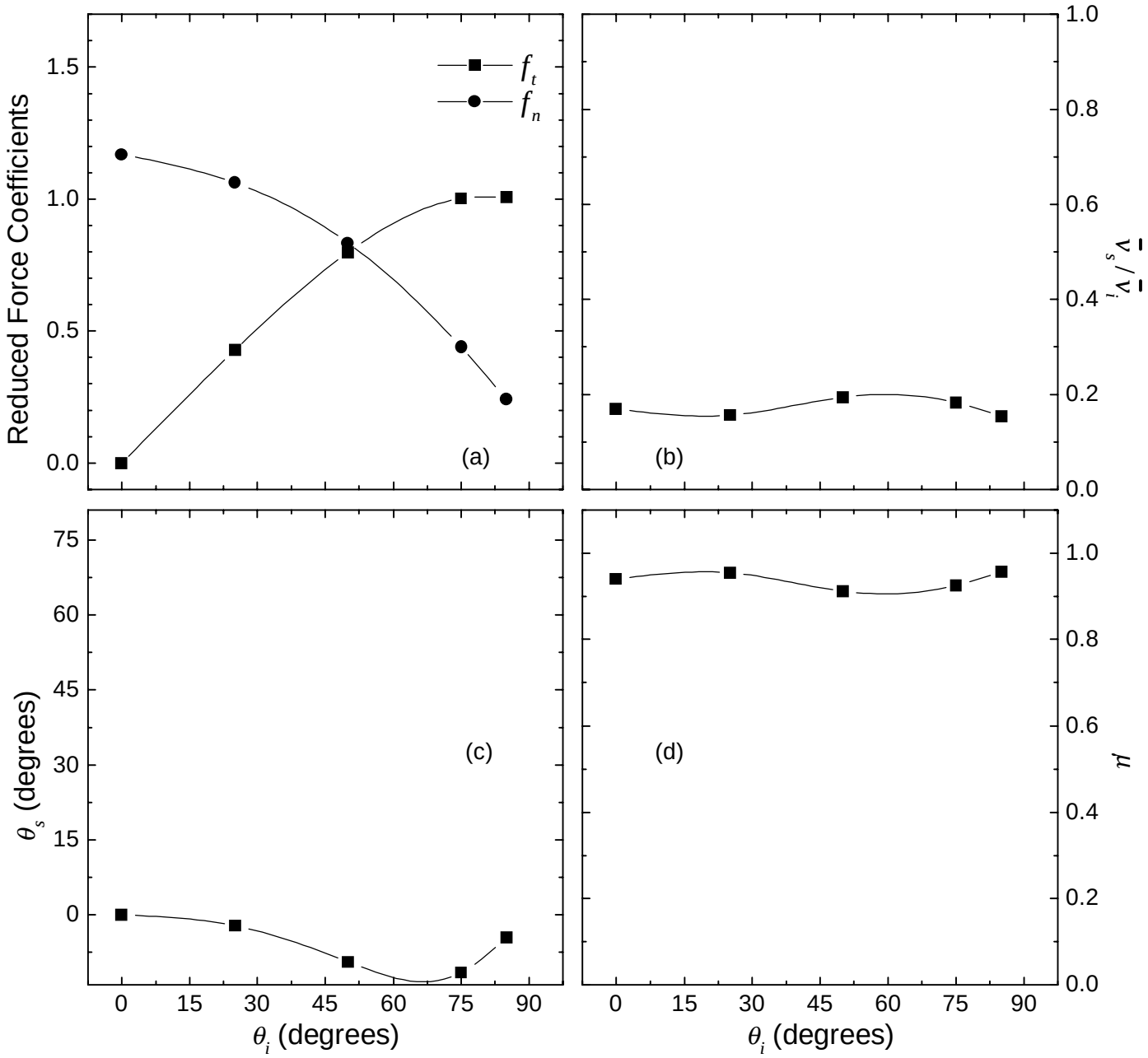

Figure 24: The data for 3180 m/s N_2 incident upon Z-93-coated aluminum.

Table 24: 3180 m/s N_2 incident upon Z-93-coated aluminum

θ_i (degrees)	f_t	f_n	$\overline{v}_s/\overline{v}_i$	$\overline{v}_s$ (m/s)	θ_s (degrees)	μ	ϵ'	$\overline{v_s^2}$ $(\mathrm{m/s})^2$
0	0	1.17	0.170	539	0	0.940	0.985	5.05×10^5
25	0.429	1.06	0.157	499	-2.20	0.954	0.989	4.62×10^5
50	0.798	0.834	0.194	617	-9.33	0.912	0.976	5.96×10^5
75	1.00	0.438	0.183	583	-11.6	0.925	0.980	5.54×10^5
85	1.01	0.241	0.155	492	-4.48	0.957	0.989	4.56×10^5

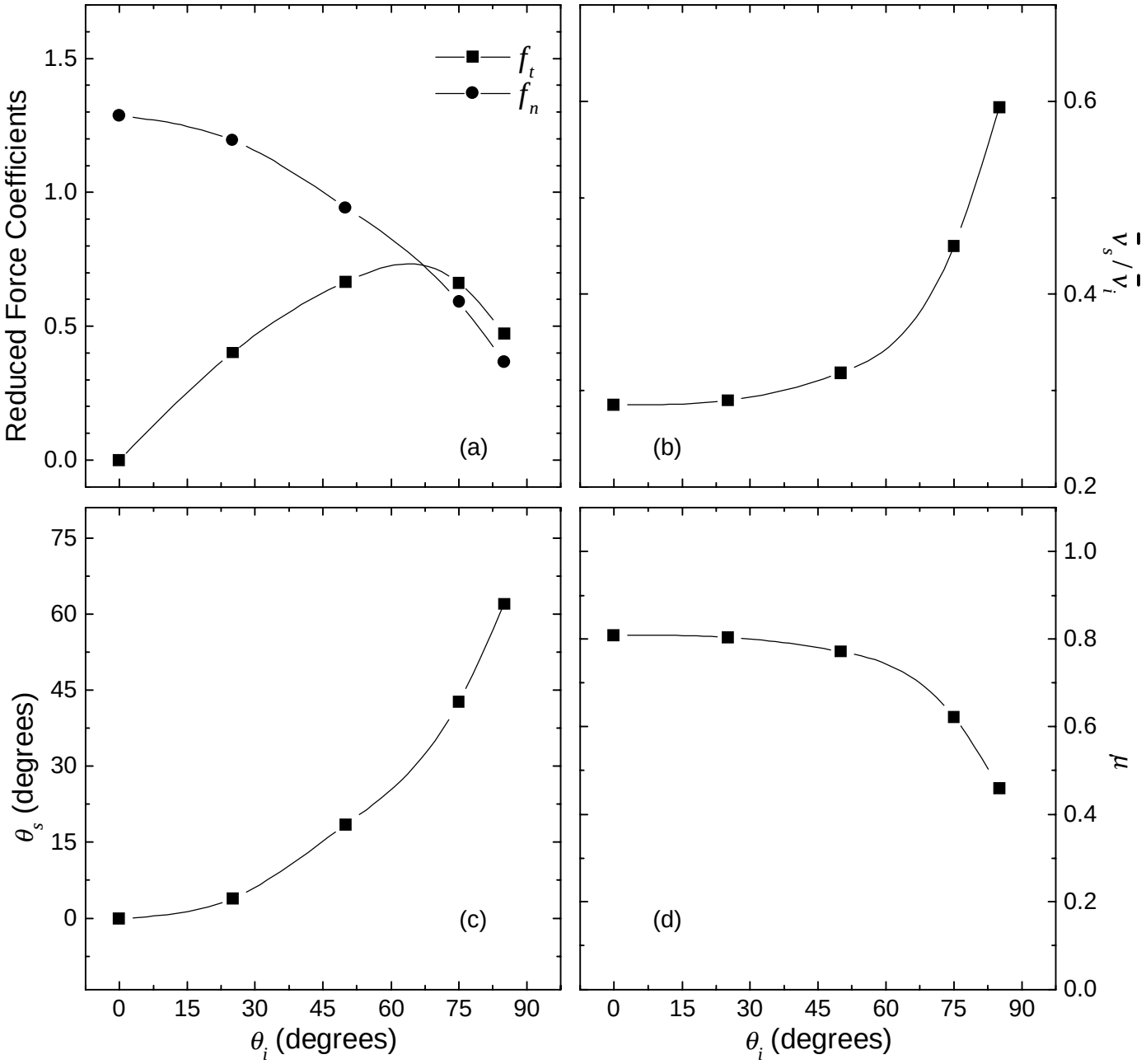

Figure 25: The data for 3200 m/s CO incident upon the solar panel.

Table 25: 3200 m/s CO incident upon the solar panel

θ_i (degrees)	f_t	f_n	$\overline{v}_s/\overline{v}_i$	$\overline{v}_s$ (m/s)	θ_s (degrees)	μ	ϵ'	$\overline{v_s^2}$ (m/s)^2
0	0	1.29	0.285	913	0	0.809	0.931	1.05×10^6
25	0.403	1.19	0.289	926	3.90	0.804	0.929	1.07×10^6
50	0.665	0.945	0.318	1020	18.5	0.771	0.911	1.26×10^6
75	0.661	0.590	0.450	1440	42.6	0.622	0.808	2.30×10^6
85	0.472	0.365	0.594	1900	62.1	0.459	0.656	3.85×10^6

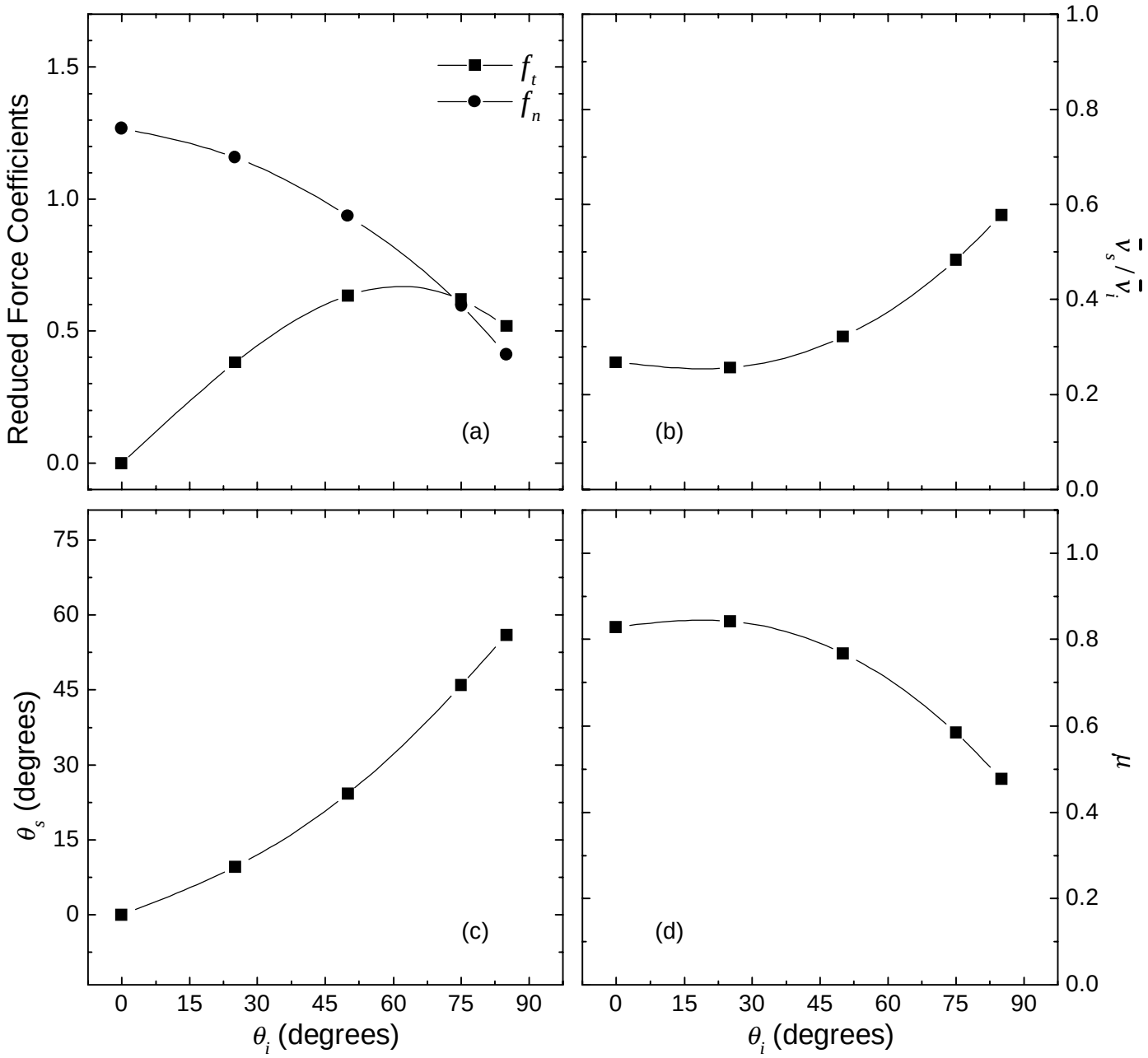

Figure 26: The data for 3200 m/s CO incident upon SiO_2-coated Kapton.

Table 26: 3200 m/s CO incident upon SiO_2-coated Kapton

θ_i (degrees)	f_t	f_n	$\overline{v}_s/\overline{v}_i$	$\overline{v}_s$ (m/s)	θ_s (degrees)	μ	ϵ'	$\overline{v_s^2}$ $(m/s)^2$
0	0	1.27	0.268	857	0	0.828	0.941	9.52×10^5
25	0.380	1.16	0.256	819	9.65	0.842	0.947	8.87×10^5
50	0.634	0.935	0.321	1030	24.3	0.768	0.909	1.27×10^6
75	0.619	0.595	0.483	1550	45.9	0.584	0.777	2.62×10^6
85	0.518	0.411	0.578	1850	56.0	0.478	0.675	3.66×10^6

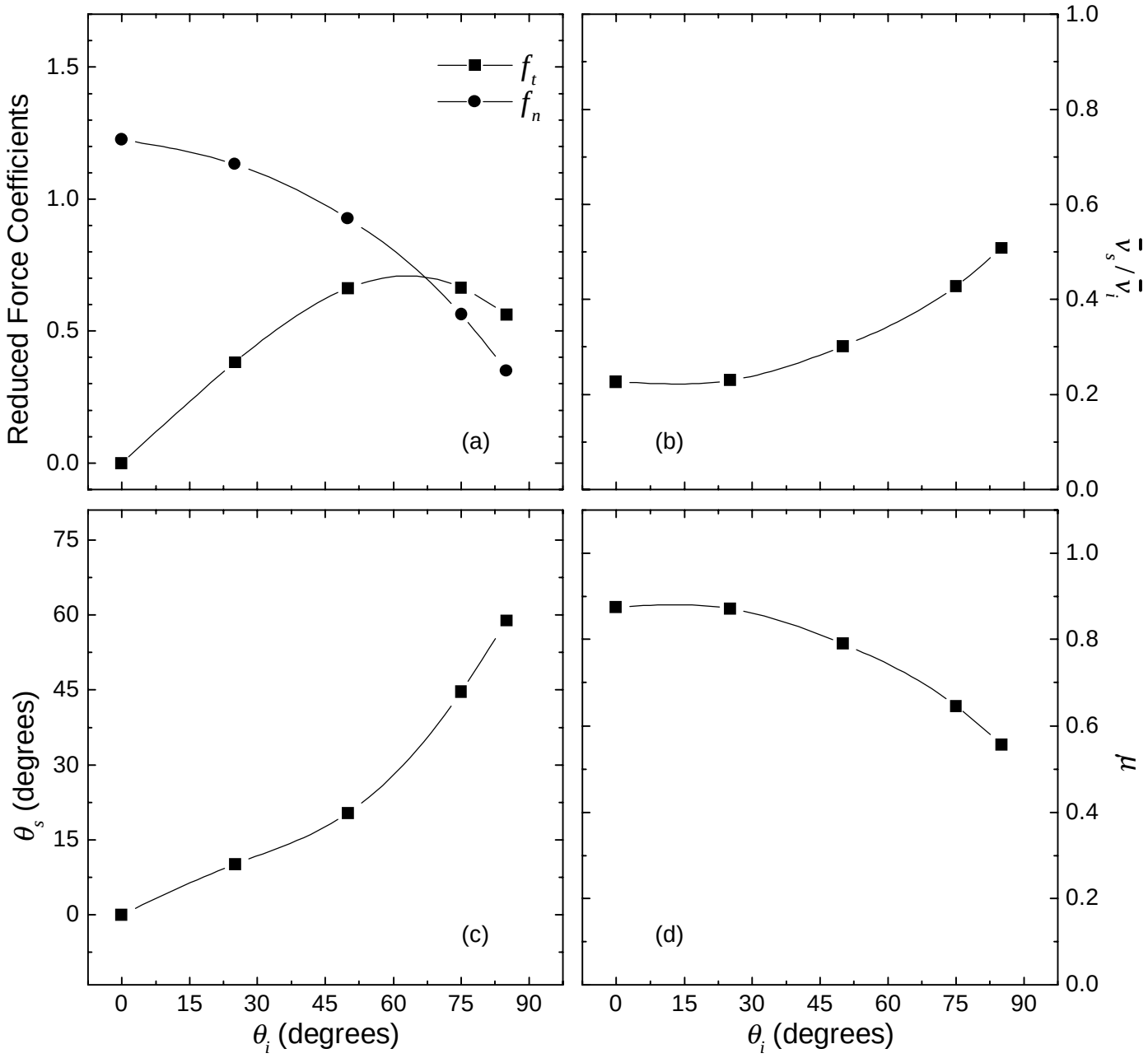

Figure 27: The data for 3200 m/s CO incident upon Kapton.

Table 27: 3200 m/s CO incident upon Kapton

θ_i (degrees)	f_t	f_n	$\overline{v}_s/\overline{v}_i$	$\overline{v}_s$ (m/s)	θ_s (degrees)	μ	ϵ'	$\overline{v_s^2}$ (m/s)^2
0	0	1.23	0.226	725	0	0.875	0.962	7.40×10^5
25	0.382	1.13	0.229	734	10.2	0.872	0.960	7.53×10^5
50	0.661	0.925	0.301	965	20.4	0.790	0.921	1.15×10^6
75	0.665	0.563	0.428	1370	44.7	0.647	0.828	2.10×10^6
85	0.562	0.350	0.507	1620	58.8	0.557	0.753	2.87×10^6

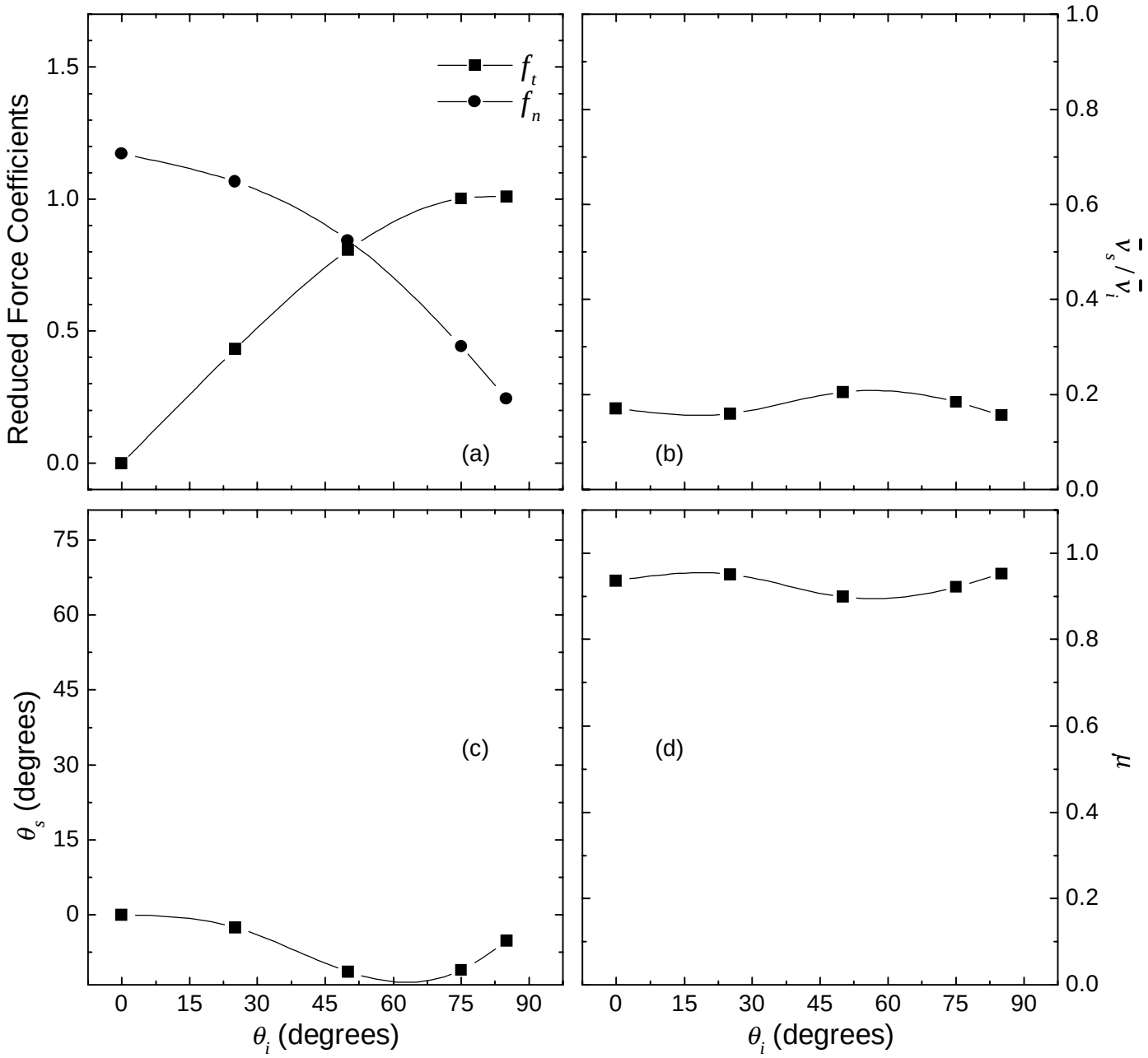

Figure 28: The data for 3200 m/s CO incident upon Z-93-coated aluminum.

Table 28: 3200 m/s CO incident upon Z-93-coated aluminum

θ_i (degrees)	f_t	f_n	$\overline{v}_s/\overline{v}_i$	$\overline{v}_s$ (m/s)	θ_s (degrees)	μ	ϵ'	$\overline{v_s^2}$ $(\mathrm{m/s})^2$
0	0	1.17	0.172	550	0	0.937	0.984	5.16×10^5
25	0.429	1.07	0.160	511	-2.46	0.951	0.988	4.74×10^5
50	0.807	0.844	0.205	658	-11.4	0.899	0.971	6.47×10^5
75	1.00	0.440	0.185	592	-11.1	0.922	0.979	5.65×10^5
85	1.01	0.244	0.157	503	-5.19	0.953	0.989	4.66×10^5

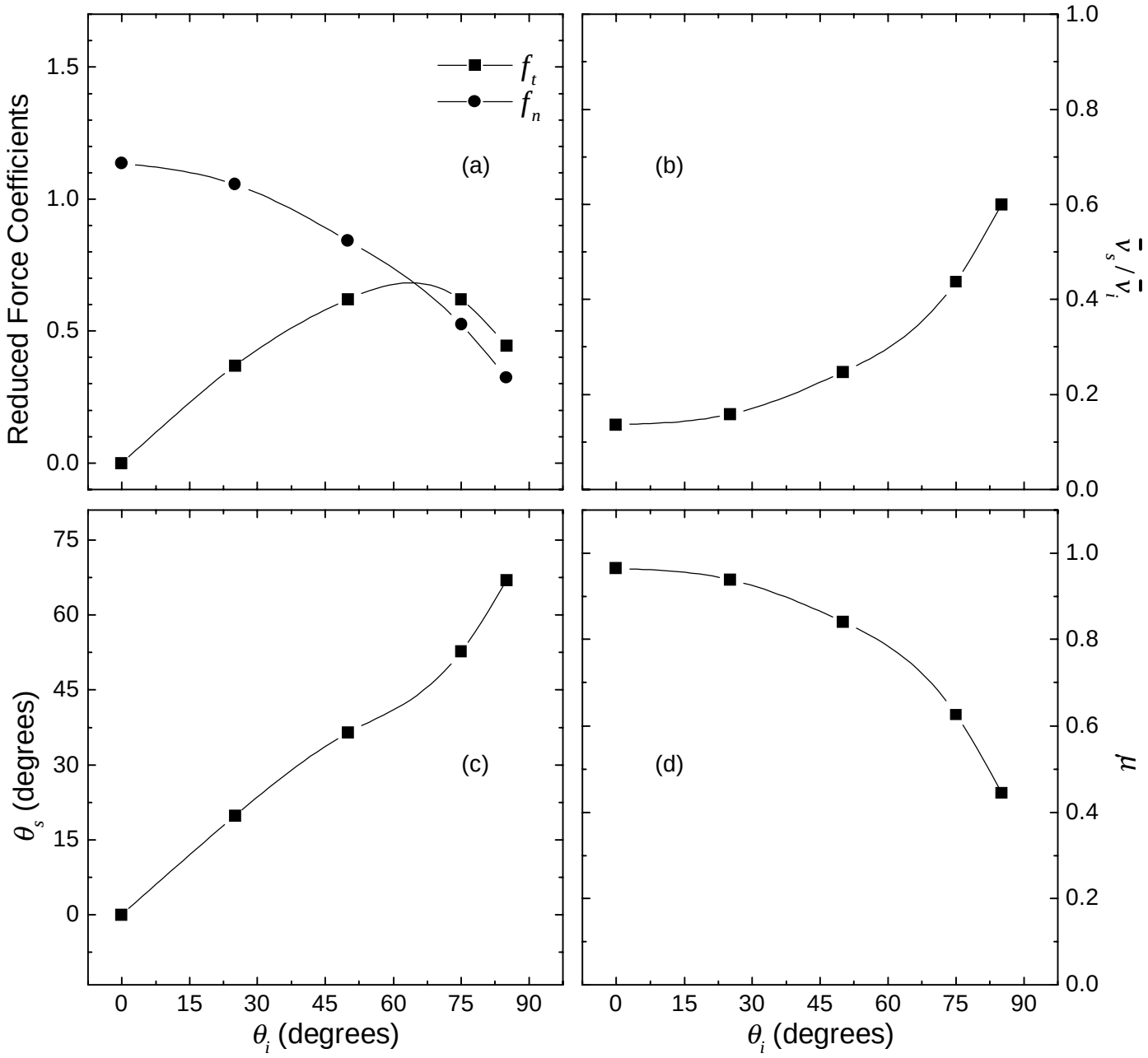

Figure 29: The data for 2840 m/s CO_2 incident upon the solar panel.

Table 29: 2840 m/s CO_2 incident upon the solar panel

θ_i (degrees)	f_t	f_n	$\overline{v}_s/\overline{v}_i$	$\overline{v}_s$ (m/s)	θ_s (degrees)	μ	ϵ'	$\overline{v_s^2}$ (m/s)^2
0	0	1.14	0.136	387	0	0.964	0.992	2.86×10^5
25	0.369	1.06	0.159	451	19.9	0.939	0.985	3.40×10^5
50	0.619	0.841	0.247	700	36.5	0.841	0.949	6.30×10^5
75	0.618	0.525	0.438	1240	52.6	0.627	0.817	1.70×10^6
85	0.444	0.322	0.600	1700	67.0	0.446	0.647	3.07×10^6

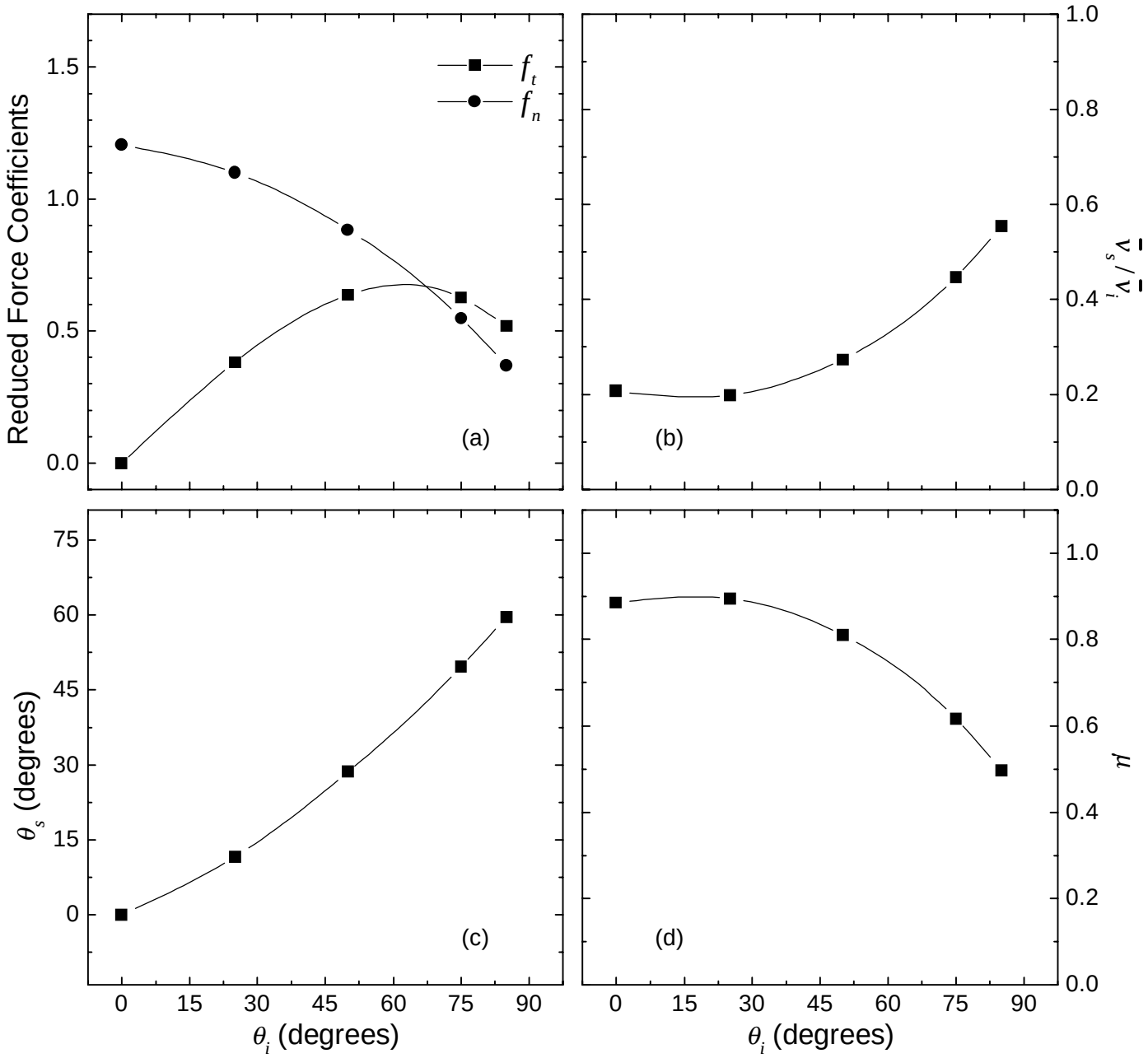

Figure 30: The data for 2840 m/s CO_2 incident upon SiO_2-coated Kapton.

Table 30: 2840 m/s CO_2 incident upon SiO_2-coated Kapton

θ_i (degrees)	f_t	f_n	$\overline{v}_s/\overline{v}_i$	$\overline{v}_s$ (m/s)	θ_s (degrees)	μ	ϵ'	$\overline{v_s^2}$ $(\mathrm{m/s})^2$
0	0	1.21	0.207	587	0	0.885	0.968	4.83×10^5
25	0.383	1.10	0.199	564	11.6	0.895	0.971	4.56×10^5
50	0.635	0.883	0.274	777	28.6	0.811	0.935	7.45×10^5
75	0.625	0.548	0.447	1270	49.6	0.617	0.809	1.76×10^6
85	0.518	0.368	0.555	1580	59.6	0.497	0.700	2.64×10^6

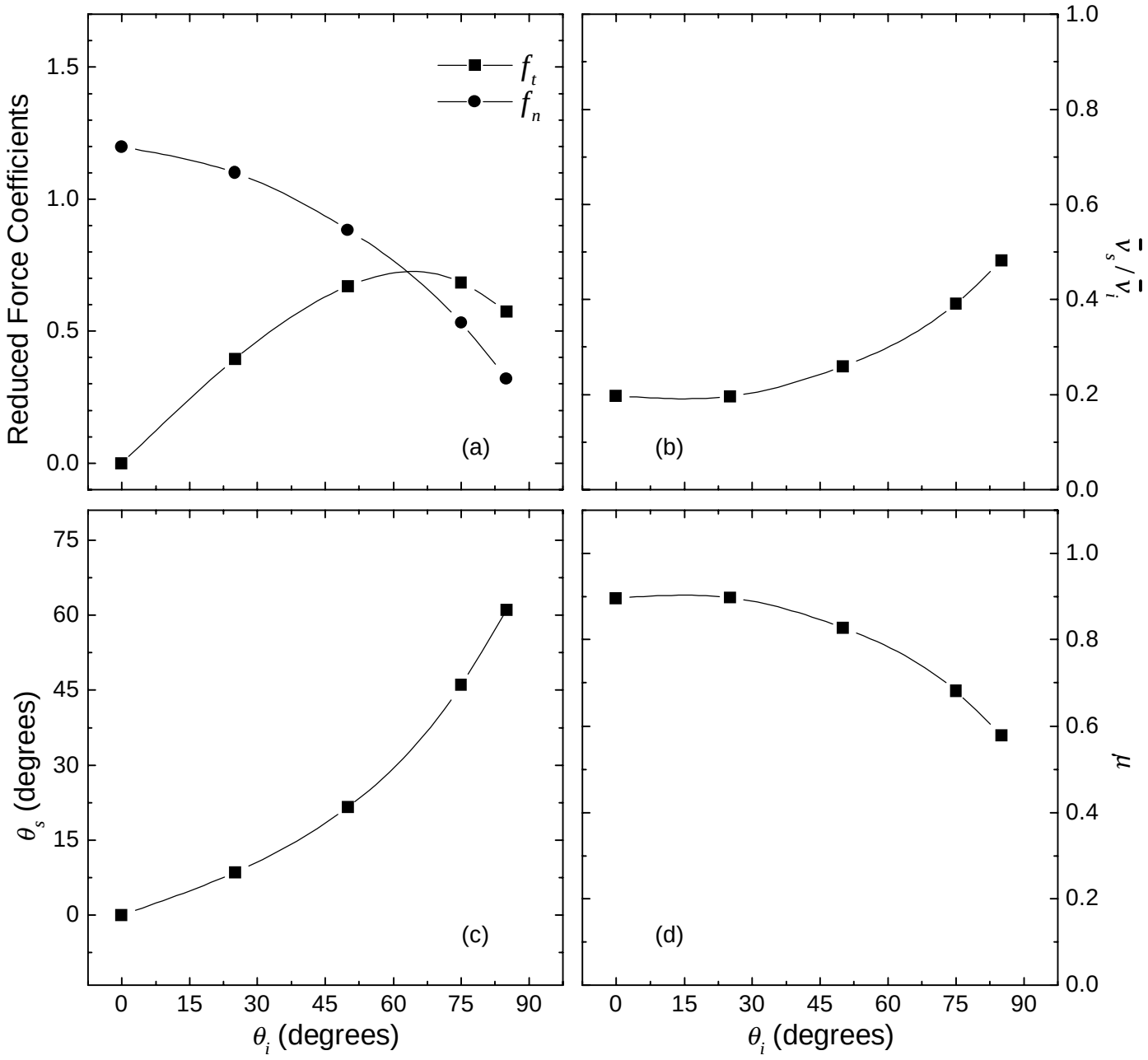

Figure 31: The data for 2840 m/s CO_2 incident upon Kapton.

Table 31: 2840 m/s CO_2 incident upon Kapton

θ_i (degrees)	f_t	f_n	$\overline{v}_s/\overline{v}_i$	$\overline{v}_s$ (m/s)	θ_s (degrees)	μ	ϵ'	$\overline{v_s^2}$ $(\mathrm{m/s})^2$
0	0	1.20	0.198	561	0	0.896	0.972	4.52×10^5
25	0.393	1.10	0.197	559	8.55	0.897	0.972	4.50×10^5
50	0.670	0.883	0.259	735	21.7	0.827	0.943	6.80×10^5
75	0.685	0.530	0.391	1110	46.1	0.680	0.857	1.38×10^6
85	0.574	0.321	0.483	1370	61.1	0.578	0.776	2.03×10^6

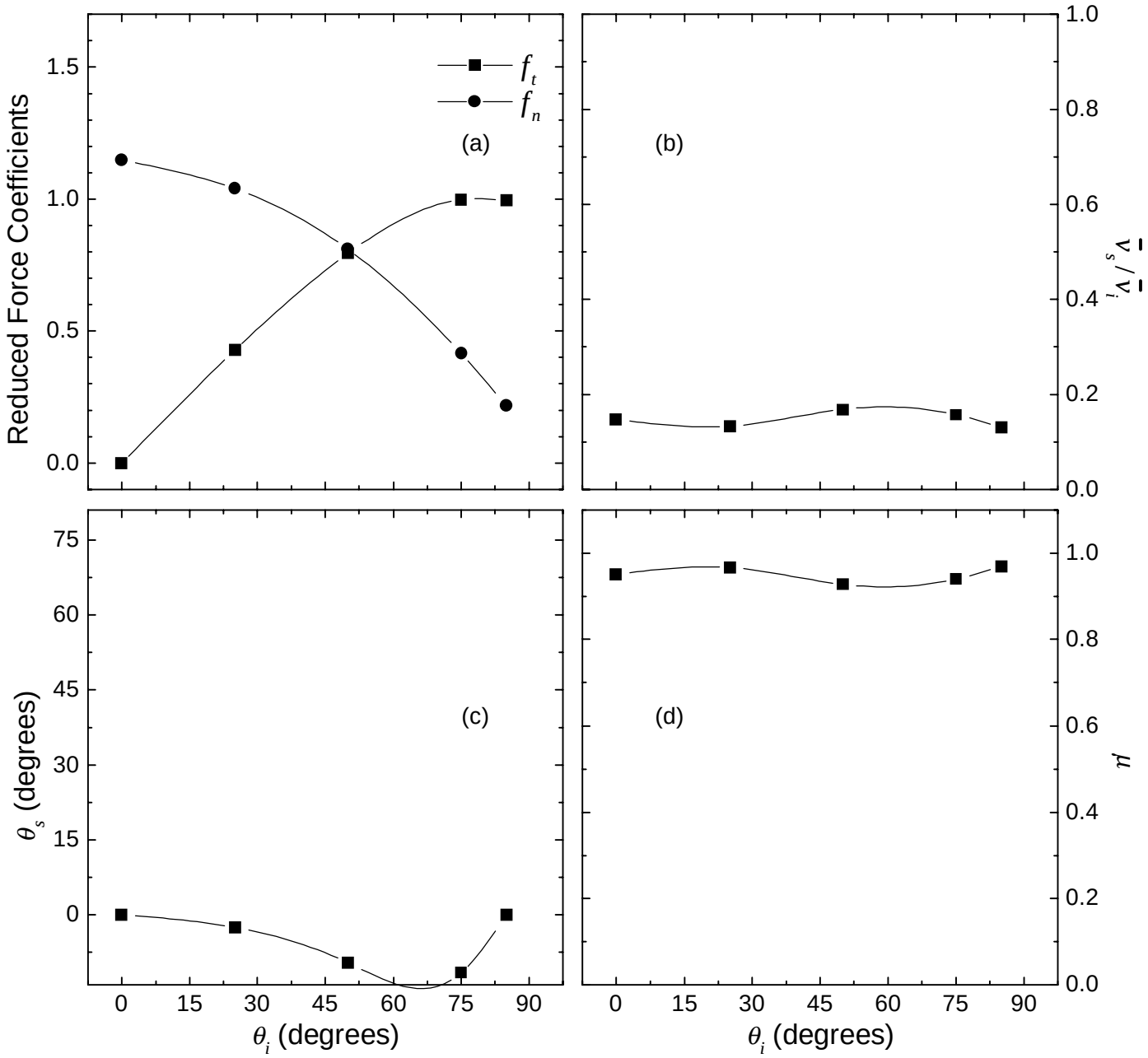

Figure 32: The data for 2840 m/s CO_2 incident upon Z-93-coated aluminum.

Table 32: 2840 m/s CO_2 incident upon Z-93-coated aluminum

θ_i (degrees)	f_t	f_n	$\overline{v}_s/\overline{v}_i$	$\overline{v}_s$ (m/s)	θ_s (degrees)	μ	ϵ'	$\overline{v_s^2}$ $(\mathrm{m/s})^2$
0	0	1.15	0.148	421	0	0.951	0.989	3.13×10^5
25	0.429	1.04	0.134	380	-2.52	0.967	0.993	2.80×10^5
50	0.794	0.809	0.169	479	-9.54	0.928	0.982	3.66×10^5
75	0.998	0.414	0.158	449	-11.6	0.940	0.986	3.38×10^5
85	0.996	0.219	0.132	373	0.076	0.969	0.993	2.75×10^5

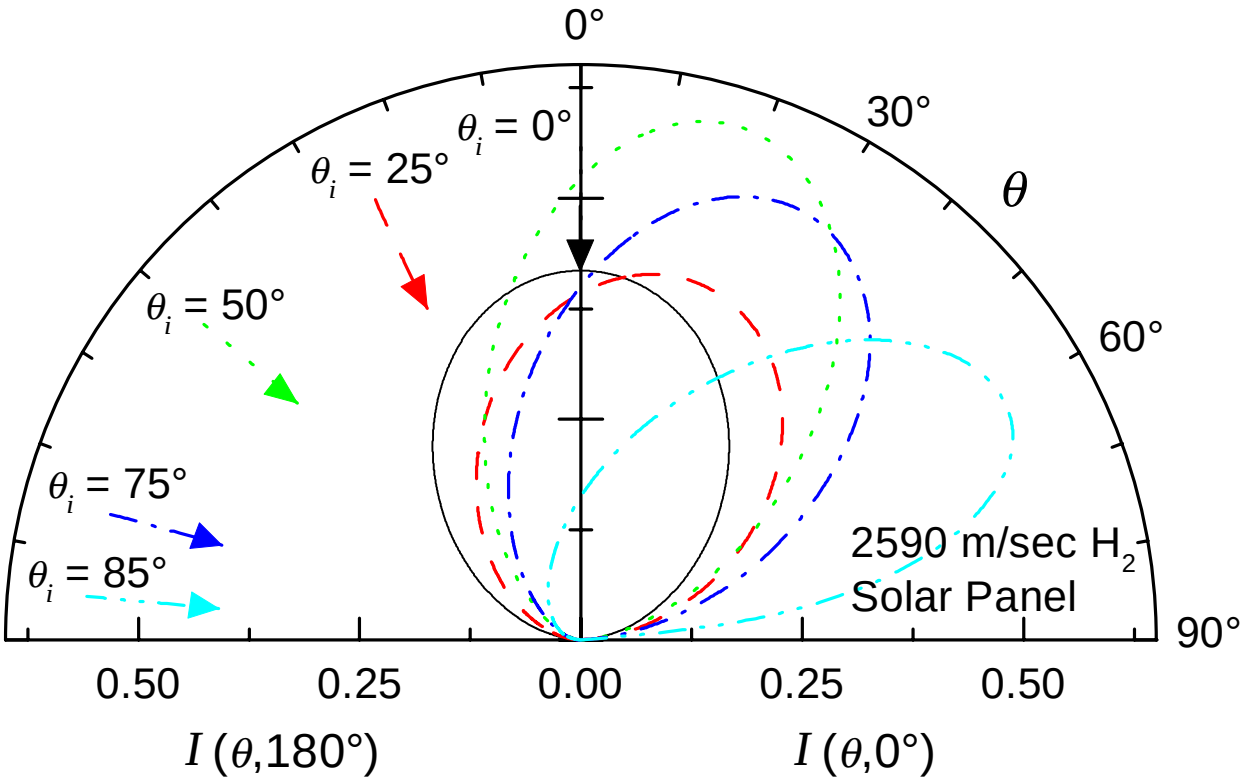

Figure 33: The angular distribution functions for 2590 m/s H_2 incident upon the solar panel.

Table 33: The Nocilla model parameters for 2590 m/s H_2 incident upon the solar panel.

θ_i (degrees)	S	U (m/s)	θ_u (degrees)	T_s (K)
0	0.309	454	0	263
25	0.334	491	33.7	263
50	0.718	968	24.3	221
75	0.594	831	42.1	237
85	0.706	1070	114	278

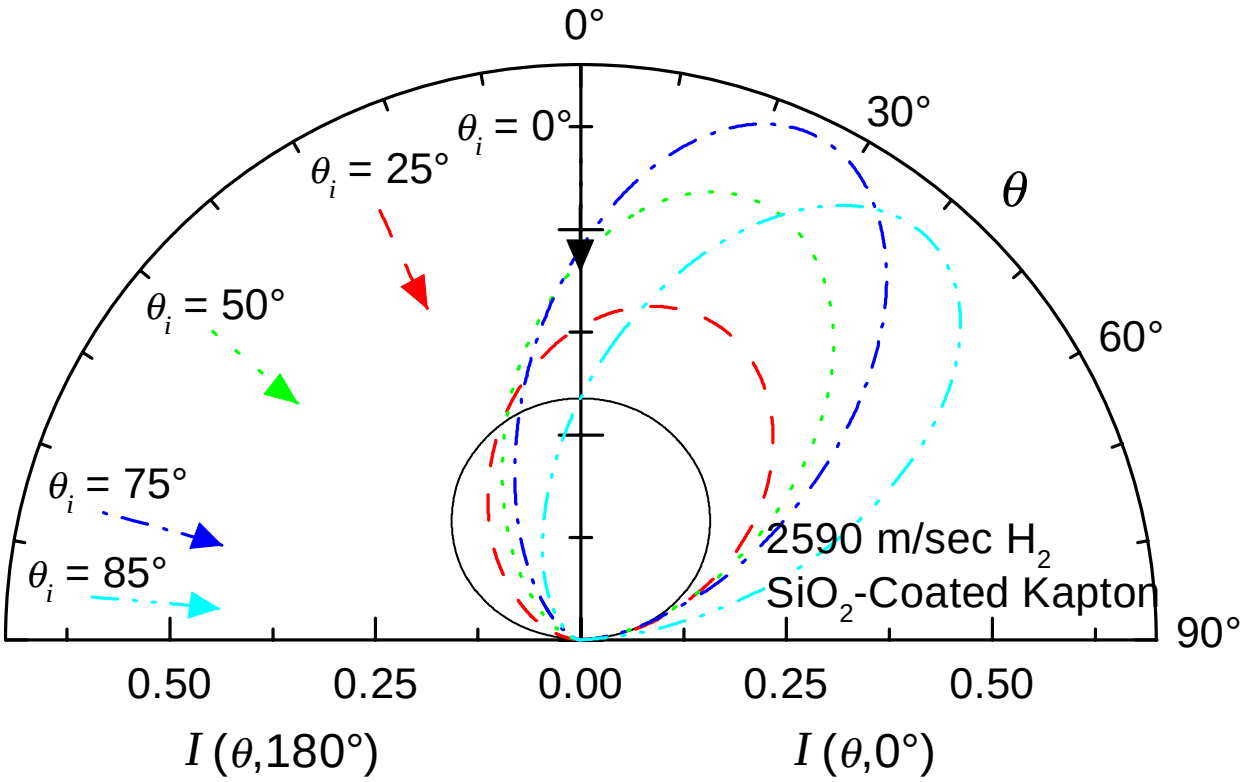

Figure 34: The angular distribution functions for 2590 m/s H_2 incident upon SiO_2-coated Kapton.

Table 34: The Nocilla model parameters for 2590 m/s H_2 incident upon SiO_2-coated Kapton.

θ_i (degrees)	S	U (m/s)	θ_u (degrees)	T_s (K)
0	0.0860	136	180	304
25	0.326	482	38.5	265
50	0.657	901	31.5	228
75	0.831	1090	33.4	210
85	0.757	1030	58.6	225

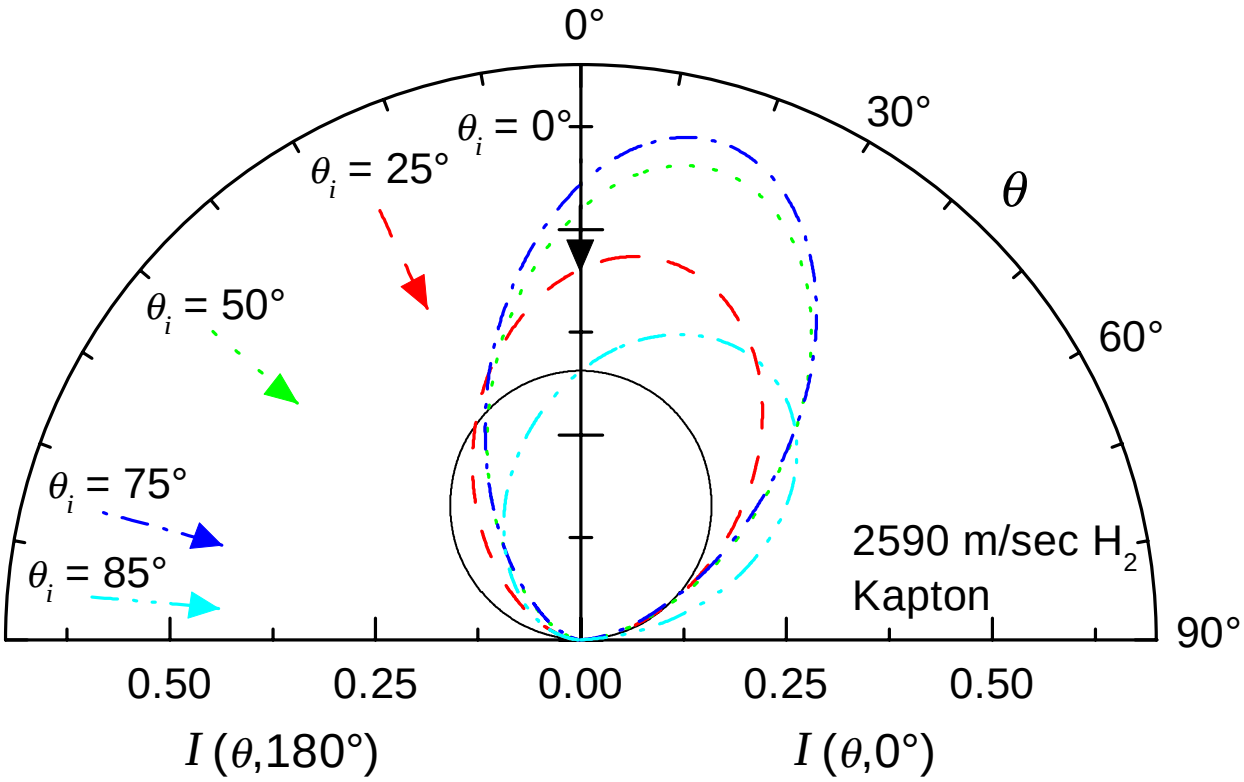

Figure 35: The angular distribution functions for 2590 m/s H_2 incident upon Kapton.

Table 35: The Nocilla model parameters for 2590 m/s H_2 incident upon Kapton.

θ_i (degrees)	S	U (m/s)	θ_u (degrees)	T_s (K)
0	0.0360	55.8	0	291
25	0.447	641	19.5	249
50	0.697	945	22.7	223
75	0.758	1010	21.0	216
85	0.308	463	65.9	275

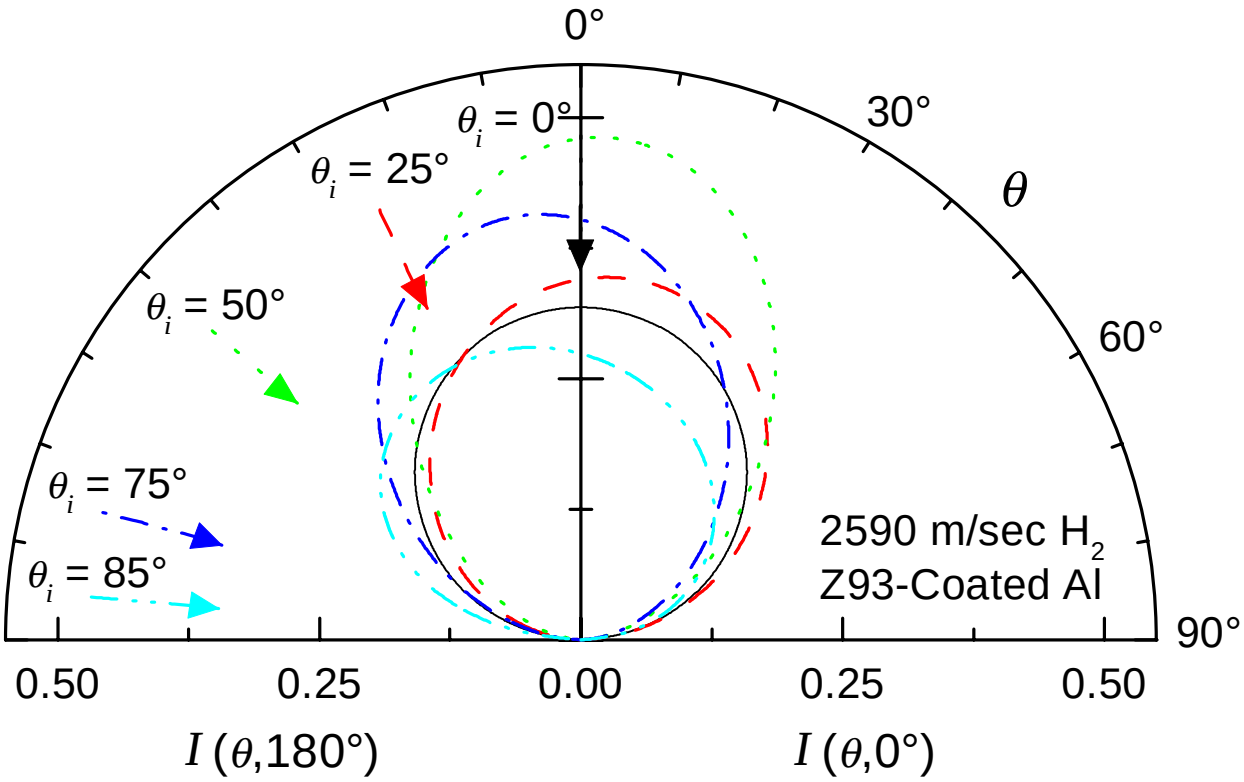

Figure 36: The angular distribution functions for 2590 m/s H_2 incident upon Z-93-coated aluminum.

Table 36: The Nocilla model parameters for 2590 m/s H_2 incident upon Z-93-coated aluminum

θ_i (degrees)	S	U (m/s)	θ_u (degrees)	T_s (K)
0	0.00438	6.83	0	291
25	0.115	177	30.4	249
50	0.466	663	4.69	223
75	0.289	428	-17.9	216
85	0.188	300	-146	275

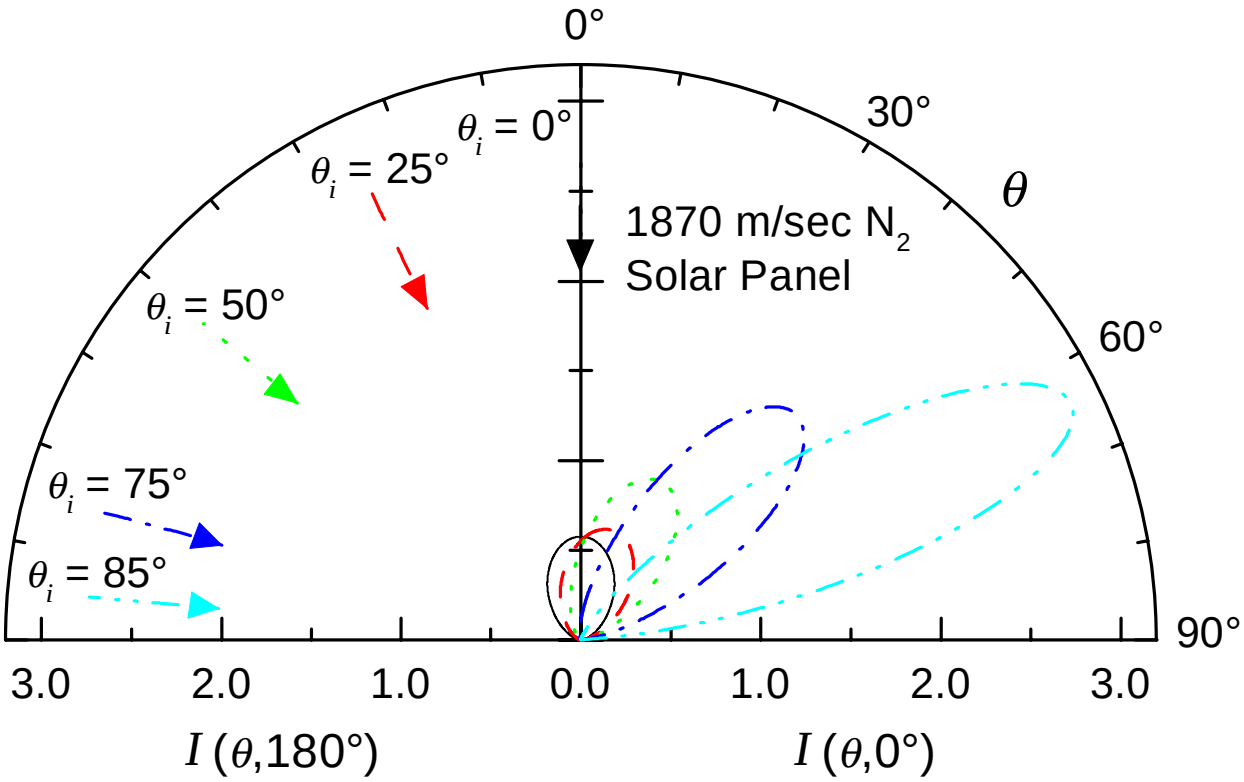

Figure 37: The angular distribution functions for 1870 m/s N_2 incident upon the solar panel.

Table 37: The Nocilla model parameters for 1870 m/s N_2 incident upon the solar panel.

θ_i (degrees)	S	U (m/s)	θ_u (degrees)	T_s (K)
0	0.669	266	0	267
25	0.774	306	21.7	264
50	1.26	484	32.3	247
75	1.94	711	49.0	226
85	2.66	938	71.4	210

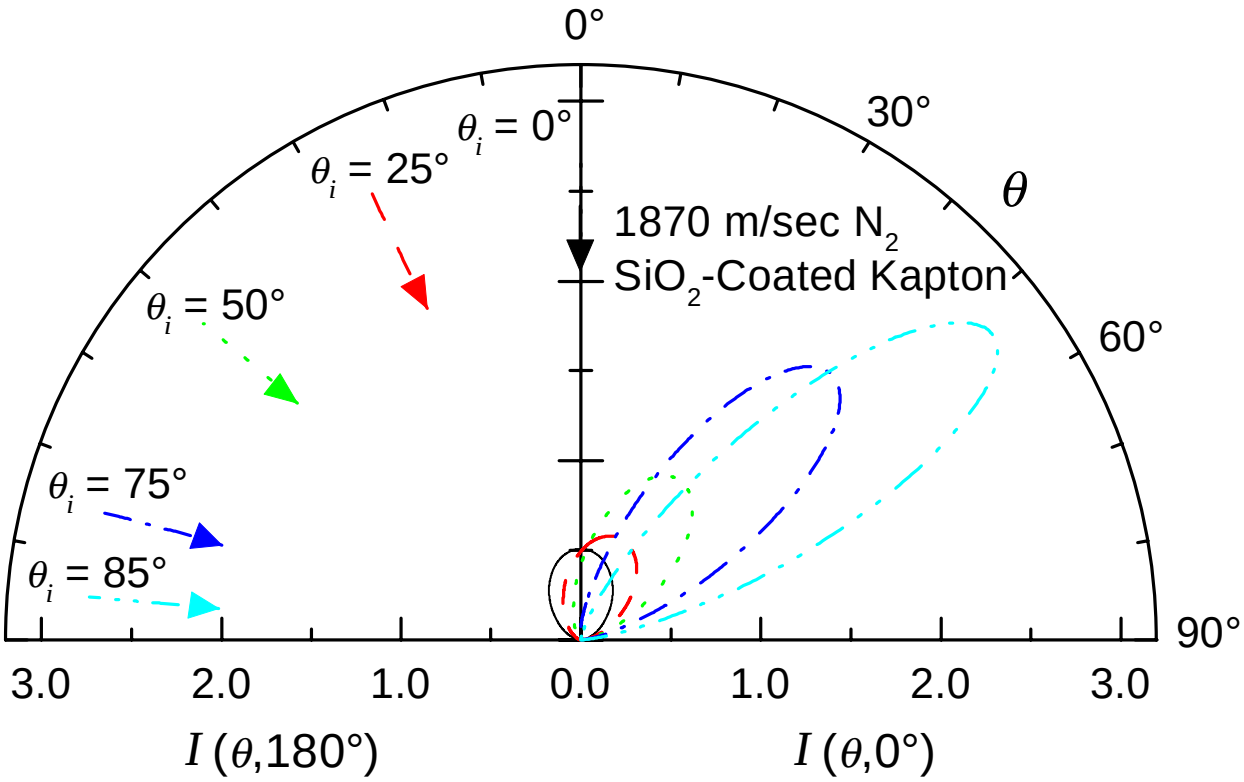

Figure 38: The angular distribution functions for 1870 m/s N_2 incident upon SiO_2-coated Kapton.

Table 38: The Nocilla model parameters for 1870 m/s N_2 incident upon SiO_2-coated Kapton.

θ_i (degrees)	S	U (m/s)	θ_u (degrees)	T_s (K)
0	0.531	214	0	273
25	0.718	286	28.4	268
50	1.32	505	37.5	246
75	2.18	781	47.7	216
85	2.68	925	58.0	202

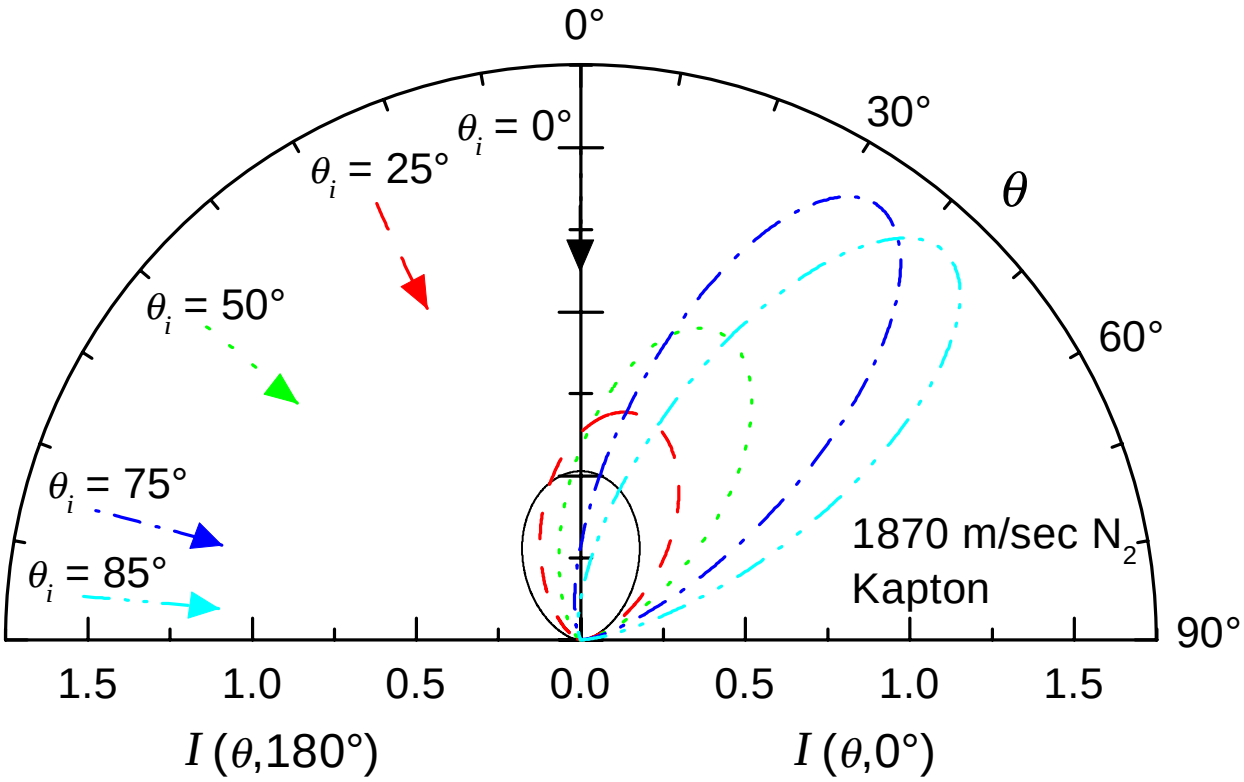

Figure 39: The angular distribution functions for 1870 m/s N_2 incident upon Kapton.

Table 39: The Nocilla model parameters for 1870 m/s N_2 incident upon Kapton.

θ_i (degrees)	S	U (m/s)	θ_u (degrees)	T_s (K)
0	0.540	217	0	273
25	0.896	351	17.5	259
50	1.31	499	28.8	244
75	1.86	682	38.4	225
85	1.85	682	48.9	229

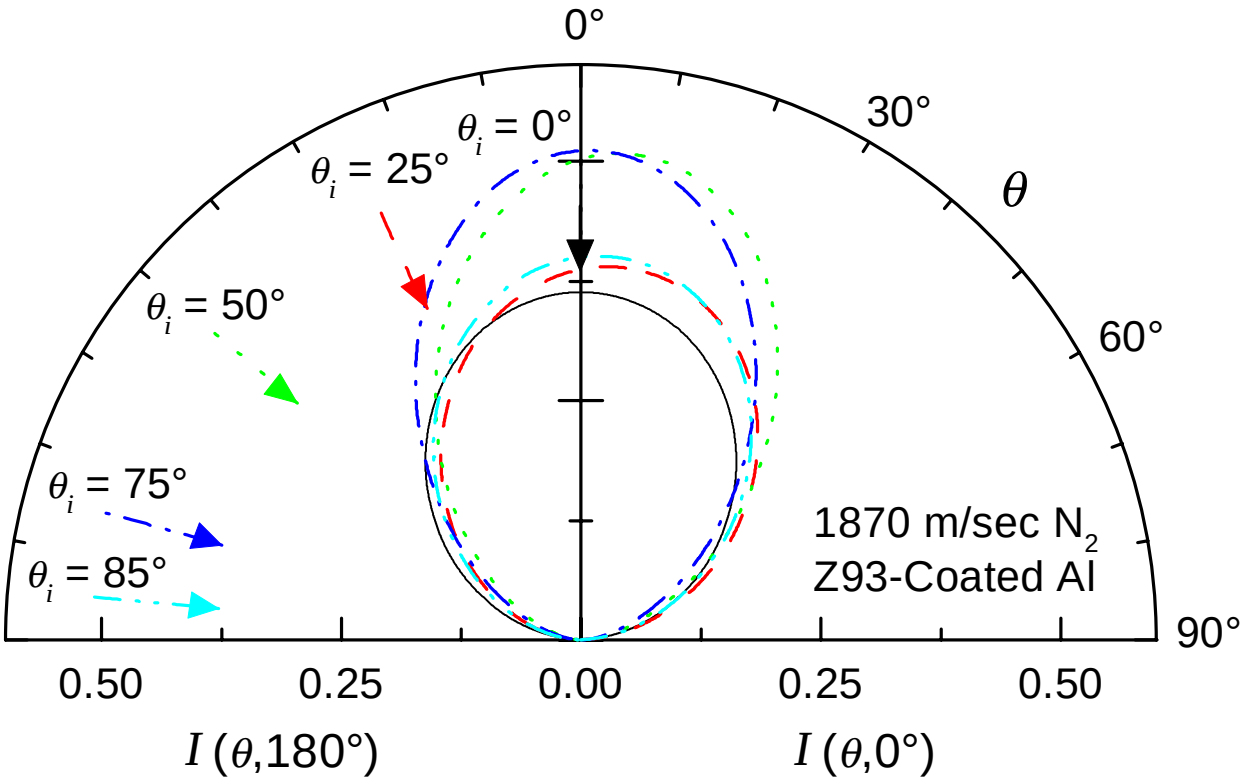

Figure 40: The angular distribution functions for 1870 m/s N_2 incident upon Z-93-coated aluminum.

Table 40: The Nocilla model parameters for 1870 m/s N_2 incident upon Z-93-coated aluminum.

θ_i (degrees)	S	U (m/s)	θ_u (degrees)	T_s (K)
0	0.153	63.4	0	289
25	0.237	97.7	16.2	286
50	0.529	213	9.71	274
75	0.532	214	1.86	273
85	0.265	109	8.92	284

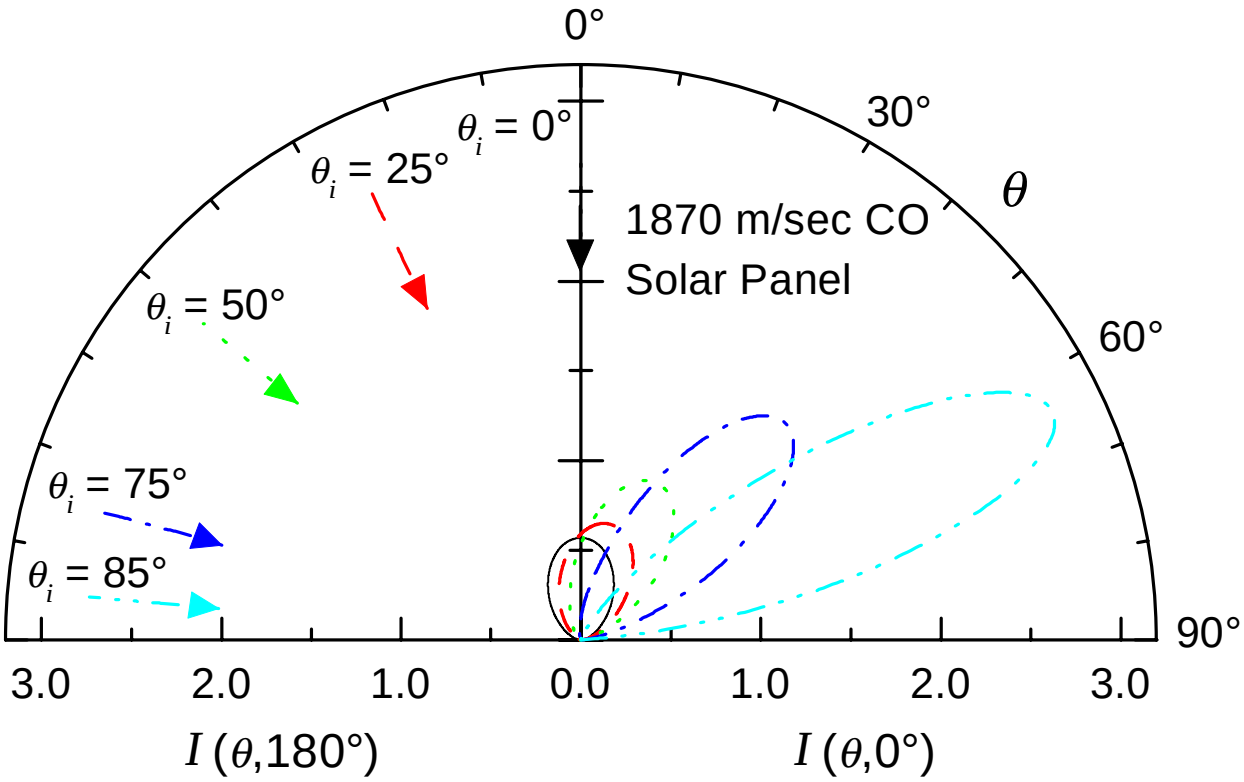

Figure 41: The angular distribution functions for 1870 m/s CO incident upon the solar panel.

Table 41: The Nocilla model parameters for 1870 m/s CO incident upon the solar panel.

θ_i (degrees)	S	U (m/s)	θ_u (degrees)	T_s (K)
0	0.655	261	0	268
25	0.822	324	19.0	262
50	1.24	477	31.2	248
75	1.88	693	48.9	229
85	2.59	921	71.7	213

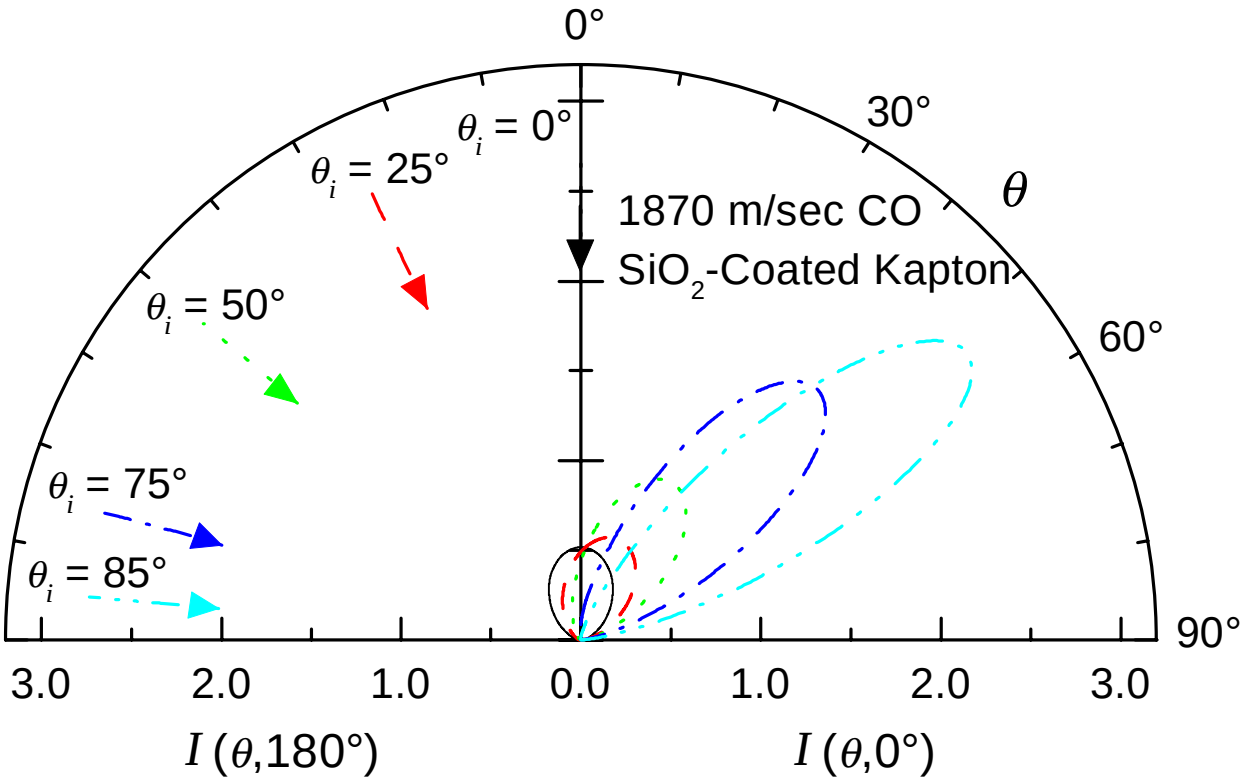

Figure 42: The angular distribution functions for 1870 m/s CO incident upon SiO_2-coated Kapton.

Table 42: The Nocilla model parameters for 1870 m/s CO incident upon SiO_2-coated Kapton.

θ_i (degrees)	S	U (m/s)	θ_u (degrees)	T_s (K)
0	0.548	220	0	273
25	0.700	279	28.2	269
50	1.28	492	36.2	247
75	2.09	756	48.0	220
85	2.57	898	58.2	206

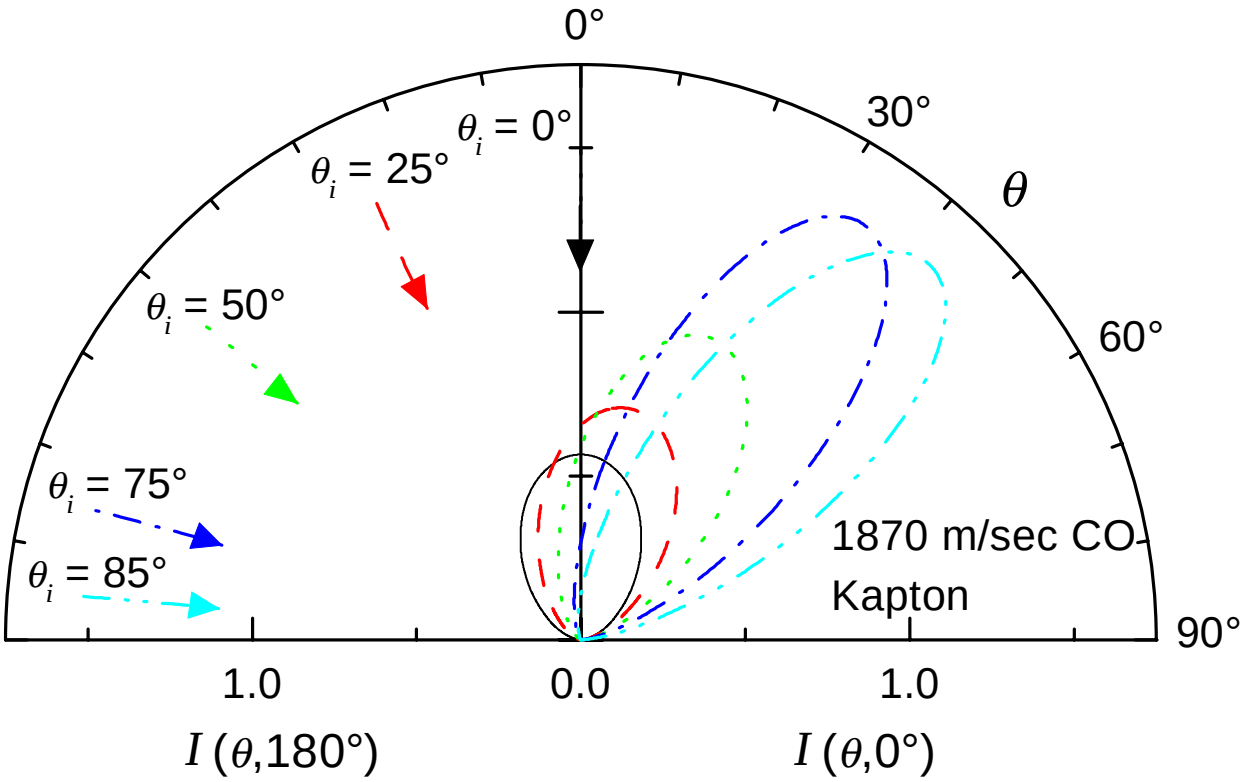

Figure 43: The angular distribution functions for 1870 m/s CO incident upon Kapton.

Table 43: The Nocilla model parameters for 1870 m/s CO incident upon Kapton.

θ_i (degrees)	S	U (m/s)	θ_u (degrees)	T_s (K)
0	0.645	257	0	269
25	0.913	358	15.7	258
50	1.28	490	28.5	245
75	1.80	663	38.6	228
85	1.80	666	48.9	232

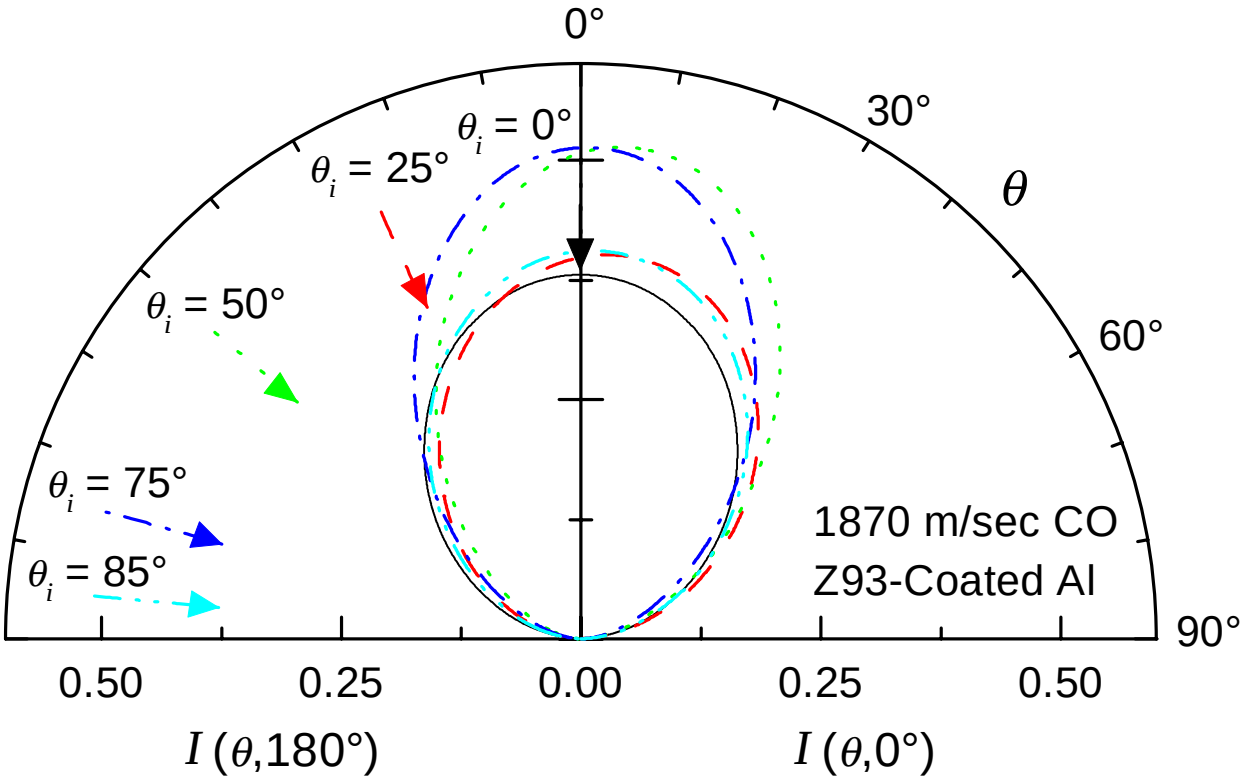

Figure 44: The angular distribution functions for 1870 m/s CO incident upon Z-93-coated aluminum.

Table 44: The Nocilla model parameters for 1870 m/s CO incident upon Z-93-coated aluminum.

θ_i (degrees)	S	U (m/s)	θ_u (degrees)	T_s (K)
0	0.204	84.1	0	287
25	0.268	110	13.3	284
50	0.542	218	9.97	273
75	0.536	216	1.48	273
85	0.277	113	5.34	284

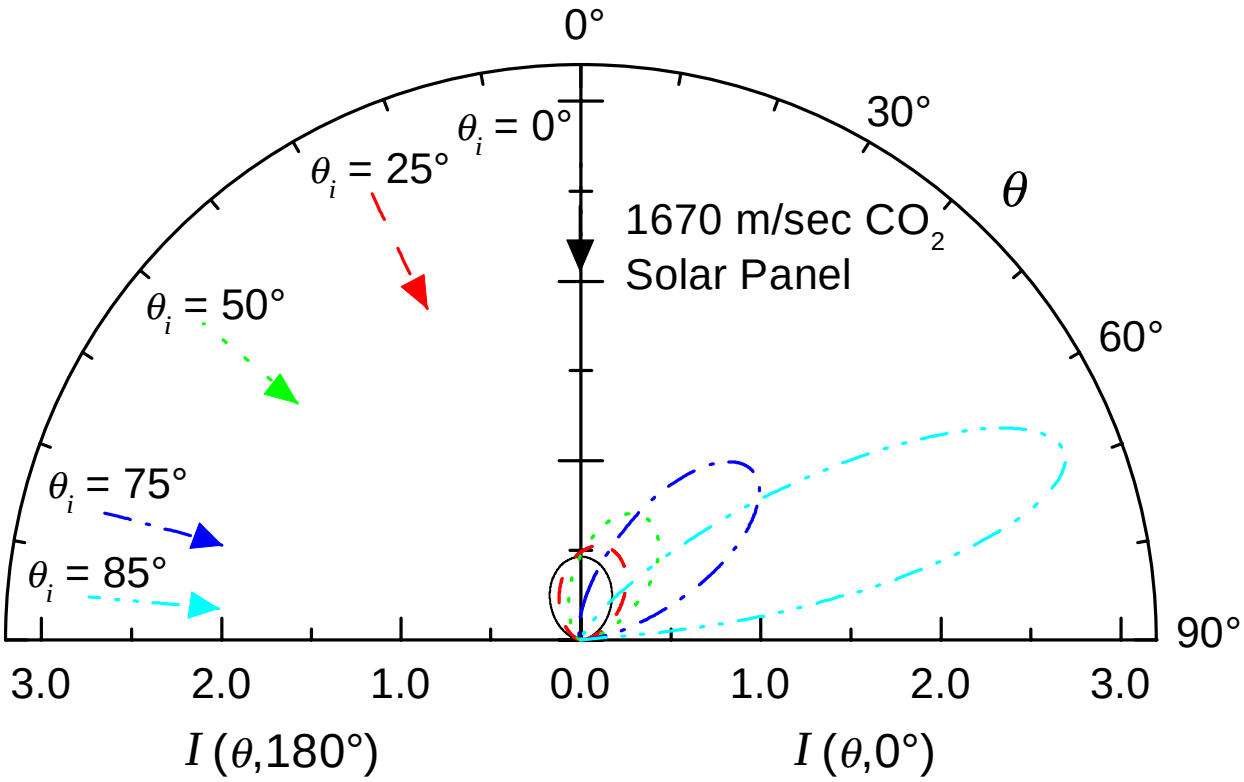

Figure 45: The angular distribution functions for 1670 m/s CO_2 incident upon the solar panel.

Table 45: The Nocilla model parameters for 1670 m/s CO_2 incident upon the solar panel.

θ_i (degrees)	S	U (m/s)	θ_u (degrees)	T_s (K)
0	0.432	140	0	279
25	0.587	189	21.6	274
50	0.975	307	34.7	262
75	1.59	485	52.9	248
85	2.47	739	78.8	236

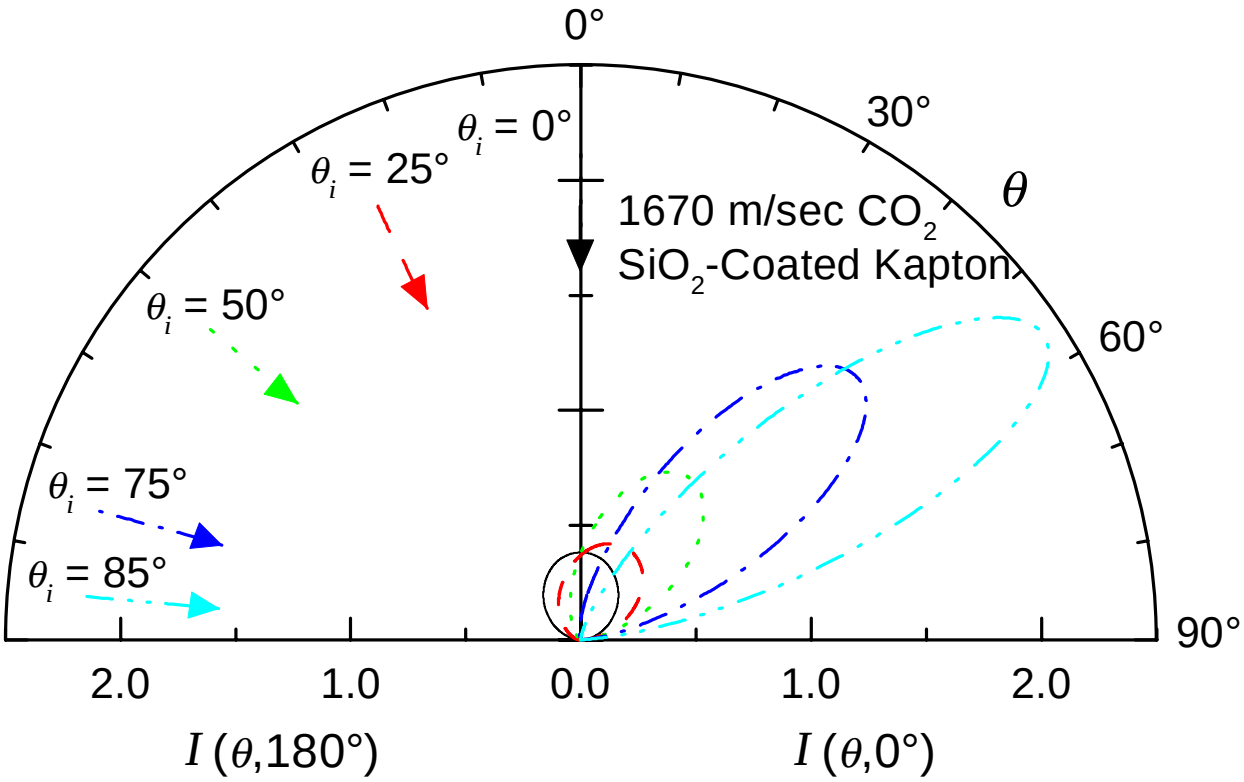

Figure 46: The angular distribution functions for 1670 m/s CO_2 incident upon SiO_2-coated Kapton.

Table 46: The Nocilla model parameters for 1670 m/s CO_2 incident upon SiO_2-coated Kapton.

θ_i (degrees)	S	U (m/s)	θ_u (degrees)	T_s (K)
0	0.212	69.7	0	287
25	0.395	129	47.1	284
50	1.07	335	42.5	261
75	1.87	560	52.8	238
85	2.36	692	63.0	227

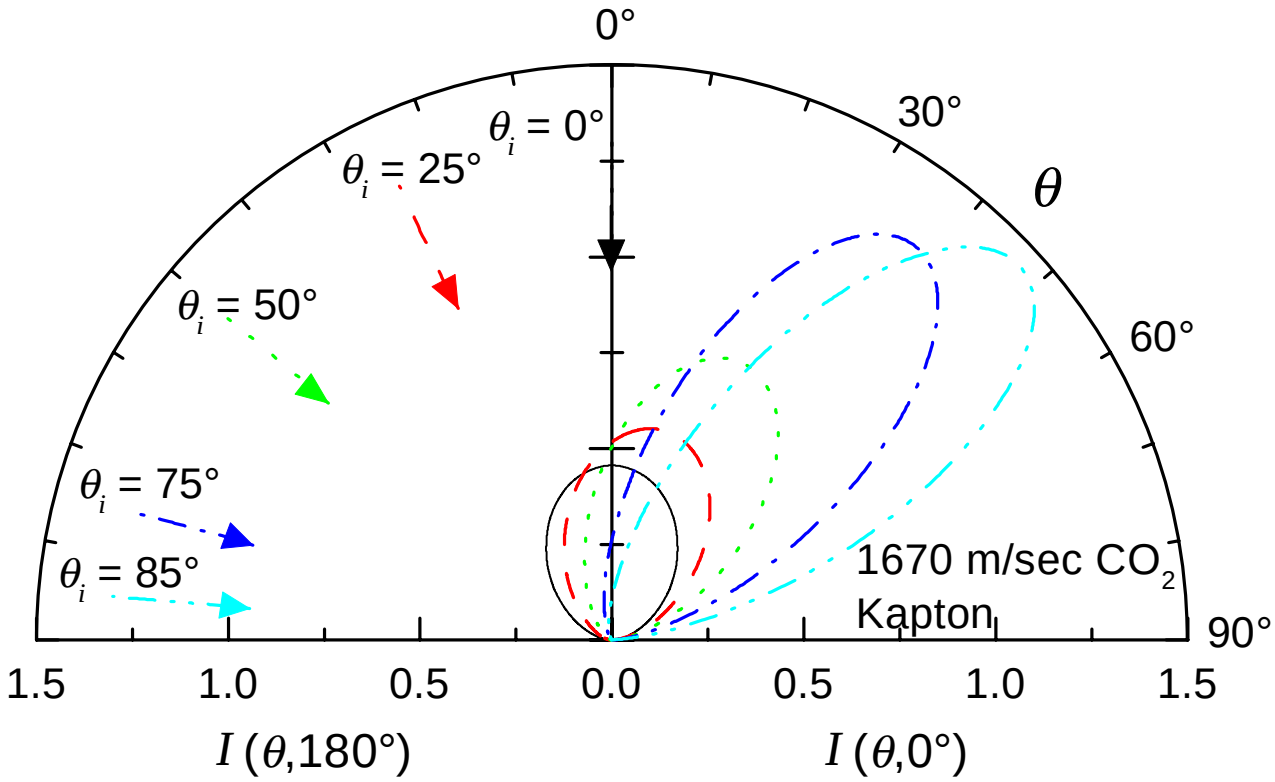

Figure 47: The angular distribution functions for 1670 m/s CO_2 incident upon Kapton.

Table 47: The Nocilla model parameters for 1670 m/s CO_2 incident upon Kapton.

θ_i (degrees)	S	U (m/s)	θ_u (degrees)	T_s (K)
0	0.405	132	0	280
25	0.637	204	19.8	272
50	1.02	318	32.4	260
75	1.57	478	43.6	244
85	1.67	509	55.4	246

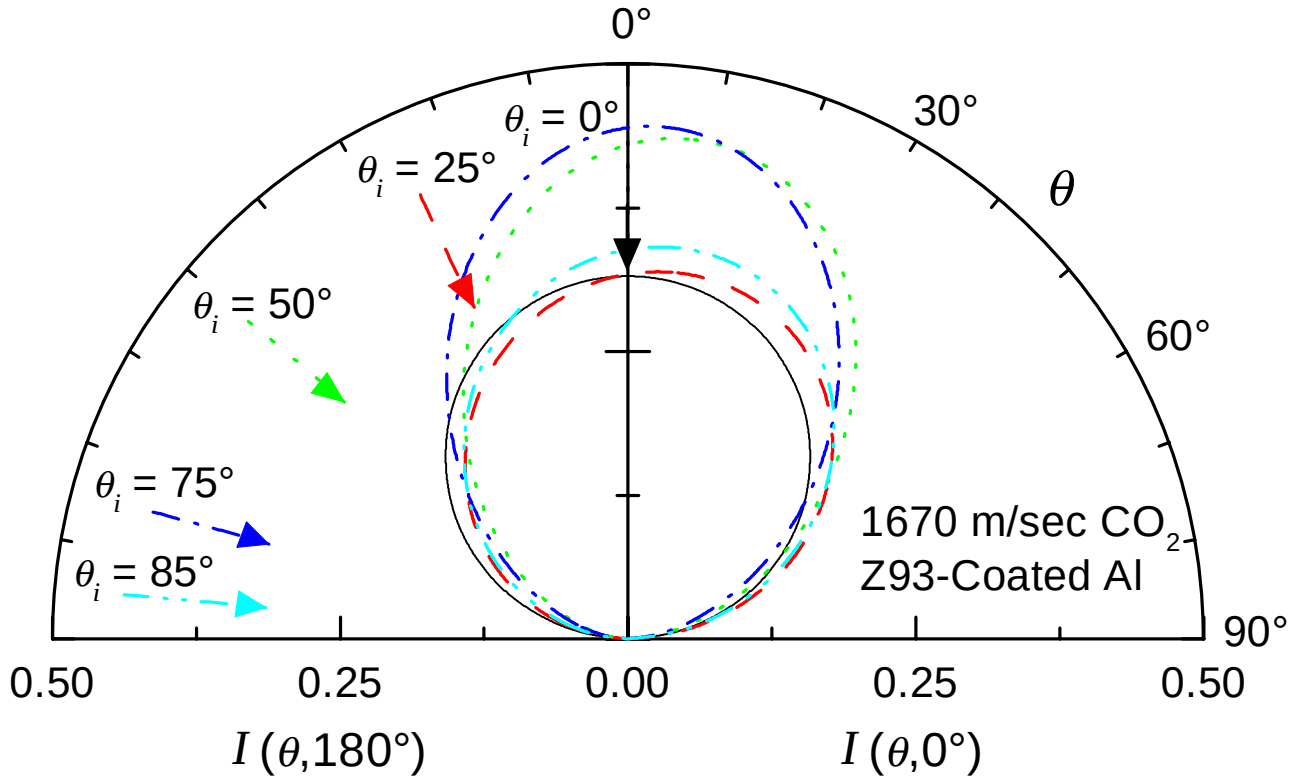

Figure 48: The angular distribution functions for 1670 m/s CO_2 incident upon Z-93-coated aluminum.

Table 48: The Nocilla model parameters for 1670 m/s CO_2 incident upon Z-93-coated aluminum.

θ_i (degrees)	S	U (m/s)	θ_u (degrees)	T_s (K)
0	0.00572	1.92	180	295
25	0.0613	20.4	85.7	295
50	0.363	118	14.9	282
75	0.382	124	6.55	281
85	0.101	33.4	38.1	292

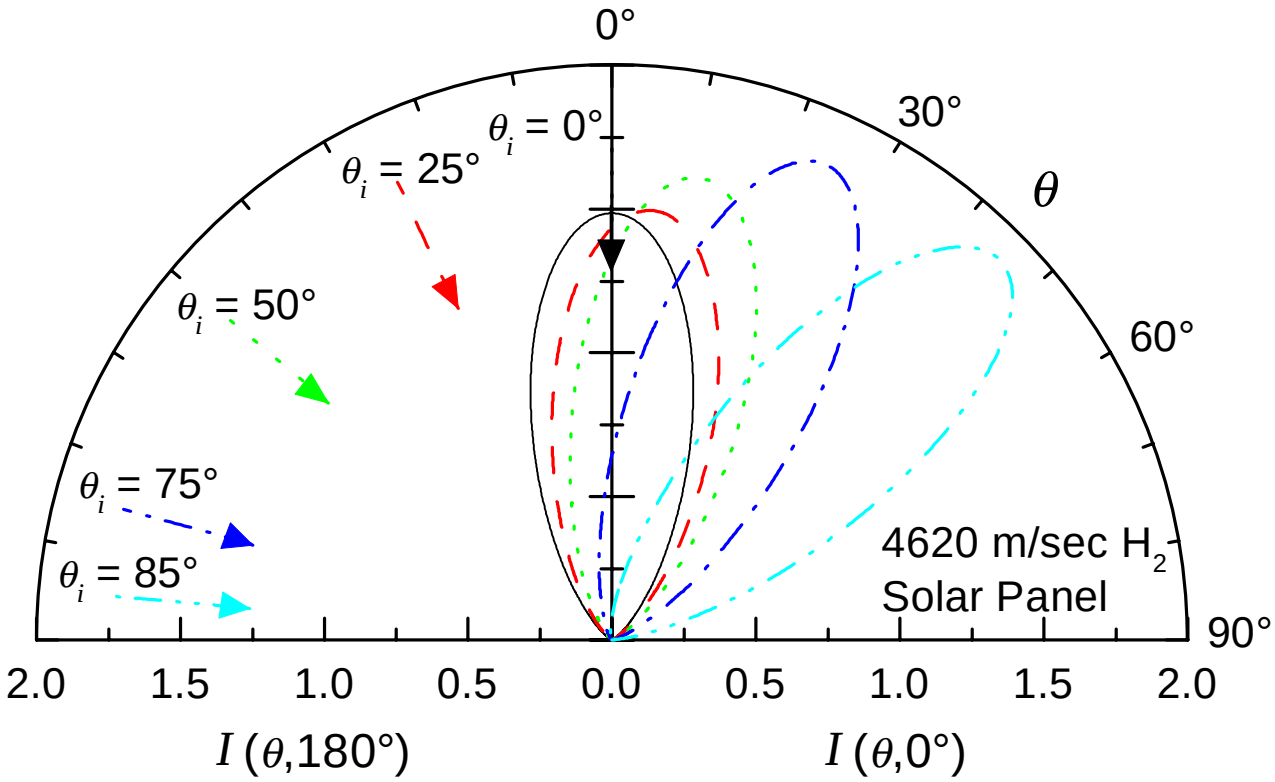

Figure 49: The angular distribution functions for 4620 m/s H_2 incident upon the solar panel.

Table 49: The Nocilla model parameters for 4620 m/s H_2 incident upon the solar panel.

θ_i (degrees)	S	U (m/s)	θ_u (degrees)	T_s (K)
0	1.80	2290	0	197
25	1.81	2310	6.05	197
50	1.93	2420	12.1	191
75	2.06	2540	26.5	185
85	2.06	2570	50.9	189

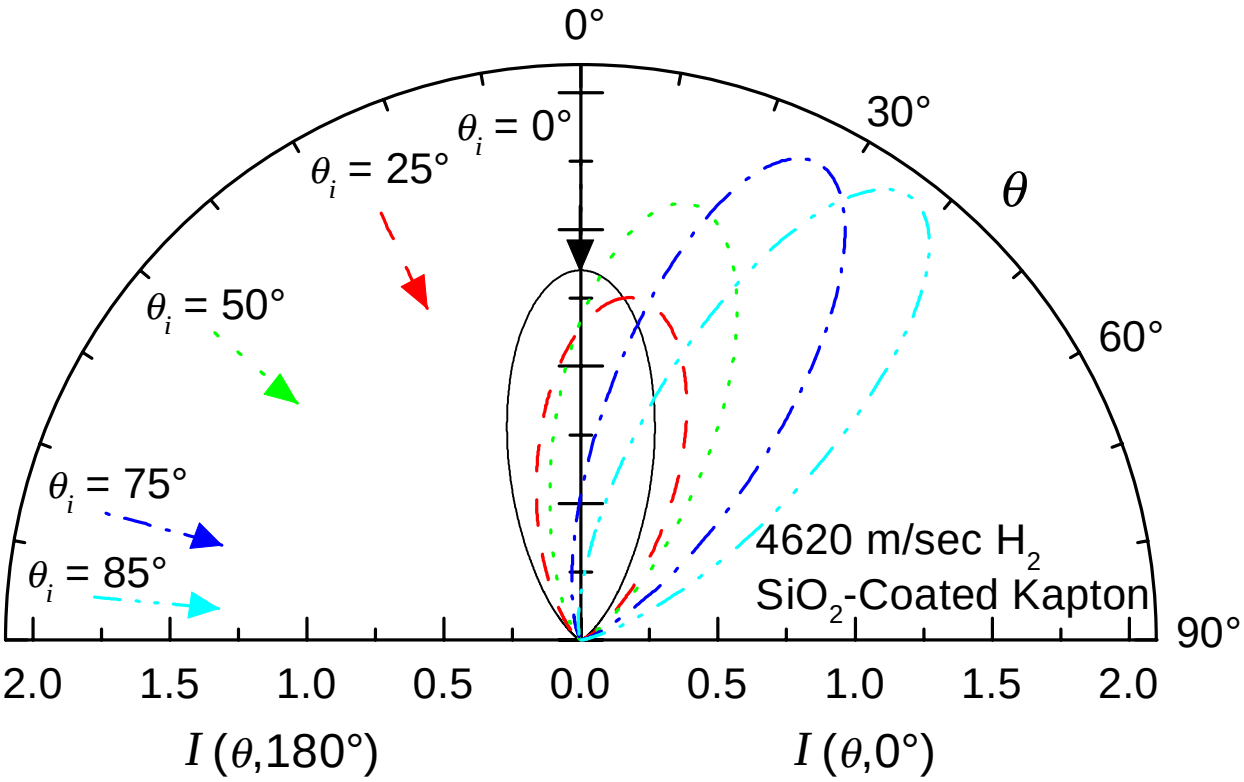

Figure 50: The angular distribution functions for 4620 m/s H_2 incident upon SiO_2-coated Kapton.

Table 50: The Nocilla model parameters for 4620 m/s H_2 incident upon SiO_2-coated Kapton.

θ_i (degrees)	S	U (m/s)	θ_u (degrees)	T_s (K)
0	1.68	2170	0	204
25	1.59	2080	10.2	208
50	1.93	2420	15.7	191
75	2.16	2630	28.6	180
85	2.19	2670	40.2	180

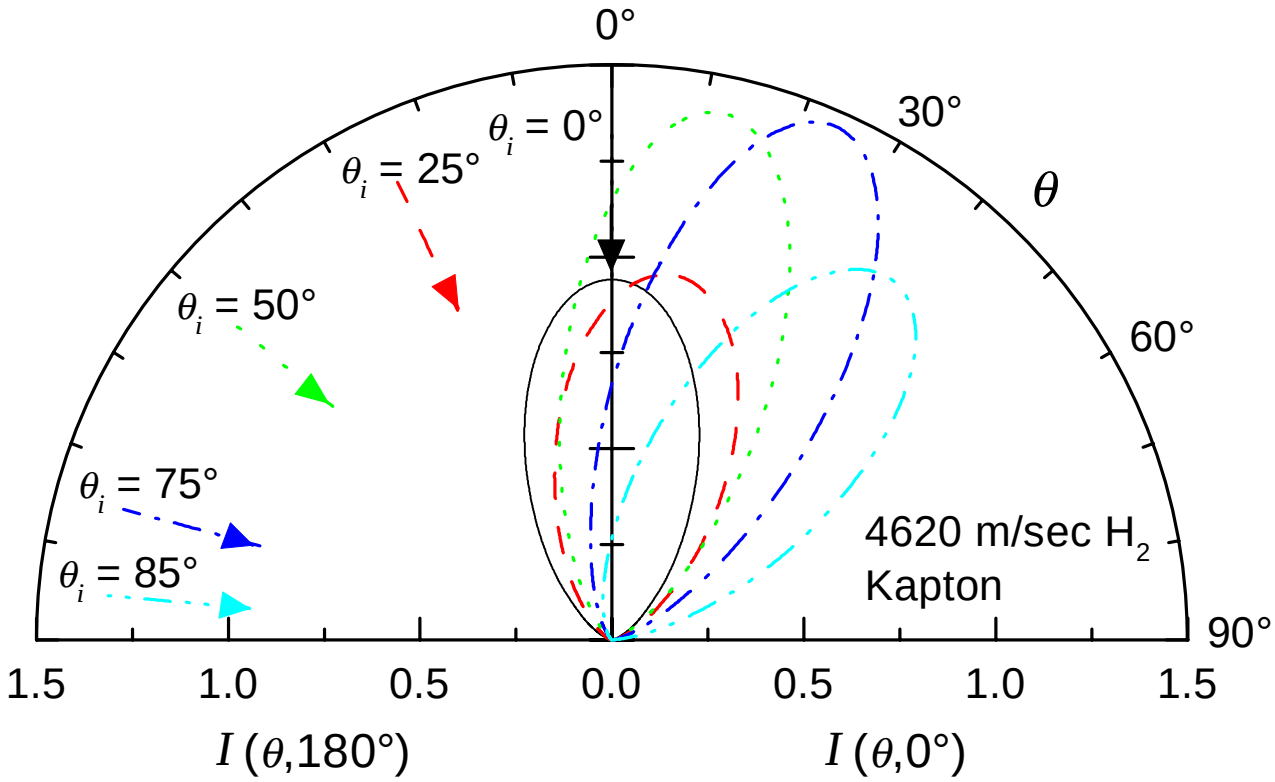

Figure 51: The angular distribution functions for 4620 m/s H_2 incident upon Kapton.

Table 51: The Nocilla model parameters for 4620 m/s H_2 incident upon Kapton.

θ_i (degrees)	S	U (m/s)	θ_u (degrees)	T_s (K)
0	1.23	1680	0	228
25	1.26	1720	11.5	226
50	1.72	2220	13.4	202
75	1.76	2260	26.4	200
85	1.46	1970	45.1	220

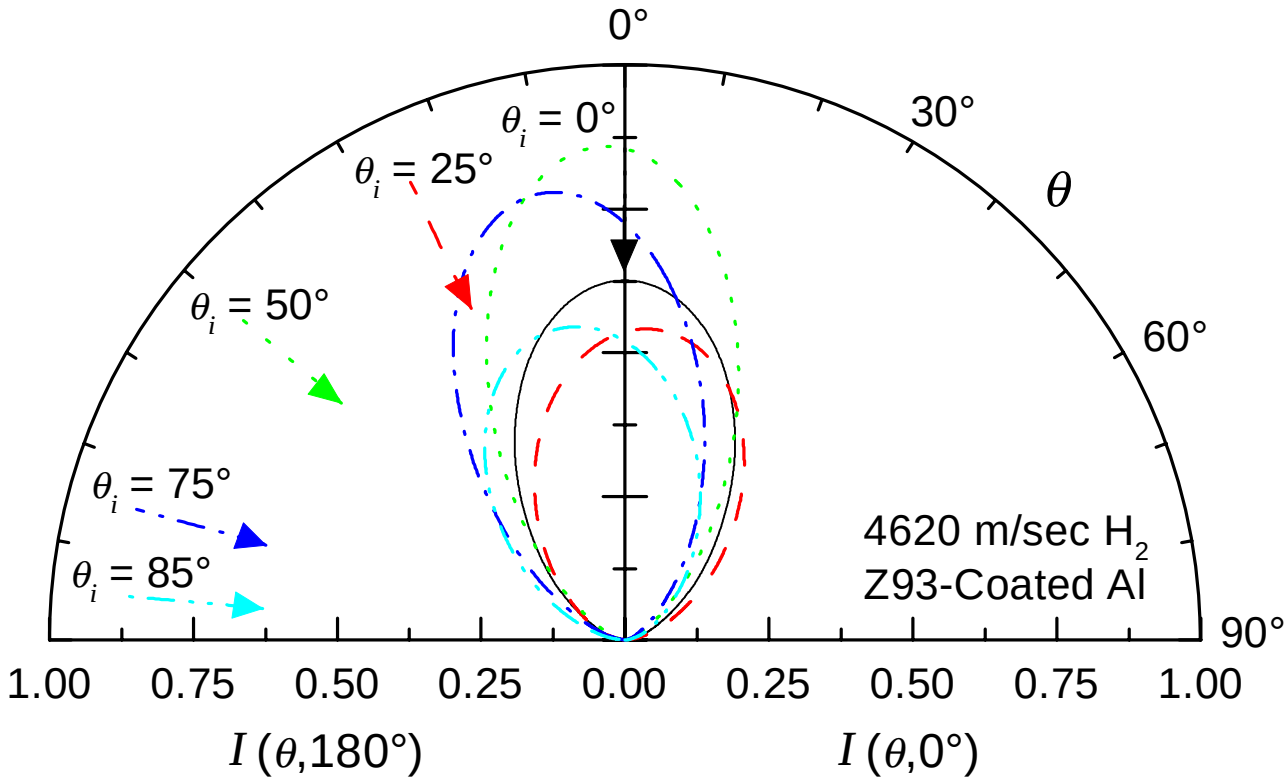

Figure 52: The angular distribution functions for 4620 m/s H_2 incident upon Z-93-coated aluminum.

Table 52: The Nocilla model parameters for 4620 m/s H_2 incident upon Z-93-coated aluminum.

θ_i (degrees)	S	U (m/s)	θ_u (degrees)	T_s (K)
0	0.760	1100	0	254
25	0.598	881	7.95	263
50	1.12	1560	-3.17	234
75	1.02	1440	-13.6	240
85	0.618	910	-17.4	263

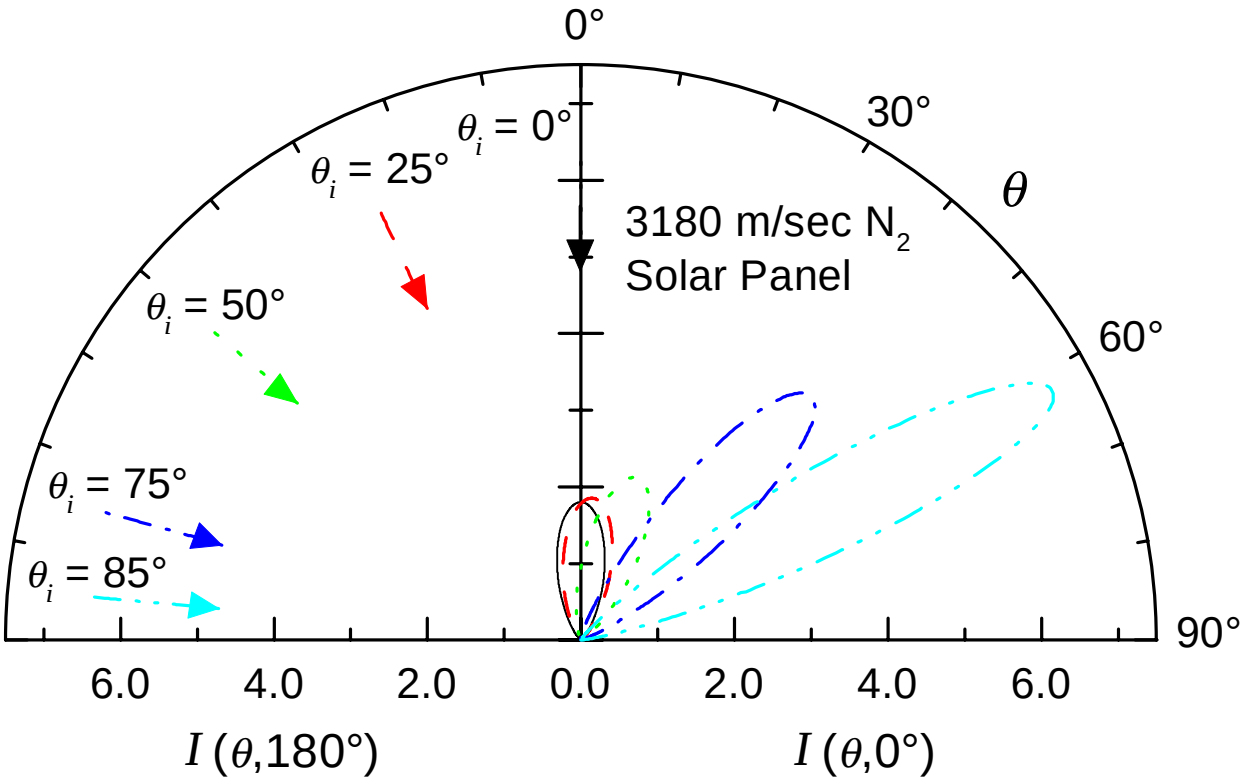

Figure 53: The angular distribution functions for 3180 m/s N_2 incident upon the solar panel.

Table 53: The Nocilla model parameters for 3180 m/s N_2 incident upon the solar panel.

θ_i (degrees)	S	U (m/s)	θ_u (degrees)	T_s (K)
0	2.06	802	0	318
25	2.11	820	5.12	255
50	2.38	926	20.8	255
75	3.54	1400	45.3	264
85	4.55	1860	64.6	283

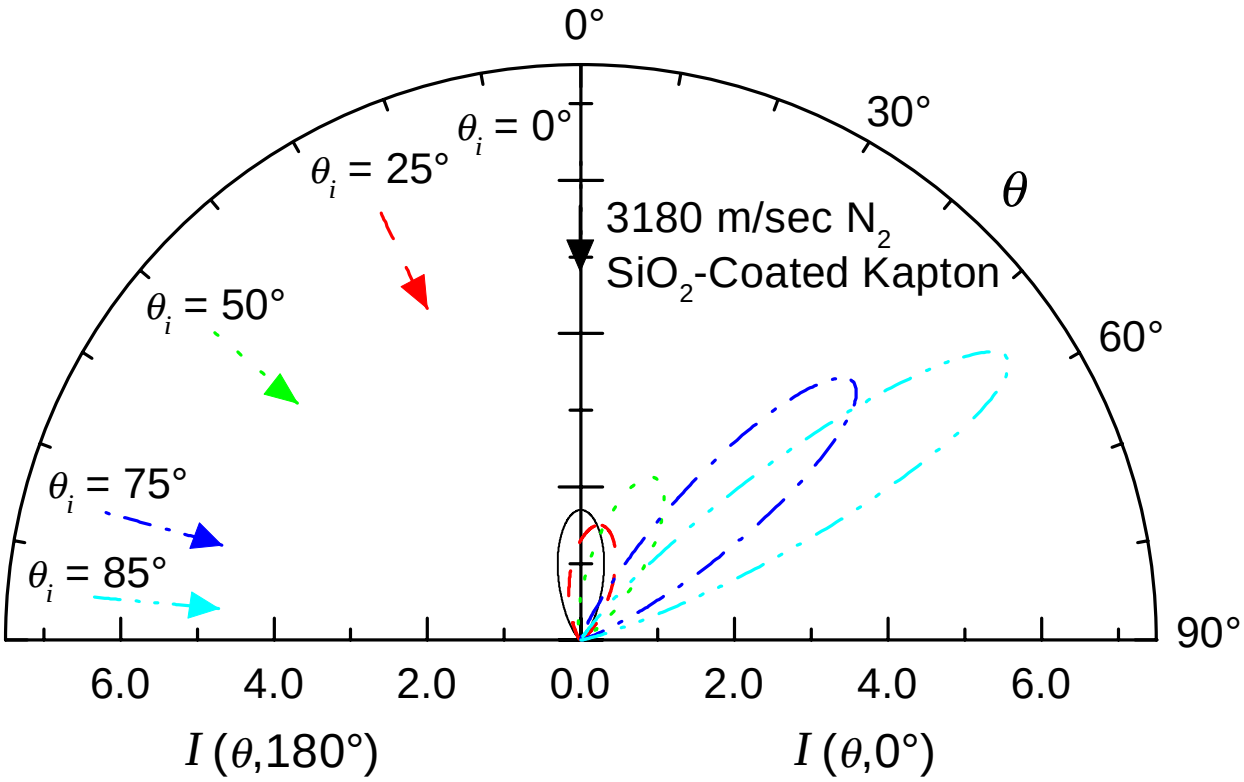

Figure 54: The angular distribution functions for 3180 m/s N_2 incident upon SiO_2-coated Kapton.

Table 54: The Nocilla model parameters for 3180 m/s N_2 incident upon SiO_2-coated Kapton.

θ_i (degrees)	S	U (m/s)	θ_u (degrees)	T_s (K)
0	1.98	771	0	255
25	1.83	714	10.9	256
50	2.43	947	26.5	256
75	3.77	1500	48.4	267
85	4.48	1820	58.5	277

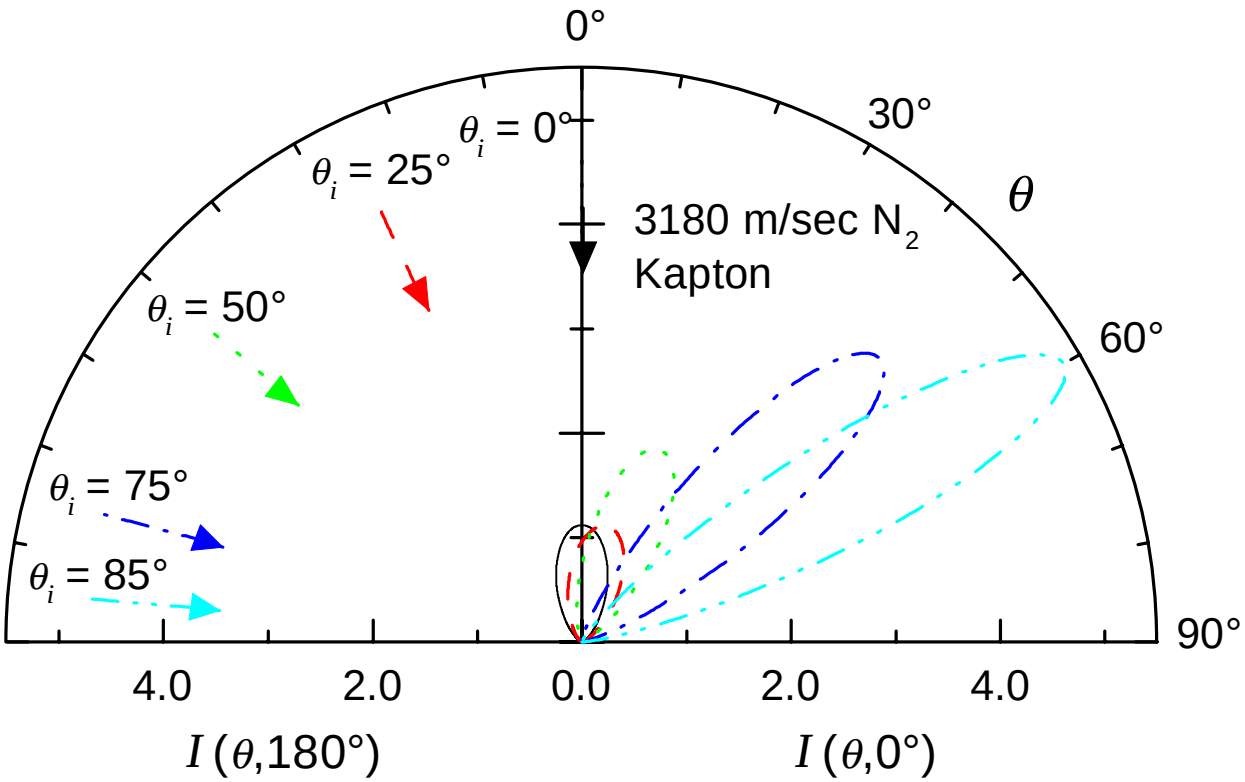

Figure 55: The angular distribution functions for 3180 m/s N_2 incident upon Kapton.

Table 55: The Nocilla model parameters for 3180 m/s N_2 incident upon Kapton.

θ_i (degrees)	S	U (m/s)	θ_u (degrees)	T_s (K)
0	1.44	565	0	260
25	1.46	572	14.1	260
50	2.19	854	24.8	256
75	3.31	1310	48.8	264
85	3.89	1570	63.1	276

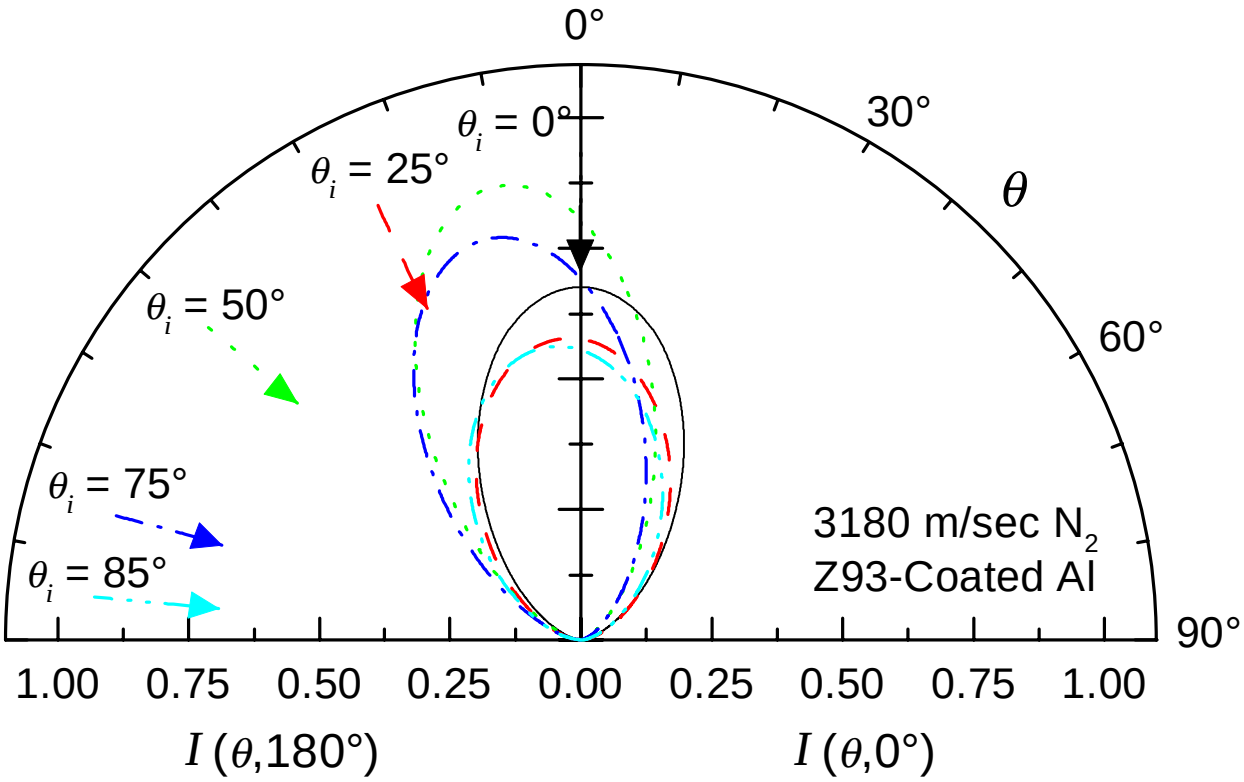

Figure 56: The angular distribution functions for 3180 m/s N_2 incident upon Z-93-coated aluminum.

Table 56: The Nocilla model parameters for 3180 m/s N_2 incident upon Z-93-coated aluminum.

θ_i (degrees)	S	U (m/s)	θ_u (degrees)	T_s (K)
0	0.846	339	0	260
25	0.669	270	-4.05	260
50	1.15	456	-12.7	256
75	1.02	405	-16.8	264
85	0.64	259	-8.51	276

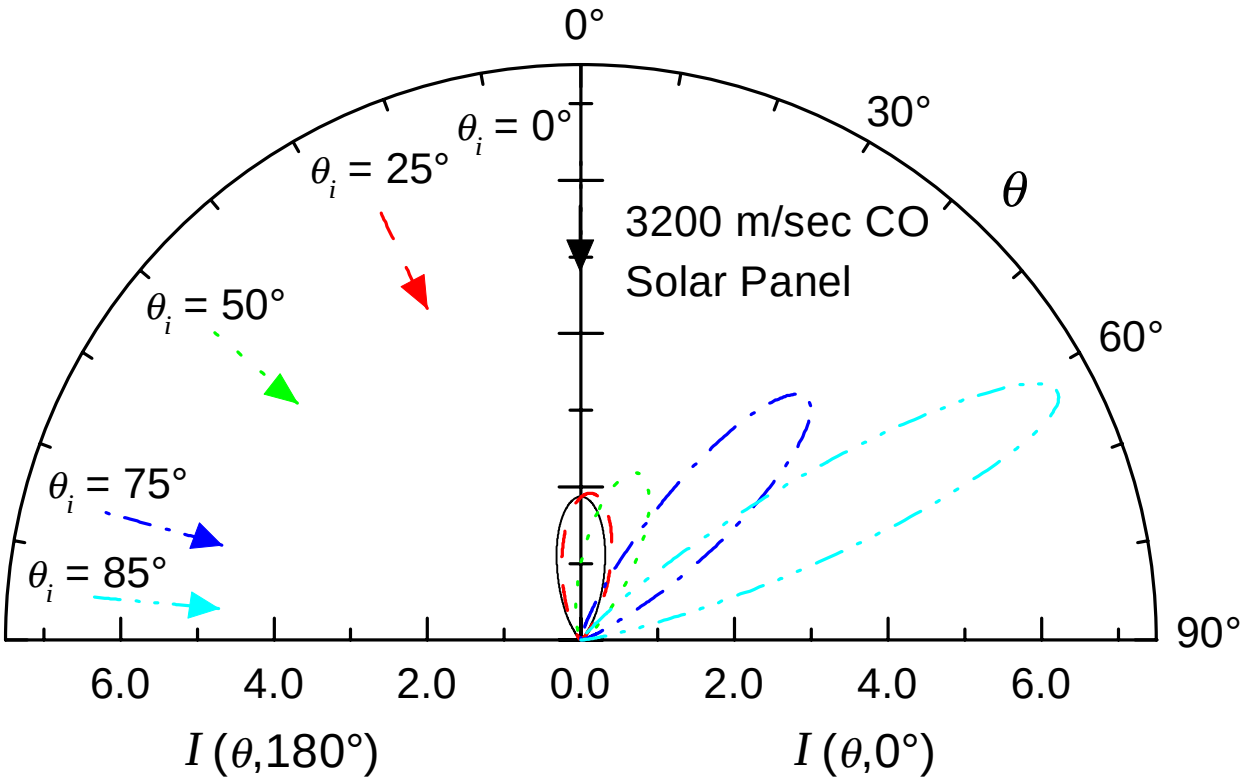

Figure 57: The angular distribution functions for 3200 m/s CO incident upon the solar panel.

Table 57: The Nocilla model parameters for 3200 m/s CO incident upon the solar panel.

θ_i (degrees)	S	U (m/s)	θ_u (degrees)	T_s (K)
0	2.12	821	0	254
25	2.16	836	4.32	254
50	2.42	939	20.1	254
75	3.51	1380	44.9	261
85	4.56	1850	64.9	278

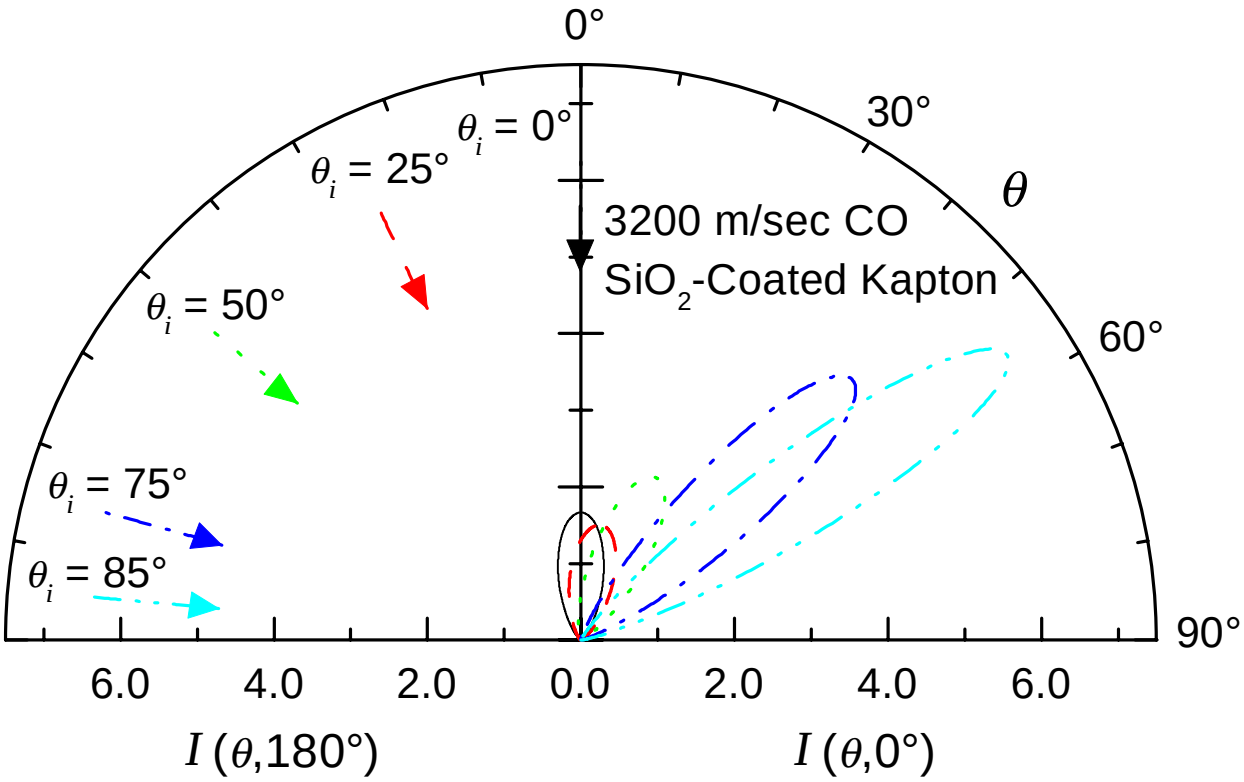

Figure 58: The angular distribution functions for 3200 m/s CO incident upon SiO_2-coated Kapton.

Table 58: The Nocilla model parameters for 3200 m/s CO incident upon SiO_2-coated Kapton.

θ_i (degrees)	S	U (m/s)	θ_u (degrees)	T_s (K)
0	1.95	758	0	254
25	1.83	713	11.1	256
50	2.44	947	26.6	255
75	3.79	1490	48.1	263
85	4.48	1800	58.2	273

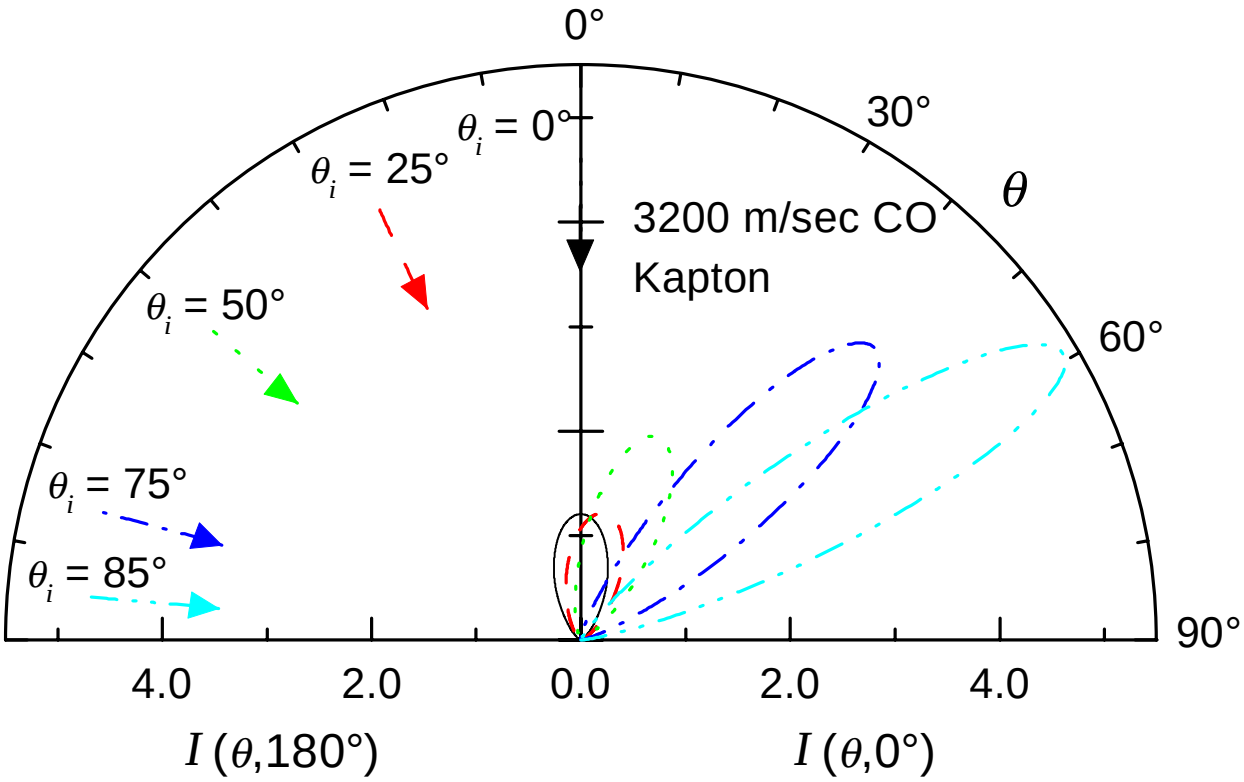

Figure 59: The angular distribution functions for 3200 m/s CO incident upon Kapton.

Table 59: The Nocilla model parameters for 3200 m/s CO incident upon Kapton.

θ_i (degrees)	S	U (m/s)	θ_u (degrees)	T_s (K)
0	1.53	599	0	258
25	1.56	610	12.3	258
50	2.26	879	22.5	255
75	3.33	1310	47.4	261
85	3.91	1570	62.2	271

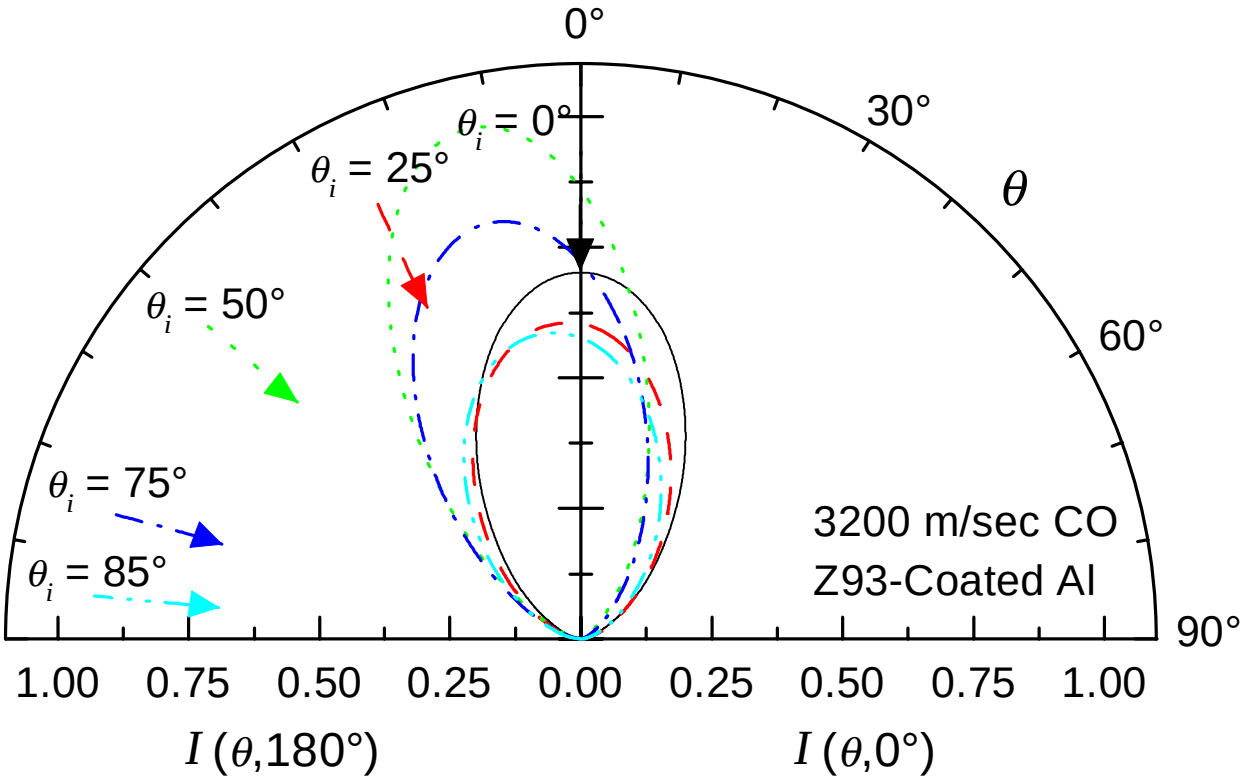

Figure 60: The angular distribution functions for 3200 m/s CO incident upon Z-93-coated aluminum.

Table 60: The Nocilla model parameters for 3200 m/s CO incident upon Z-93-coated aluminum.

θ_i (degrees)	S	U (m/s)	θ_u (degrees)	T_s (K)
0	0.889	356	0	270
25	0.724	292	-4.31	274
50	1.30	511	-14.7	262
75	1.06	420	-15.7	267
85	0.688	278	-9.42	275

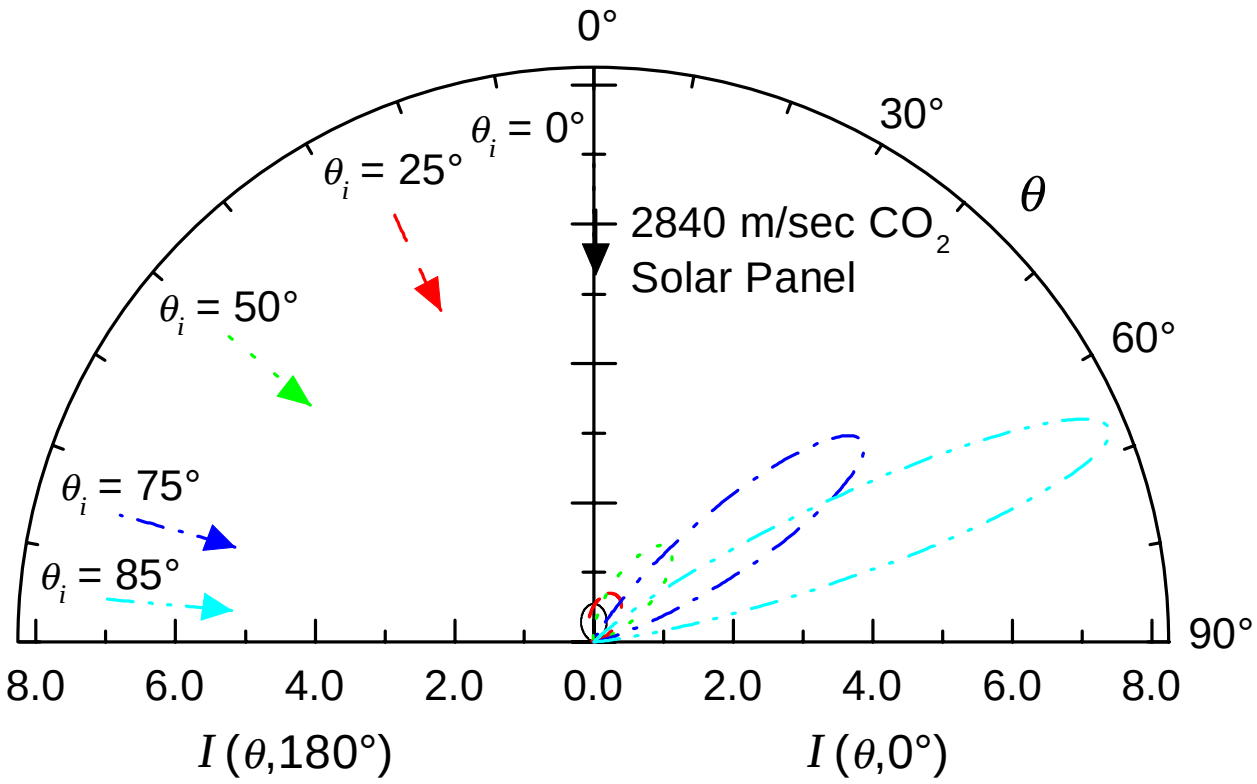

Figure 61: The angular distribution functions for 2840 m/s CO_2 incident upon the solar panel.

Table 61: The Nocilla model parameters for 2840 m/s CO_2 incident upon the solar panel.

θ_i (degrees)	S	U (m/s)	θ_u (degrees)	T_s (K)
0	0.605	196	0	278
25	0.942	302	30.5	273
50	1.95	618	42.4	264
75	3.71	1200	55.5	277
85	4.87	1670	70.3	310

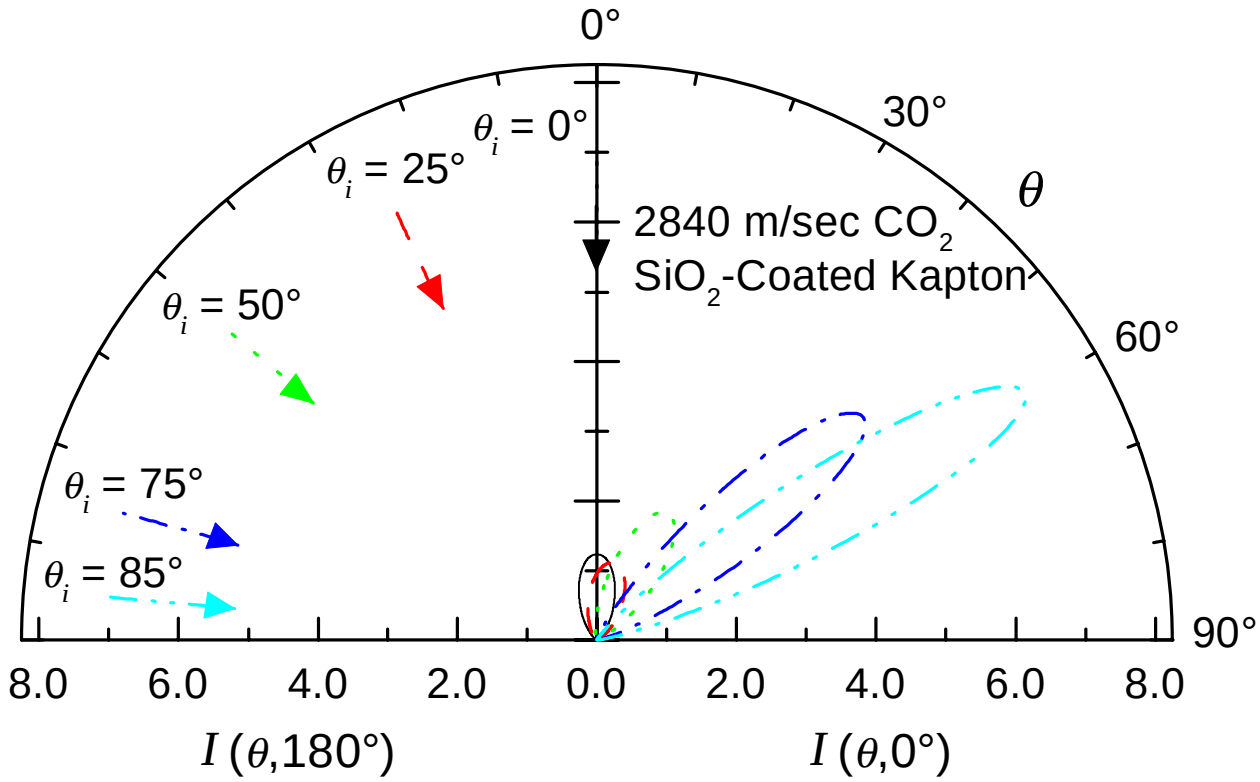

Figure 62: The angular distribution functions for 2840 m/s CO_2 incident upon SiO_2-coated Kapton.

Table 62: The Nocilla model parameters for 2840 m/s CO_2 incident upon SiO_2-coated Kapton.

θ_i (degrees)	S	U (m/s)	θ_u (degrees)	T_s (K)
0	1.56	489	0	260
25	1.46	459	14.3	262
50	2.26	707	31.8	260
75	3.80	1230	52.1	276
85	4.61	1540	62.1	295

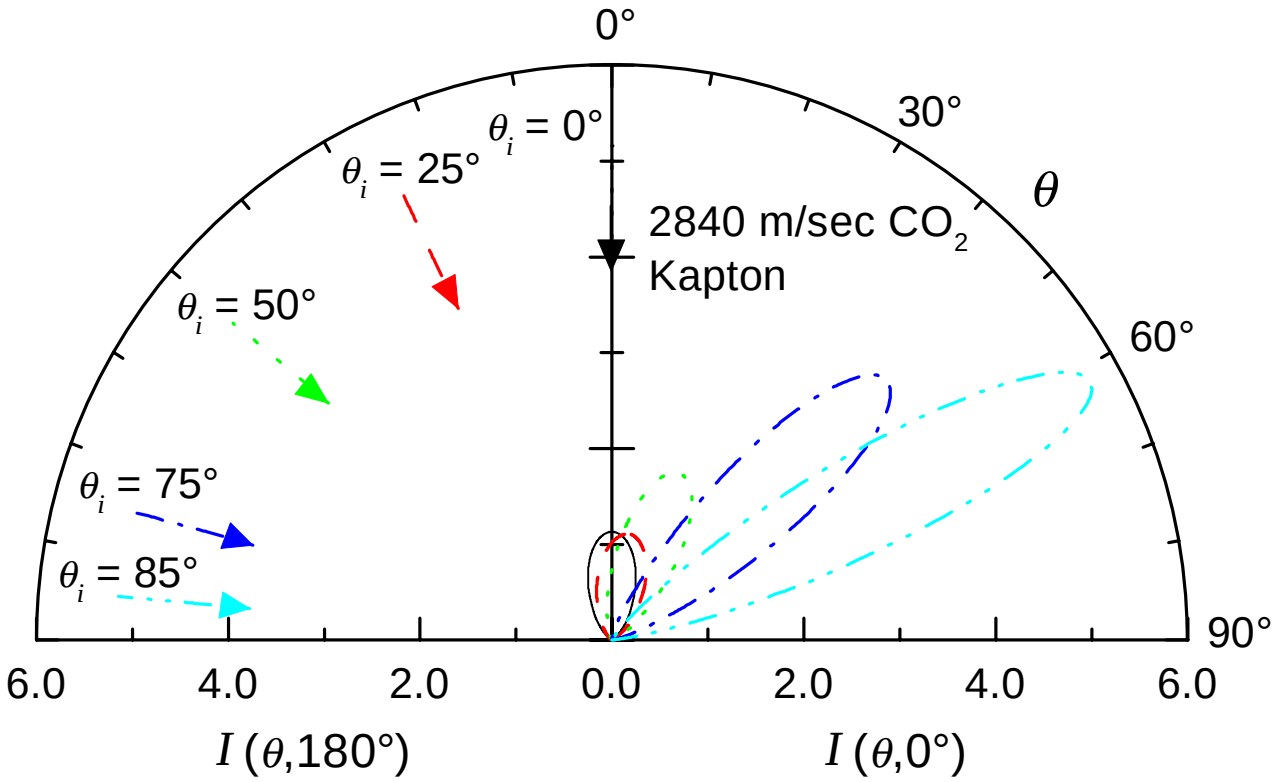

Figure 63: The angular distribution functions for 2840 m/s CO_2 incident upon Kapton.

Table 63: The Nocilla model parameters for 2840 m/s CO_2 incident upon Kapton.

θ_i (degrees)	S	U (m/s)	θ_u (degrees)	T_s (K)
0	1.45	455	0	261
25	1.44	452	10.6	261
50	2.11	660	24.3	259
75	3.32	1060	48.9	270
85	4.03	1380	64.7	288

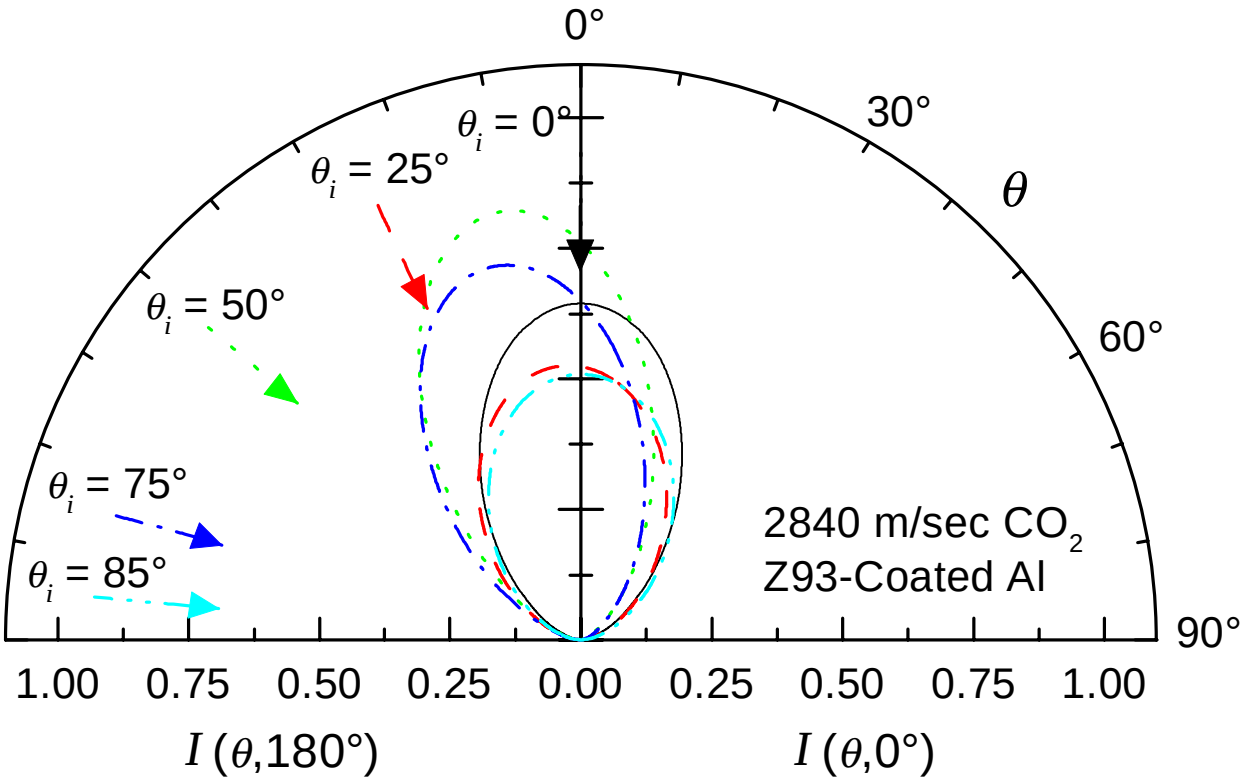

Figure 64: The angular distribution functions for 2840 m/s CO_2 incident Z-93-coated aluminum.

Table 64: The Nocilla model parameters for 2840 m/s CO_2 incident upon Z-93-coated aluminum.

θ_i (degrees)	S	U (m/s)	θ_u (degrees)	T_s (K)
0	0.792	254	0	273
25	0.564	183	-5.25	279
50	1.08	344	-13.3	267
75	0.935	299	17.6	271
85	0.526	171	0.166	280

Table 65: Comparison of the Reduced Force Coefficient measurements for 1870 m/s N_2 incident upon the solar panel made with the carrier gases H_2 and He.

θ_i (degrees)	f_t He	f_t H_2	f_t % Diff.	f_n He	f_n H_2	f_n % Diff.
0	0	0	0	1.34	1.26	6.0
25	0.379	0.362	4.6	1.24	1.17	6.4
50	0.648	0.628	3.2	1.02	0.949	7.7
75	0.696	0.679	2.6	0.643	0.581	10.7
85	0.578	0.522	10.7	0.430	0.340	26.6

Table 66: Comparison of the Reduced Force Coefficient measurements for 1870 m/s CO incident upon the solar panel made with the carrier gases H_2 and He.

θ_i (degrees)	f_t He	f_t H_2	f_t % Diff.	f_n He	f_n H_2	f_n % Diff.
0	0	0	0	1.33	1.26	5.6
25	0.382	0.366	4.3	1.24	1.18	5.1
50	0.656	0.634	3.5	0.997	0.948	5.1
75	0.725	0.688	5.3	0.632	0.577	9.6
85	0.595	0.530	12.2	0.414	0.338	22.5

Table 67: Comparison of the Reduced Force Coefficient measurements for 1670 m/s CO_2 incident upon the solar panel made with the carrier gases H_2 and He.

θ_i (degrees)	f_t He	f_t H_2	f_t % Diff.	f_n He	f_n H_2	f_n % Diff.
0	0	0	0	1.27	1.21	5.3
25	0.374	0.381	1.7	1.19	1.13	5.3
50	0.653	0.661	1.2	0.961	0.891	7.8
75	0.719	0.734	2.1	0.588	0.519	13.4
85	0.608	0.562	8.3	0.368	0.288	27.6

REPORT DOCUMENTATION PAGE

Form Approved
OMB No. 0704-0188

1. AGENCY USE ONLY *(Leave Blank)*	2. REPORT DATE	3. REPORT TYPE AND DATES COVERED
	November 1997	NASA Technical Paper

4. TITLE AND SUBTITLE
Measurement of Momentum Transfer Coefficients for H2, N2, CO, and CO2 Incident Upon Spacecraft Surfaces

5. FUNDING NUMBERS

6. AUTHOR(S)
Steven R. Cook* and Mark A. Hoffbauer*

7. PERFORMING ORGANIZATION NAME(S) AND ADDRESS(ES)
Lyndon B. Johnson Space Center
Houston, Texas 77058

8. PERFORMING ORGANIZATION REPORT NUMBERS
S-834

9. SPONSORING/MONITORING AGENCY NAME(S) AND ADDRESS(ES)
National Aeronautics and Space Administration
Washington, D.C. 20546-0001

10. SPONSORING/MONITORING AGENCY REPORT NUMBER
TP 3701

11. SUPPLEMENTARY NOTES
* Los Alamos National Laboratory

12a. DISTRIBUTION/AVAILABILITY STATEMENT
Unclassified/unlimited
Available from the NASA Center for AeroSpace Information (CASI)
800 Elkridge Landing Rd
Linthicum Heights, MD 21090-2934 (301) 621-0390 Subject Category: 15

12b. DISTRIBUTION CODE

13. ABSTRACT *(Maximum 200 words)*
Measurements of momentum transfer coefficients were made for gas-surface interactions between the Space Shuttle reaction control jet plume gases and the solar panel array materials to be used on the International Space Station. Actual conditions were simulated using a supersonic nozzle source to produce beams of the gases with approximately the same average velocities as the gases have in the Shuttle plumes. Samples of the actual solar panel materials were mounted on a torsion balance that was used to measure the force exerted on the surfaces by the molecular beams. Measurements were made with H2, N2, CO, and CO2 incident upon the solar array material, Kapton, SiO2-coated Kapton, and Z93-coated Al. The measurements showed that molecules scatter from the surfaces more specularly as the angle of incidence increases and that the scattering behavior has a strong dependence upon both the incident gas and velocity. These results show that for some technical surfaces the simple assumption of diffuse scattering with complete thermal accommodation is entirely inadequate. It is clear that additional measurements are required to produce models that more accurately describe the gas-surface interactions encountered in rarefied flow regimes.

14. SUBJECT TERMS	15. NUMBER OF PAGES	16. PRICE CODE
solar arrays, plumes, momentum transfer, rarefied gas dynamics	81	

17. SECURITY CLASSIFICATION OF REPORT	18. SECURITY CLASSIFICATION OF THIS PAGE	19. SECURITY CLASSIFICATION OF ABSTRACT	20. LIMITATION OF ABSTRACT
Unclassified	Unclassified	Unclassified	None

Standrard Form 298 (Rev Feb 89) (MS Word Mar 97)
Prescribed by ANSI Std. 239-18
298-102
NSN 7540-01-280-5500